

Particle Dark Matter: Evidence, Candidates and Constraints

Gianfranco Bertone¹, Dan Hooper² and Joseph Silk²

¹ NASA/Fermilab Theoretical Astrophysics Group, Batavia, IL 60510

² University of Oxford, Astrophysics Dept., Oxford, UK OX1 3RH

February 1, 2008

Abstract

In this review article, we discuss the current status of particle dark matter, including experimental evidence and theoretical motivations. We discuss a wide array of candidates for particle dark matter, but focus on neutralinos in models of supersymmetry and Kaluza-Klein dark matter in models of universal extra dimensions. We devote much of our attention to direct and indirect detection techniques, the constraints placed by these experiments and the reach of future experimental efforts.

Contents

1	Introduction	4
1.1	Overview	4
1.2	Standard Cosmology	5
1.3	The Standard Model of Particle Physics	8
1.4	A very brief history of the Universe	9
1.5	Relic Density	10
1.5.1	The standard calculation	11
1.5.2	Including coannihilations	13
1.6	Links with Physics Beyond the Standard Model	14
2	Evidence and Distribution	15
2.1	The Galactic Scale	15
2.2	The Scale of Galaxy Clusters	19
2.3	Cosmological Scales	21
2.4	N-Body Simulations	23
2.5	The Case of the Milky Way	25
2.5.1	The Galactic center	26
2.5.2	The local density	30
3	Candidates	31
3.1	The Non-Baryonic Candidate Zoo	31
3.2	Supersymmetry	36
3.2.1	Basics of supersymmetry	36
3.2.2	Minimal supersymmetric Standard Model	38
3.2.3	The lightest neutralino	41
3.2.4	Supersymmetric models	42
3.3	Extra Dimensions	47
3.3.1	Universal extra dimensions	48
3.3.2	The lightest Kaluza–Klein particle	49
3.4	Superheavy Candidates	51
3.5	Collider Constraints	52
3.5.1	Current collider constraints	52
3.5.2	The reach of future collider experiments	55
4	Experiments	57
4.1	Direct Detection Experiments	57
4.1.1	Scattering classifications	59
4.1.2	Experimental Efforts	60
4.2	Gamma-Ray Experiments	60
4.2.1	Ground-based telescopes	61
4.2.2	Space-based telescopes	64
4.3	Neutrino Telescopes	65
4.4	Positron and Anti-Proton Experiments	68
4.5	Observations at Radio Wavelengths	69

5	Direct Detection	70
6	Indirect Detection	71
6.1	Gamma-rays and neutrinos from the Galactic center	73
6.1.1	Prospects for Neutralinos	74
6.1.2	Prospects for Kaluza-Klein dark matter	74
6.1.3	The gamma-ray source at the Galactic center	81
6.1.4	Upper Limit for the Neutrino Flux from the GC	81
6.2	Synchrotron Radiation from the Galactic Center	82
6.3	Annihilation Radiation from External or Dwarf Galaxies	89
6.4	High-Energy Neutrinos from the Sun or Earth	90
6.4.1	Capture and annihilation in the Sun	90
6.4.2	Detection of high-energy neutrinos from the Sun	93
6.5	e^+ and \bar{p} from Annihilations in the Galactic Halo	95
6.5.1	The positron excess	95
6.5.2	Anti-protons	98
6.6	The Role of Substructures	99
6.7	Constraints from Helioseismology	100
6.8	Constraints on Superheavy Dark Matter	101
7	Conclusions	102
8	Acknowledgements	103
A	Neutralino Mass Eigenstates	104
B	Neutralino Annihilation Cross Sections in the Low Velocity Limit	106
B.1	Annihilation Into Fermions	106
B.2	Annihilation Into Gauge Bosons	108
B.3	Annihilation Into Higgs Bosons	110
B.4	Annihilation Into Photons	112
C	Elastic Scattering Processes	116
C.1	Scalar Interactions	116
C.2	Axial-Vector Interactions	119
C.3	Vector Interactions	120

1 Introduction

1.1 Overview

A great deal of effort has been made since 1687, the year of publication of Issac Newton’s classic work “*Philosophiae Naturalis Principia Mathematica*”, towards explaining the motion of astrophysical objects in terms of the laws of gravitation. Since then, the deviations of observed motions from expected trajectories have proved very effective in deepening our understanding of the Universe. Whenever anomalies were observed in the motion of planets in the Solar system, the question arose: should such anomalies be regarded as a refutation of the laws of gravitation or as an indication of the existence of unseen (today we would say “dark”) objects?

The second approach proved to be correct in the case of the anomalous motion of Uranus, which led the French astronomer U. Le Verrier and the English astronomer John Couch Adams to conjecture the existence of Neptune, eventually discovered in 1846 by J.G. Galle. Conversely, the attempt to explain the anomalies in the motion of Mercury as due to the existence of a new planet, called Vulcan, failed, and the final solution had to wait for the advent of Einstein’s theory of general relativity, *i.e.* the introduction of a more refined description of the laws of gravitation.

The modern problem of dark matter is conceptually very similar to the old problem of unseen planets. We observe in large astrophysical systems, with sizes ranging from galactic to cosmological scales, some “anomalies” that can only be explained either by assuming the existence of a large amount of unseen, *dark*, matter, or by assuming a deviation from the known laws of gravitation and the theory of general relativity.

About ten years ago, Jungman, Kamionkowski and Griest wrote a review of supersymmetric dark matter for Physics Reports [319]. This article, although incredibly useful, complete and popular, has gradually become outdated over the last decade. With this in mind, we have endeavored to write a new review of particle dark matter. As with the Jungman *et al.* article, our review is intended to be suitable for a wide range of readers. It could be used as an introduction for graduate students interested in this subject or for more experienced scientists whose research focuses in other areas. It is also intended to be a useful reference in day-to-day research for particle physicists and astrophysicists actively working on the problem of dark matter. Unlike the review by Jungman *et al.*, we do not limit our discussion to supersymmetric dark matter.

The article is organized as follows: we first present, in this chapter, a brief review of the Standard Model of particle physics and cosmology, and review our present understanding of the history of the Universe. We focus in particular on the freeze-out of dark matter particles and on the calculation of their relic abundance, and discuss the possible relationship between dark matter and physics beyond the Standard Model of particle physics.

Chapter 2 is devoted to the compelling evidence for dark matter at all astrophysical length scales. We review the key observations and discuss the theoret-

ical predictions (from N-body simulations) for the distribution of dark matter, focusing in particular on the innermost regions of galaxies, and discuss how they compare with observations. Particular attention is devoted to the galactic center, where the presence of a supermassive black hole could significantly modify the dark matter distribution.

Dark matter candidates are presented in chapter 3. We start with an introduction to the “dark matter zoo”, *i.e.* a description of the many candidates that have been proposed in the literature. We then focus on two particularly interesting dark matter candidates: the supersymmetric neutralino and Kaluza-Klein dark matter. For each of these candidates, we give a brief introduction to the physical motivations and underlying theories. We conclude chapter 3 with a review of the constraints put on dark matter from collider experiments, and discuss the prospects for future experiments.

The second part of this review is devoted to the astrophysical constraints on particle dark matter. We begin in chapter 4 with a review of existing and next-generation experiments that will probe the nature of dark matter. This chapter is propedeutical to chapter 5, which discusses the many possible direct and indirect searches of dark matter and which constitutes the heart of this review. We give our conclusions in chapter 6. Some useful particle physics details are given in the appendices.

1.2 Standard Cosmology

Although the exact definition of the *Standard* cosmological model evolves with time, following the progress of experiments in measuring the cosmological parameters, most cosmologists agree on a fundamental picture, the so-called *Big Bang* scenario, which describes the Universe as a system evolving from a highly compressed state existing around 10^{10} years ago.

This picture has its roots in the discovery of Hubble’s law early in the past century, and has survived all sorts of cosmological observations, unlike alternative theories such as the “steady state cosmology”, with continuous creation of baryons, which, among other problems, failed to explain the existence and features of the cosmic microwave background.

We now have at our disposal an extremely sophisticated model, allowing us to explain in a satisfactory way the thermal history, relic background radiation, abundance of elements, large scale structure and many other properties of the Universe. Nevertheless, we are aware that our understanding is still only partial. It is quite clear that new physics is necessary to investigate the first instants of our Universe’s history (see section 1.6).

To “build” a cosmological model, in a modern sense, three fundamental ingredients are needed:

- *Einstein equations*, relating the geometry of the Universe with its matter and energy content
- *metrics*, describing the symmetries of the problem

- *Equation of state*, specifying the physical properties of the matter and energy content

The Einstein field equation can be derived almost from first principles, assuming that: 1) the equation is invariant under general coordinate transformations, 2) the equation tends to Newton’s law in the limit of weak fields, and 3) the equation is of second differential order and linear in second derivatives [400]. The resulting equation reads

$$R_{\mu\nu} - \frac{1}{2}g_{\mu\nu}R = -\frac{8\pi G_N}{c^4}T_{\mu\nu} + \Lambda g_{\mu\nu}, \quad (1)$$

where $R_{\mu\nu}$ and R are, respectively, the Ricci tensor and scalar (obtained by contraction of the Riemann curvature tensor). $g_{\mu\nu}$ is the metric tensor, G_N is Newton’s constant, $T_{\mu\nu}$ is the energy-momentum tensor, and Λ is the so-called cosmological constant.

Ignoring for a moment the term involving the cosmological constant, this equation is easily understood. We learn that *the geometry of the Universe*, described by the terms on the left-hand-side, *is determined by its energy content*, described by the energy-momentum tensor on the right-hand-side. This is the well known relationship between the matter content and geometry of the Universe, which is the key concept of general relativity.

The addition of the cosmological constant term, initially introduced by Einstein to obtain a stationary solution for the Universe and subsequently abandoned when the expansion of the Universe was discovered, represents a “vacuum energy” associated with space-time itself, rather than its matter content, and is a source of gravitational field even in the absence of matter. The contribution of such “vacuum energy” to the total energy of the Universe can be important, if one believes recent analyses of type Ia supernovae and parameter estimates from the cosmic microwave background (for further discussion see section 2.3).

To solve the Einstein equations one has to specify the symmetries of the problem. Usually one assumes the properties of statistical *homogeneity* and *isotropy* of the Universe, which greatly simplifies the mathematical analysis. Such properties, made for mathematical convenience, are confirmed by many observations. In particular, observations of the Cosmic Microwave Background (CMB) have shown remarkable isotropy (once the dipole component, interpreted as due to the Earth motion with respect to the CMB frame, and the contribution from the galactic plane were subtracted). Isotropy alone, if combined with the Copernican principle, or “mediocrity” principle, would imply homogeneity. Nevertheless, direct evidence of homogeneity comes from galaxy surveys, suggesting a homogeneous distribution at scales in excess of ~ 100 Mpc. More specifically, spheres with diameters larger than ~ 100 Mpc centered in any place of the Universe should contain, roughly, the same amount of matter.

The properties of isotropy and homogeneity imply a specific form of the metric: the line element can in fact be expressed as

$$ds^2 = -c^2 dt^2 + a(t)^2 \left(\frac{dr^2}{1 - kr^2} + r^2 d\Omega^2 \right), \quad (2)$$

where $a(t)$ is the so-called *scale factor* and the constant k , describing the spatial curvature, can take the values $k = -1, 0, +1$. For the simplest case, $k = 0$, the spatial part of Eq. 2 reduces to the metric of ordinary (flat) Euclidean space.

The Einstein equations can be solved with this metric, one of its components leading to the Friedmann equation

$$\left(\frac{\dot{a}}{a}\right)^2 + \frac{k}{a^2} = \frac{8\pi G_N}{3}\rho_{tot}, \quad (3)$$

where ρ_{tot} is the total average energy density of the universe. It is common to introduce the Hubble parameter

$$H(t) = \frac{\dot{a}(t)}{a(t)}. \quad (4)$$

A recent estimate [159] of the present value of the Hubble parameter, H_0 , (also referred to as the Hubble *constant*) is $H_0 = 73 \pm 3 \text{ km s}^{-1} \text{ Mpc}^{-1}$. We see from Eq. 3 that the universe is flat ($k = 0$) when the energy density equals the *critical density*, ρ_c :

$$\rho_c \equiv \frac{3H^2}{8\pi G_N}. \quad (5)$$

In what follows we will frequently express the abundance of a substance in the Universe (matter, radiation or vacuum energy), in units of ρ_c . We thus define the quantity Ω_i of a substance of species i and density ρ_i as

$$\Omega_i \equiv \frac{\rho_i}{\rho_c}. \quad (6)$$

It is also customary to define

$$\Omega = \sum_i \Omega_i \equiv \sum_i \frac{\rho_i}{\rho_c}, \quad (7)$$

in terms of which the Friedmann equation (Eq. 3) can be written

$$\Omega - 1 = \frac{k}{H^2 a^2}. \quad (8)$$

The sign of k is therefore determined by whether Ω is greater than, equal to, or less than one (see table 1).

Following Ref. [86], we note that the various Ω_i evolve with time differently, depending on the equation of state of the component. A general expression for the expansion rate is

$$\begin{aligned} \frac{H^2(z)}{H_0^2} = & \left[\Omega_X (1+z)^{3(1+\alpha_X)} + \Omega_K (1+z)^2 \right. \\ & \left. + \Omega_M (1+z)^3 + \Omega_R (1+z)^4 \right] \end{aligned} \quad (9)$$

$\rho < \rho_c$	$\Omega < 1$	$k = -1$	open
$\rho = \rho_c$	$\Omega = 1$	$k = 0$	flat
$\rho > \rho_c$	$\Omega > 1$	$k = 1$	closed

Table 1: Classification of cosmological models based on the value of the average density, ρ , in terms of the critical density, ρ_c .

where M and R are labels for matter and radiation, $\Omega_K = \frac{-k}{a_0^2 H_0^2}$ and X refers to a generic substance with equation of state $p_X = \alpha_X \rho_X$ (in particular, for the cosmological constant, $\alpha_\Lambda = -1$). z is the redshift.

We discuss in Sec. 2.3 recent estimates of cosmological parameters using CMB measurements, combined with various astrophysical observations.

1.3 The Standard Model of Particle Physics

The Standard Model (SM) of particle physics has, for many years, accounted for all observed particles and interactions¹. Despite this success, it is by now clear that a more fundamental theory must exist, whose low-energy realization should coincide with the SM.

In the SM, the fundamental constituents of matter are fermions: *quarks* and *leptons*. Their interactions are mediated by integer spin particles called *gauge bosons*. Strong interactions are mediated by gluons G_a , electroweak interaction by W^\pm , Z_0 , γ and the Higgs boson H^0 . The left-handed leptons and quarks are arranged into three generations of $SU(2)_L$ doublets

$$\begin{pmatrix} \nu_e \\ e^- \end{pmatrix}_L, \quad \begin{pmatrix} \nu_\mu \\ \mu^- \end{pmatrix}_L, \quad \begin{pmatrix} \nu_\tau \\ \tau^- \end{pmatrix}_L \quad (10)$$

$$\begin{pmatrix} u \\ d' \end{pmatrix}_L, \quad \begin{pmatrix} c \\ s' \end{pmatrix}_L, \quad \begin{pmatrix} t \\ b' \end{pmatrix}_L \quad (11)$$

with the corresponding right-handed fields transforming as singlets under $SU(2)_L$. Each generation contains two flavors of quarks with *baryon number* $B = 1/3$ and *lepton number* $L = 0$ and two leptons with $B = 0$ and $L = 1$. Each particle also has a corresponding antiparticle with the same mass and opposite quantum numbers.

The quarks which are primed are *weak eigenstates* related to *mass eigenstates* by the Cabibbo-Kobayashi-Maskawa (CKM) matrix

$$\begin{pmatrix} d' \\ s' \\ b' \end{pmatrix} = \begin{pmatrix} V_{ud} & V_{us} & V_{ub} \\ V_{cd} & V_{cs} & V_{cb} \\ V_{td} & V_{ts} & V_{tb} \end{pmatrix} \begin{pmatrix} d \\ s \\ b \end{pmatrix} = \hat{V}_{\text{CKM}} \begin{pmatrix} d \\ s \\ b \end{pmatrix}. \quad (12)$$

¹It is a matter of definition whether one considers neutrino masses as part of the SM or as physics beyond the SM.

Gauge symmetries play a fundamental role in particle physics. It is in fact in terms of symmetries and using the formalism of gauge theories that we describe electroweak and strong interactions. The SM is based on the $SU(3)_C \otimes SU(2)_L \otimes U(1)_Y$ gauge theory, which undergoes the spontaneous breakdown:

$$SU(3)_C \otimes SU(2)_L \otimes U(1)_Y \rightarrow SU(3)_C \otimes U(1)_Q \quad (13)$$

where Y and Q denote the weak hypercharge and the electric charge generators, respectively, and $SU(3)_C$ describes the strong (color) interaction, known as Quantum Chromodynamics (QCD). This spontaneous symmetry breaking results in the generation of the massive W^\pm and Z gauge bosons as well as a massive scalar Higgs field.

1.4 A very brief history of the Universe

Our description of the early Universe is based on an extrapolation of known physics back to the Planck epoch, when the Universe was only $t = 10^{-43}$ seconds old, or equivalently up to energies at which the gravitational interaction becomes strong (of the order of the Planck mass, $M_{Pl} = 10^{19}$ GeV). Starting at this epoch we take now a brief tour through the evolution of the Universe:

- $T \sim 10^{16}$ GeV. It is thought that at this scale, some (unknown) grand unified group, G , breaks down into the Standard Model gauge group, $SU(3)_C \otimes SU(2)_L \otimes U(1)_Y$. Little is known about this transition, however.
- $T \sim 10^2$ GeV. The Standard Model gauge symmetry breaks into $SU(3)_C \otimes U(1)_Q$ (see Eq. 13). This transition, called electroweak symmetry breaking, could be the origin of baryogenesis (see *e.g.* Ref. [13]) and possibly of primordial magnetic fields (*e.g.* Ref. [317]).
- $T \sim 10^1 - 10^3$ GeV. Weakly interacting dark matter candidates with GeV-TeV scale masses *freeze-out*, as discussed in next section. This is true in particular for the *neutralino* and the $B^{(1)}$ Kaluza-Klein excitation that we discuss in Chapter 3.
- $T \sim 0.3$ GeV. The QCD phase transition occurs, which drives the confinement of quarks and gluons into hadrons.
- $T \sim 1$ MeV. Neutron freeze-out occurs.
- $T \sim 100$ keV. Nucleosynthesis: protons and neutrons fuse into light elements (D, ^3He , ^4He , Li). The standard Big Bang nucleosynthesis (BBN) provides by far the most stringent constraints to the Big Bang theory, and predictions remarkably agree with observations (see Fig. 1).
- $T \sim 1$ eV. The matter density becomes equal to that of the radiation, allowing for the formation of structure to begin.
- $T \sim 0.4$ eV. Photon decoupling produces the cosmic background radiation (CMB), discussed in Sec. 2.3.

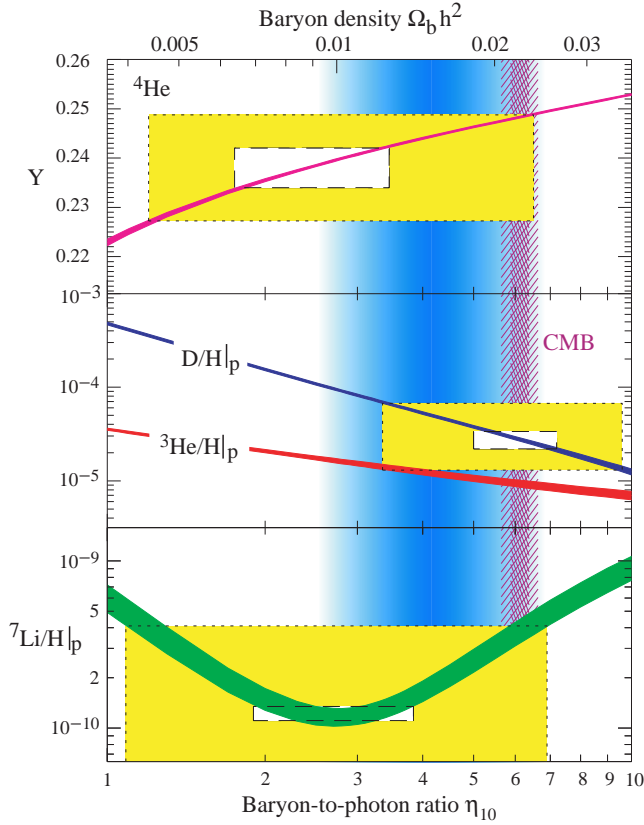


Figure 1: Big Bang nucleosynthesis predictions for the abundances of light elements as a function of the baryon over photon ratio η or $\Omega_b h^2$ [156]. From Ref. [235].

- $T = 2.7K \sim 10^{-4}$ eV. Today.

1.5 Relic Density

We briefly recall here the basics of the calculation of the density of a thermal relic. The discussion is based on Refs. [340, 260, 447] and we refer to them for further comments and details.

A particle species in the early Universe has to interact sufficiently or it will fall out of local thermodynamic equilibrium. Roughly speaking, when its interaction rate drops below the expansion rate of the Universe, the equilibrium can no longer be maintained and the particle is said to be *decoupled*.

1.5.1 The standard calculation

The evolution of the phase space distribution function, $f(\mathbf{p}, \mathbf{x})$, is governed by the Boltzmann equation

$$\mathbf{L}[f] = \mathbf{C}[f], \quad (14)$$

where \mathbf{L} is the Liouville operator, and \mathbf{C} is the collision operator, describing the interactions of the particle species considered.

After some manipulation, the Boltzmann equation can be written as an equation for the particle number density n :

$$\frac{dn}{dt} + 3Hn = -\langle \sigma v \rangle (n^2 - (n^{eq})^2), \quad (15)$$

where σv is the total annihilation cross section multiplied by velocity, brackets denote thermal average, H is Hubble constant, and n^{eq} is the number density at thermal equilibrium. For massive particles, *i.e.* in the non-relativistic limit, and in the Maxwell-Boltzmann approximation, one has

$$n^{eq} = g \left(\frac{mT}{2\pi} \right)^{3/2} e^{-m/T}, \quad (16)$$

where m is the particle mass and T is the temperature. We next introduce the variables

$$Y \equiv \frac{n}{s}, \quad Y^{eq} \equiv \frac{n^{eq}}{s} \quad (17)$$

where s is the entropy density $s = 2\pi^2 g_* T^3/45$ and g_* counts the number of relativistic degrees of freedom. Using the conservation of entropy per co-moving volume ($sa^3 = \text{constant}$), it follows that $\dot{n} + 3Hn = s\dot{Y}$ and Eq. 15 reads

$$s\dot{Y} = -\langle \sigma v \rangle s^2 (Y^2 - (Y^{eq})^2). \quad (18)$$

If we further introduce the variable $x \equiv \frac{m}{T}$, Eq. 18 can be expressed as

$$\frac{dY}{dx} = -\frac{\langle \sigma v \rangle s}{Hx} (Y^2 - (Y^{eq})^2). \quad (19)$$

For heavy states, we can approximate $\langle \sigma v \rangle$ with the non-relativistic expansion in powers of v^2

$$\langle \sigma v \rangle = a + b\langle v^2 \rangle + \mathcal{O}(\langle v^4 \rangle) \approx a + 6b/x, \quad (20)$$

which leads to our final version of Eq. 19 in terms of the variable $\Delta = Y - Y^{eq}$:

$$\Delta' = -Y^{eq'} - f(x)\Delta(2Y^{eq} + \Delta), \quad (21)$$

where prime denotes d/dx and

$$f(x) = \sqrt{\frac{\pi g_*}{45}} m M_{Pl} (a + 6b/x) x^{-2}. \quad (22)$$

Following Ref. [340] we introduce the quantity $x_F \equiv m/T_F$, where T_F is the freeze-out temperature of the relic particle, and we notice that Eq. 21 can be solved analytically in the two extreme regions $x \ll x_F$ and $x \gg x_F$

$$\Delta = -\frac{Y^{eq'}}{2f(x)Y^{eq}} \text{ for } x \ll x_F \quad (23)$$

$$\Delta' = -f(x)\Delta^2 \text{ for } x \gg x_F. \quad (24)$$

These regions correspond to long before freeze-out and long after freeze-out, respectively. Integrating the last equation between x_F and ∞ and using $\Delta_{x_F} \gg \Delta_\infty$, we can derive the value of Δ_∞ and arrive at

$$Y_\infty^{-1} = \sqrt{\frac{\pi g_*}{45}} M_{Pl} m x_F^{-1} (a + 3b/x_F). \quad (25)$$

The present density of a generic relic, X , is simply given by $\rho_X = m_X n_X = m_X s_0 Y_\infty$, where $s_0 = 2889.2 \text{ cm}^{-3}$ is the present entropy density (assuming three Dirac neutrino species). The relic density can finally be expressed in terms of the critical density (see Eq. 6)

$$\Omega_X h^2 \approx \frac{1.07 \times 10^9 \text{ GeV}^{-1}}{M_{Pl}} \frac{x_F}{\sqrt{g_*}} \frac{1}{(a + 3b/x_F)}, \quad (26)$$

where a and b are expressed in GeV^{-2} and g_* is evaluated at the freeze-out temperature. It is conventional to write the relic density in terms of the Hubble parameter, $h = H_0/100 \text{ km s}^{-1} \text{ Mpc}^{-1}$.

To estimate the relic density, one is thus left with the calculation of the annihilation cross sections (in all of the possible channels) and the extraction of the parameters a and b , which depend on the particle mass. The freeze-out temperature x_F can be estimated through the iterative solution of the equation

$$x_F = \ln \left[c(c+2) \sqrt{\frac{45}{8}} \frac{g}{2\pi^3} \frac{m M_{Pl} (a + 6b/x_F)}{g_*^{1/2} x_F^{1/2}} \right], \quad (27)$$

where c is a constant of order one determined by matching the late-time and early-time solutions.

It is sometimes useful to perform an order-of-magnitude estimate using an approximate version of Eq. 26 [319]:

$$\Omega_X h^2 \approx \frac{3 \times 10^{-27} \text{ cm}^3 \text{ s}^{-1}}{\langle \sigma v \rangle}. \quad (28)$$

We note that the approximation introduced in Eq. 20 is not always justified (see *e.g.* Ref. [319]). For example, Ref. [437] suggests a scenario where the presence of a scalar field in the early Universe could significantly affect the value of the relic density. Furthermore, a dramatic change in the relic density can be induced by resonance enhancements or so-called *coannihilations*. We discuss the effects of coannihilations in the next section.

1.5.2 Including coannihilations

Following earlier works (see Ref. [103]), Griest and Seckel [279] noticed that if one or more particles have a mass similar to the relic particle and share a quantum number with it, the standard calculation of relic density fails.

Let us consider N particles X_i ($i = 1, \dots, N$) with masses m_i and internal degrees of freedom (statistical weights) g_i . Also assume that $m_1 \leq m_2 \leq \dots \leq m_{N-1} \leq m_N$, and that the lightest particle is protected against decay thanks to some symmetry (*i.e.* R-parity or KK-parity, for neutralinos or Kaluza-Klein particles, respectively. See section 3). We will also denote the lightest particle by X_1 .

In this case, Eq. 15 becomes

$$\frac{dn}{dt} = -3Hn - \sum_{i,j=1}^N \langle \sigma_{ij} v_{ij} \rangle (n_i n_j - n_i^{\text{eq}} n_j^{\text{eq}}), \quad (29)$$

where n is the number density of the relic particle and $n = \sum_{i=1}^N n_i$, due to the fact that the decay rate of particles, X_i , other than the lightest is much faster than the age of the Universe. Here,

$$\sigma_{ij} = \sum_X \sigma(X_i X_j \rightarrow X_{SM}) \quad (30)$$

is the total annihilation rate for $X_i X_j$ annihilations into a Standard Model particle. Finally,

$$v_{ij} = \frac{\sqrt{(p_i \cdot p_j)^2 - m_i^2 m_j^2}}{E_i E_j} \quad (31)$$

is the relative particle velocity, with p_i and E_i being the four-momentum and energy of particle i .

The thermal average $\langle \sigma_{ij} v_{ij} \rangle$ is defined with equilibrium distributions and is given by

$$\langle \sigma_{ij} v_{ij} \rangle = \frac{\int d^3 \mathbf{p}_i d^3 \mathbf{p}_j f_i f_j \sigma_{ij} v_{ij}}{\int d^3 \mathbf{p}_i d^3 \mathbf{p}_j f_i f_j}, \quad (32)$$

where f_i are distribution functions in the Maxwell-Boltzmann approximation.

The scattering rate of supersymmetric particles off particles in the thermal background is much faster than their annihilation rate. We then obtain

$$\frac{dn}{dt} = -3Hn - \langle \sigma_{\text{eff}} v \rangle (n^2 - n_{\text{eq}}^2), \quad (33)$$

where

$$\langle \sigma_{\text{eff}} v \rangle = \sum_{ij} \langle \sigma_{ij} v_{ij} \rangle \frac{n_i^{\text{eq}} n_j^{\text{eq}}}{n_{\text{eq}}^2}. \quad (34)$$

Edsjo and Gondolo [202] reformulated the thermal average into the more convenient expression

$$\langle \sigma_{\text{eff}} v \rangle = \frac{\int_0^\infty dp_{\text{eff}} p_{\text{eff}}^2 W_{\text{eff}} K_1 \left(\frac{\sqrt{s}}{T} \right)}{m_1^4 T \left[\sum_i \frac{g_i}{g_1} \frac{m_i^2}{m_1^2} K_2 \left(\frac{m_i}{T} \right) \right]^2}, \quad (35)$$

where K_i are the modified Bessel functions of the second kind and of order i . The quantity W_{eff} is defined as

$$W_{\text{eff}} = \sum_{ij} \frac{p_{ij}}{p_{11}} \frac{g_i g_j}{g_1^2} W_{ij} = \sum_{ij} \sqrt{\frac{[s - (m_i - m_j)^2][s - (m_i + m_j)^2]}{s(s - 4m_1^2)}} \frac{g_i g_j}{g_1^2} W_{ij}, \quad (36)$$

where $W_{ij} = 4E_i E_j \sigma_{ij} v_{ij}$ and p_{ij} is the momentum of the particle X_i (or X_j) in the center-of-mass frame of the pair $X_i X_j$, and $s = m_i^2 + m_j^2 + 2E_i E_j - 2|\mathbf{p}_i||\mathbf{p}_j| \cos \theta$, with the usual meaning of the symbols.

The details of coannihilations in the framework of supersymmetric models are well established (see *e.g.* the recent work of Edsjo *et al.* [206]), and numerical codes now exist including coannihilations with all supersymmetric particles, *e.g.* MicrOMEGAs [68] and the new version of DarkSusy [263, 264], publicly released in 2004. The case of coannihilations with a light top squark, such as the one required for the realization of the electroweak baryogenesis mechanism, has been discussed in Ref.[55].

1.6 Links with Physics Beyond the Standard Model

The concepts of dark energy and dark matter do not find an explanation in the framework of the Standard Model of particle physics. Nor are they understood in any quantitative sense in terms of astrophysics. It is interesting that also in the realm of particle physics, evidence is accumulating for the existence of physics *beyond* the Standard Model, based on theoretical and perhaps experimental arguments.

On the experimental side, there is strong evidence for oscillations of atmospheric neutrinos (originating from electromagnetic cascades initiated by cosmic rays in the upper atmosphere) and solar neutrinos. The oscillation mechanism can be explained under the hypothesis that neutrinos *do* have mass, in contrast to the zero mass neutrinos of the Standard Model (see Ref. [369] for a recent review).

On the theoretical side, many issues make the Standard Model unsatisfactory, for example the *hierarchy problem*, *i.e.* the enormous difference between the weak and Planck scales in the presence of the Higgs field (this will be discussed in some detail in Sec. 3.2.1), or the problem of unification addressing the question of whether there exists a unified description of all known forces, possibly including gravity.

The list of problems could be much longer, and it is natural to conjecture that our Standard Model is the low-energy limit of a more fundamental theory.

Two examples of popular extensions of the Standard Model include:

- *Supersymmetry*. As a complete symmetry between fermions and bosons, supersymmetry’s theoretical appeal is very great [498]. So great, in fact, is this appeal, that it appears to many as a necessary ingredient of future extensions of the Standard Model. Many interesting features make it attractive, including its role in understanding the fundamental distinction between bosons and fermions, and the problems of hierarchy and unification discussed above. Last, but not least, it provides an excellent dark matter candidate in terms of its lightest stable particle, the *neutralino*. We will present the basics of supersymmetry and the properties of the neutralino in Sec. 3.2.
- *Extra dimensions*. In the search of a fundamental theory with a unified description of all interactions, physicists developed theories with extra spatial dimensions, following an early idea of Kaluza [322], who extended to four the number of space dimensions to include electromagnetism into a “geometric” theory of gravitation. In theories with *unified* extra dimensions, in which all particles and fields of the Standard Model can propagate in the extra dimensions, the lightest Kaluza-Klein particle, *i.e.* the lightest of all the states corresponding to the first excitations of the particles of the Standard Model, is a viable dark matter candidate, as we discuss in Sec. 3.3.

Despite the fact that neutrinos are thought to be massive, they are essentially ruled out as dark matter candidates (see Sec. 3.1). Consequently, the Standard Model does not provide a viable dark matter candidate. This is further supported by the fact that most of the dark matter is non-baryonic (see section 2.3). Dark matter is therefore a motivation to search for physics beyond the Standard Model (others might say that this is *evidence* for physics beyond the Standard Model).

This is a typical example of the strong interplay between particle physics, theoretical physics, cosmology and astrophysics. From one side, theoretical particle physics stimulates the formulation of new theories predicting new particles that turn out to be excellent dark matter candidates. On the other side, cosmological and astrophysical observations constrain the properties of such particles and consequently the parameters of the new theories.

2 Evidence and Distribution

2.1 The Galactic Scale

The most convincing and direct evidence for dark matter on galactic scales comes from the observations of the *rotation curves* of galaxies, namely the graph of circular velocities of stars and gas as a function of their distance from the galactic center.

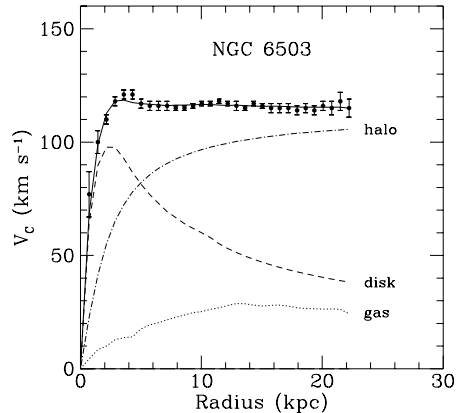


Figure 2: Rotation curve of NGC 6503. The dotted, dashed and dash-dotted lines are the contributions of gas, disk and dark matter, respectively. From Ref. [50].

Rotation curves are usually obtained by combining observations of the 21cm line with optical surface photometry. Observed rotation curves usually exhibit a characteristic *flat* behavior at large distances, *i.e.* out towards, and even far beyond, the edge of the visible disks (see a typical example in Fig. 2).

In Newtonian dynamics the circular velocity is expected to be

$$v(r) = \sqrt{\frac{GM(r)}{r}}, \quad (37)$$

where, as usual, $M(r) \equiv 4\pi \int \rho(r)r^2 dr$, and $\rho(r)$ is the mass density profile, and should be falling $\propto 1/\sqrt{r}$ beyond the optical disc. The fact that $v(r)$ is approximately constant implies the existence of an halo with $M(r) \propto r$ and $\rho \propto 1/r^2$.

Among the most interesting objects, from the point of view of the observation of rotation curves, are the so-called Low Surface Brightness (LSB) galaxies, which are probably everywhere dark matter-dominated, with the observed stellar populations making only a small contribution to rotation curves. Such a property is extremely important because it allows one to avoid the difficulties associated with the deprojection and disentanglement of the dark and visible contributions to the rotation curves.

Although there is a consensus about the shape of dark matter halos at large distances, it is unclear whether galaxies present cuspy or shallow profiles in their innermost regions, which is an issue of crucial importance for the effects we will be discussing in the following chapters.

Using high-resolution data of 13 LSB galaxies, de Blok *et al.* [179] recently showed, that the distribution of inner slopes, *i.e.* the power-law indices of the density profile in the innermost part of the galaxies, suggests the presence of

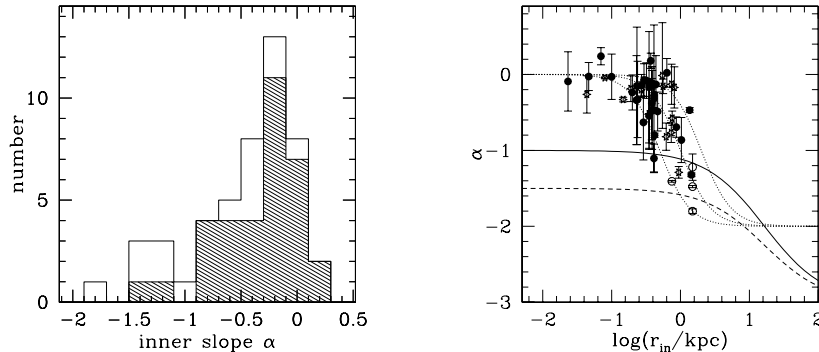


Figure 3: Left panel: The distribution of inner slopes, α , of dark matter density profiles in LSB galaxies. The hatched (blank) histogram represents well-resolved (unresolved) galaxies. Right panel: The value of α as a function of the radius of the innermost point. From Ref. [179].

shallow, or even flat, cores (see Fig. 3). Furthermore, the highest values of the power-law index are obtained in correspondence to galaxies with the poorest resolution, as can be seen from the right panel of the same figure.

Following Salucci and Borriello [439], rotation curves of both low and high surface luminosity galaxies appear to suggest a universal density profile, which can be expressed as the sum of an exponential thin stellar disk, and a spherical dark matter halo with a flat core of radius r_0 and density $\rho_0 = 4.5 \times 10^{-2}(r_0/\text{kpc})^{-2/3} M_\odot \text{pc}^{-3}$ (here, M_\odot denotes a solar mass, 2×10^{30} kg). In a similar way the analysis of Reed *et al.* [425] leads to the conclusion that simulated halos have significantly steeper density profiles than are inferred from observations.

Nevertheless, claims have been made in the literature about the possibility of reconciling these results with the steep profiles predicted by numerical simulations (see section 2.4 for a discussion on the state of art of N-body simulations and for further discussions, see Refs. [179, 483, 427]). In particular, Hayashi *et al.* [291] have claimed consistency between most observations and their simulated profiles and have argued that the remaining discrepancies could be explained by taking into account the difference between the circular velocity and gas rotation speed, likely to arise in gaseous disks embedded within realistic, triaxial cold dark matter halos.

Another area of contention is that of the dark matter content in the inner halos of massive disk galaxies. It has been argued that barred galaxies cannot contain substantial amounts of dark matter out to the outermost extent of the observed bars, otherwise the rapidly rotating bars would have slowed down due to dynamical friction on the dark matter [177, 178]. One counterargument is the contention that bars may be dynamically young systems that formed by

secular evolution of unstable cold disks and hence poor dynamical probes [158]. Another is that the slowing down of bars, perhaps in an earlier phase of the forming galaxy, actually heated the dark matter and generated a core.

Despite the uncertainties of the slope in the innermost regions of galaxies, rotation curves of disk galaxies provide strong evidence for the existence of a spherical dark matter halo. The total amount of dark matter present is difficult to quantify, however, as we do not know to what distances halos extend. Additional evidence for dark matter at galactic scales comes from mass modelling of the detailed rotation curves, including spiral arm features. Submaximal disks are often, although not always, required [455].

Some elliptical galaxies show evidence for dark matter via strong gravitational lensing [341]. X-ray evidence reveals the presence of extended atmospheres of hot gas that fill the dark halos of isolated ellipticals and whose hydrostatic support provides evidence for dark matter. In at least one case, an elliptical contains a cold gas disk whose HI rotation curve is flat out to about 5 half light radii. In contrast, however, planetary nebula studies to a similar distance for other ellipticals can be explained only with a constant mass-to-light ratio. There may be some dark matter in these cases, but its relative dominance does not appear to increase with increasing galactocentric distance. Rather, it is associated with the stellar distribution.

Other arguments for dark matter, both on subgalactic and inter-galactic scales, also comes from a great variety of data. Without attempting to be complete, we cite among them:

- *Weak modulation of strong lensing* around individual massive elliptical galaxies. This provides evidence for substructure on scales of $\sim 10^6 M_\odot$ [382, 388].
- The so-called *Oort discrepancy* in the disk of the Milky Way (see *e.g.* Ref. [51]). The argument follows an early suggestion of Oort, inferring the existence of unobserved matter from the inconsistency between the amount of stars, or other tracers in the solar neighborhood, and the gravitational potential implied by their distribution.
- *Weak gravitational lensing* of distant galaxies by foreground structure (see, *e.g.* Ref. [299]).
- The *velocity dispersions of dwarf spheroidal galaxies* which imply mass-to-light ratios larger than those observed in our “local” neighborhood. While the profiles of individual dwarfs show scatter, there is no doubt about the overall dark matter content (see Refs. [486, 373]).
- The *velocity dispersions of spiral galaxy satellites* which suggest the existence of dark halos around spiral galaxies, similar to our own, extending at galactocentric radii $\gtrsim 200$ kpc, *i.e.* well behind the optical disc. This applies in particular to the Milky Way, where both dwarf galaxy satellites and globular clusters probe the outer rotation curve (see Refs. [507, 46]).

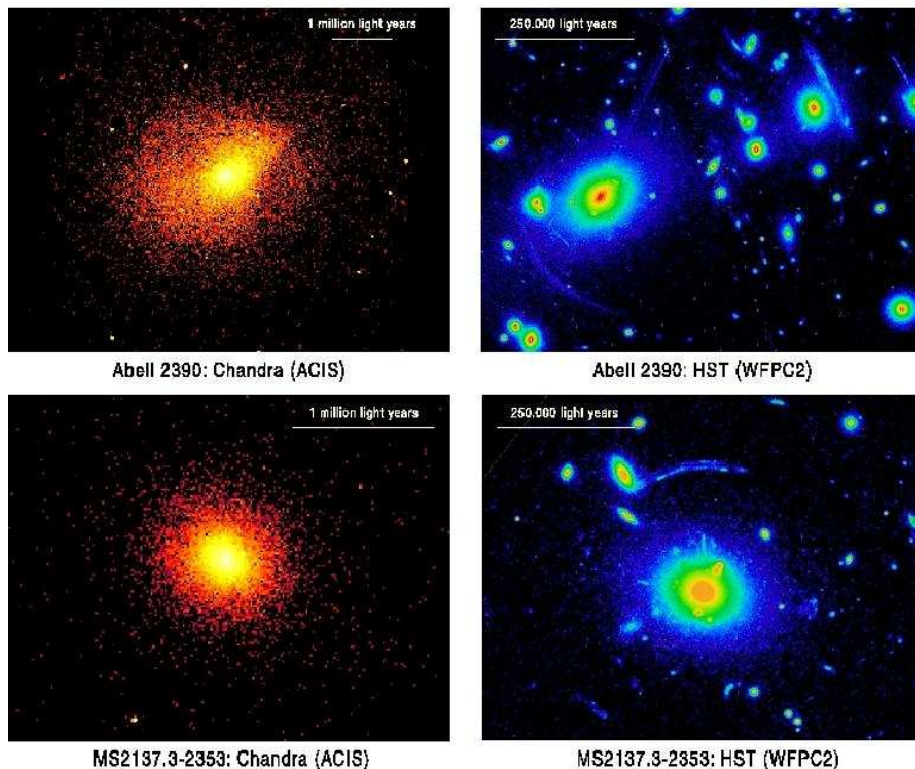


Figure 4: Chandra X-ray (left) and Hubble Space Telescope Wide Field Planetary Camera 2 optical (right) images of Abell 2390 ($z = 0.230$) and MS2137.3-2353 ($z = 0.313$). Note the clear gravitational arcs in the Hubble images. From Ref. [225].

2.2 The Scale of Galaxy Clusters

A cluster of galaxies gave the first hints of dark matter (in the modern sense). In 1933, F.Zwicky [510] inferred, from measurements of the velocity dispersion of galaxies in the Coma cluster, a mass-to-light ratio of around 400 solar masses per solar luminosity, thus exceeding the ratio in the solar neighborhood by two orders of magnitude. Today, most dynamical estimates [52, 331, 139] are consistent with a value $\Omega_M \sim 0.2-0.3$ on cluster scales. A convenient calibration is $\Omega_M = (M/L)/1000$.

The mass of a cluster can be determined via several methods, including application of the virial theorem to the observed distribution of radial velocities, by weak gravitational lensing, and by studying the profile of X-ray emission that traces the distribution of hot emitting gas in rich clusters.

Consider the equation of hydrostatic equilibrium for a system with spherical symmetry

$$\frac{1}{\rho} \frac{dP}{dr} = -a(r) , \quad (38)$$

where P , ρ , and a are, respectively, the pressure, density, and gravitational acceleration of the gas, at radius r . For an ideal gas, this can be rewritten in terms of the temperature, T , and the average molecular weight, $\mu \approx 0.6$,

$$\frac{d \log \rho}{d \log r} + \frac{d \log T}{d \log r} = -\frac{r}{T} \left(\frac{\mu m_p}{k} \right) a(r), \quad (39)$$

where m_p is the proton mass. The temperature of clusters is roughly constant outside of their cores and the density profile of the observed gas at large radii roughly follows a power-law with an index between -2 and -1.5 . We then find that the temperature should obey the relation

$$kT \approx (1.3 - 1.8) \text{keV} \left(\frac{M_r}{10^{14} M_\odot} \right) \left(\frac{1 \text{Mpc}}{r} \right) \quad (40)$$

for the baryonic mass of a typical cluster, where M_r is the mass enclosed within the radius r . The disparity between the temperature obtained using Eq. 40 and the corresponding observed temperature, $T \approx 10 \text{keV}$, when M_r is identified with the baryonic mass, suggests the existence of a substantial amount of dark matter in clusters.

These conclusions can be checked against estimates from gravitational lensing data (see Fig. 4). Following Einstein's theory of general relativity, light propagates along geodesics which deviate from straight lines when passing near intense gravitational fields. The distortion of the images of background objects due to the gravitational mass of a cluster can be used to infer the shape of the potential well and thus the mass of the cluster (see *e.g.* Ref. [477] for a spectacular demonstration of gravitational lensing in clusters).

The fraction of baryons inside a cluster, crucial to disentangle the contributions of ordinary (visible) and dark matter, can also be inferred through the so-called Sunyaev-Zel'dovich effect by which the cosmic microwave background (see section 2.3) gets spectrally distorted through Compton scattering on hot electrons.

Despite general agreement between dark matter density profiles at large radii and numerical simulations (see section 2.4), it is unclear whether there is agreement with the predicted profiles in the cores of clusters. Gravitational lensing measurements appear to be in conflict with cuspy profiles, excluding at the 99% confidence level cusps with power-law indices of about -1 (see *e.g.* Ref. [440]).

This argument is strengthened by use of radial arcs which probe the mass gradient, but is weakened if the cluster is not spherically symmetric. Indeed an asymmetry of a few percent allows the cluster profiles to be consistent with NFW. Moreover, recent *Chandra* observations of X-ray emission from Abell 2029 suggest a full compatibility of dark matter distributions with cuspy profiles (see Ref. [358]). For a critique of gravitational lensing constraints on dark matter halo profiles, see Ref. [171].

2.3 Cosmological Scales

We have seen in the previous sections that, on distance scales of the size of galaxies and clusters of galaxies, evidence of dark matter appears to be compelling. Despite this, the observations discussed do not allow us to determine the *total* amount of dark matter in the Universe. We discuss in this section how such information can be extracted from the analysis of the Cosmic Microwave Background (CMB).

Excellent introductions to CMB theory exist in the literature [312, 313]. Here, we limit ourselves to a brief review of the implications of recent CMB data on the determination of cosmological parameters. In particular, we discuss the stringent constraints on the abundances of baryons and matter in the Universe placed by the Wilkinson Microwave Anisotropy Probe (WMAP) data.

The existence of background radiation originating from the propagation of photons in the early Universe (once they decoupled from matter) was predicted by George Gamow and his collaborators in 1948 and inadvertently discovered by Arno Penzias and Robert Wilson in 1965. After many decades of experimental effort, the CMB is known to be isotropic at the 10^{-5} level and to follow with extraordinary precision the spectrum of a black body corresponding to a temperature $T = 2.726$ K.

Today, the analysis of CMB anisotropies enables accurate testing of cosmological models and puts stringent constraints on cosmological parameters.

The observed temperature anisotropies in the sky are usually expanded as

$$\frac{\delta T}{T}(\theta, \phi) = \sum_{\ell=2}^{+\infty} \sum_{m=-\ell}^{+\ell} a_{\ell m} Y_{\ell m}(\theta, \phi) \quad (41)$$

where $Y_{\ell m}(\theta, \phi)$ are spherical harmonics. The variance C_ℓ of $a_{\ell m}$ is given by

$$C_\ell \equiv \langle |a_{\ell m}|^2 \rangle \equiv \frac{1}{2\ell+1} \sum_{m=-\ell}^{\ell} |a_{\ell m}|^2. \quad (42)$$

If the temperature fluctuations are assumed to be Gaussian, as appears to be the case, all of the information contained in CMB maps can be compressed into the power spectrum, essentially giving the behavior of C_ℓ as a function of ℓ . Usually plotted is $\ell(\ell+1)C_\ell/2\pi$ (see Fig. 6).

The methodology, for extracting information from CMB anisotropy maps, is simple, at least in principle. Starting from a cosmological model with a fixed number of parameters (usually 6 or 7), the best-fit parameters are determined from the peak of the N-dimensional likelihood surface.

From the analysis of the WMAP data alone, the following values are found for the abundance of baryons and matter in the Universe

$$\Omega_b h^2 = 0.024 \pm 0.001 \quad \Omega_M h^2 = 0.14 \pm 0.02. \quad (43)$$

Taking into account data from CMB experiments studying smaller scales (with respect to WMAP), such as ACBAR [348] and CBI [411], and astronomical

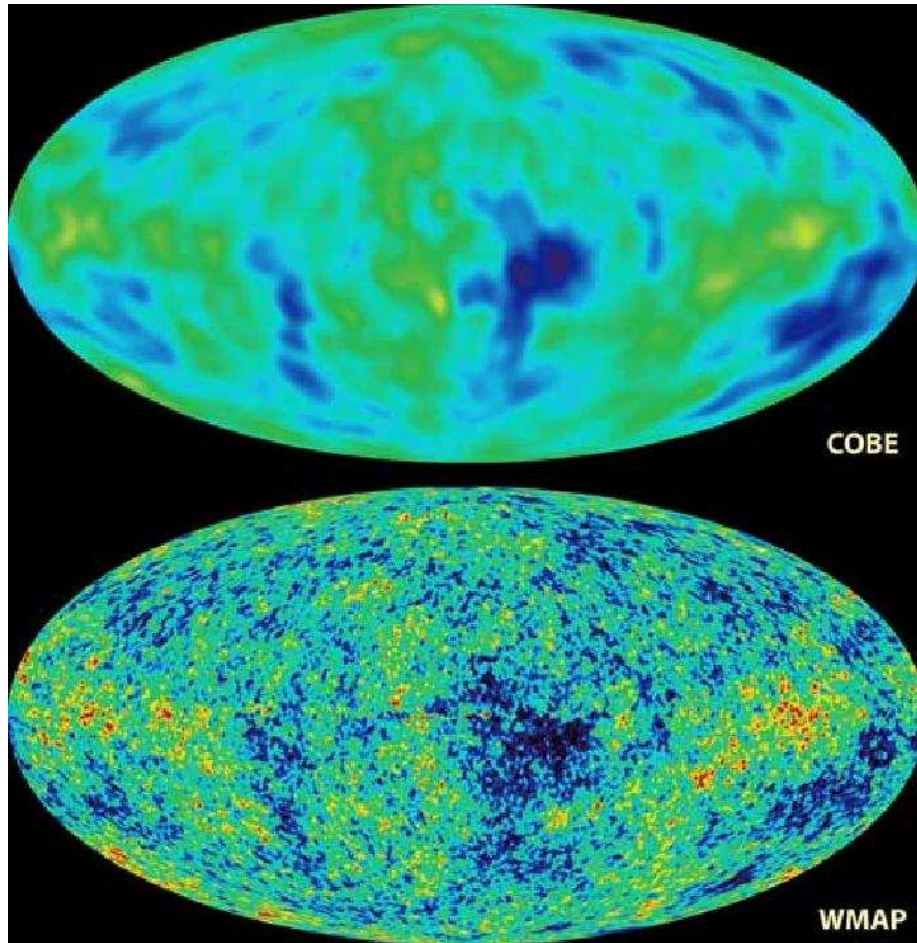


Figure 5: CMB Temperature fluctuations: A comparison between COBE and WMAP. Image from <http://map.gsfc.nasa.gov/>.

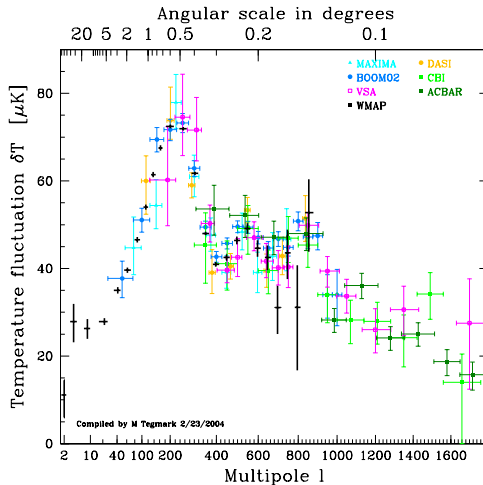


Figure 6: The observed power spectrum of CMB anisotropies. From Ref. [470].

measurements of the power spectrum from large scale structure (2dFGRS, see Ref. [414]) and the Lyman α forest (see *e.g.* Ref.[167]), the constraints become [457]

$$\Omega_b h^2 = 0.0224 \pm 0.0009 \quad \text{and} \quad \Omega_M h^2 = 0.135^{+0.008}_{-0.009}. \quad (44)$$

The value of $\Omega_b h^2$ thus obtained is consistent with predictions from Big Bang nucleosynthesis (*e.g.* [403])

$$0.018 < \Omega_b h^2 < 0.023. \quad (45)$$

Besides those provided by CMB studies, the most reliable cosmological measurements are probably those obtained by Sloan Digital Sky Survey (SDSS) team, which has recently measured the three-dimensional power spectrum, $P(k)$, using over 200,000 galaxies. An estimate of the cosmological parameters combining the SDSS and WMAP measurements can be found in Ref. [469].

2.4 N-Body Simulations

Our understanding of large scale structure is still far from a satisfactory level. The description of the evolution of structures from seed inhomogeneities, *i.e.* primordial density fluctuations, is complicated by the action of many physical processes like gas dynamics, radiative cooling, photoionization, recombination and radiative transfer. Furthermore, any theoretical prediction has to be compared with the observed luminous Universe, *i.e.* with regions where dissipative effects are of crucial importance.

	α	β	γ	R (kpc)
Kra	2.0	3.0	0.4	10.0
NFW	1.0	3.0	1.0	20.0
Moore	1.5	3.0	1.5	28.0
Iso	2.0	2.0	0	3.5

Table 2: Parameters of some widely used profile models for the dark matter density in galaxies (See Eq. 46). Values of R can vary from system to system.

The most widely adopted approach to the problem of large-scale structure formation involves the use of N-body simulations. The first simulation of interacting galaxies was performed by means of an analog optical computer (Holmberg 1941 [301]) using the flux from 37 light-bulbs, with photo-cells and galvanometers to measure and display the inverse square law of gravitational force. Modern, high resolution simulations make full use of the tremendous increase in computational power over the last few decades.

The evolution of structure is often approximated with non-linear gravitational clustering from specified initial conditions of dark matter particles and can be refined by introducing the effects of gas dynamics, chemistry, radiative transfer and other astrophysical processes. The reliability of an N-body simulation is measured by its mass and length resolution. The mass resolution is specified by the mass of the smallest (“elementary”) particle considered, being the scale below which fluctuations become negligible. Length resolution is limited by the so-called softening scale, introduced to avoid infinities in the gravitational force when elementary particles collide.

Recent N-body simulations suggest the existence of a *universal* dark matter profile, with the same shape for all masses, epochs and input power spectra [393]. The usual parametrisation for a dark matter halo density is

$$\rho(r) = \frac{\rho_0}{(r/R)^\gamma [1 + (r/R)^\alpha]^{(\beta-\gamma)/\alpha}} . \quad (46)$$

Various groups have ended up with different results for the spectral shape in the innermost regions of galaxies and galaxy clusters. In particular, several groups have failed to reproduce the initial results of Navarro, Frenk and White [393], which find a value for the power-law index in the innermost part of galactic halos of $\gamma = 1$. In table 2, we give the values of the parameters (α, β, γ) for some of the most widely used profile models, namely the Kravtsov et al. (Kra, [346]), Navarro, Frenk and White (NFW, [393]), Moore et al. (Moore, [384]) and modified isothermal (Iso, e.g. Ref. [80]) profiles.

Although it is definitely clear that the slope of the density profile should increase as one moves from the center of a galaxy to the outer regions, the precise value of the power-law index in the innermost galactic regions is still under

debate. Attention should be paid when comparing the results of different groups, as they are often based on a single simulation, sometimes at very different length scales.

Taylor and Navarro [468, 394] studied the behaviour of the phase-space density (defined as the ratio of spatial density to velocity dispersion cubed, ρ/σ^3) as a function of the radius, finding excellent agreement with a power-law extending over several decades in radius, and also with the self-similar solution derived by Bertschinger [96] for secondary infall onto a spherical perturbation. The final result of their analysis is a “critical” profile, following a NFW profile in the outer regions, but with a central slope converging to the value $\gamma_{TN} = 0.75$, instead of $\gamma_{NFW} = 1$.

The most recent numerical simulations (see Navarro *et al.* [395], Reed *et al.* [425] and Fukushige *et al.* [242]) appear to agree on a new paradigm, suggesting that density profiles do not converge to any specific power-law at small radii. The logarithmic slope of the profile continuously flattens when moving toward the galactic center. The slope at the innermost resolved radius varies between 1 and 1.5, *i.e.* between the predictions of the NFW and Moore profiles. It is important to keep in mind that predictions made adopting such profiles probably overestimate the density near the Galactic center and should be used cautiously.

Recently, Prada *et al.* [421] have suggested that the effects of adiabatic compression on the dark matter profile near the Galactic center could play an important role, possibly enhancing the dark matter density by an order of magnitude in the inner parsecs of the Milky Way.

The extrapolations of cuspy profiles at small radii have appeared in the past (and still appear to some) to be in disagreement with the flat cores observed in astrophysical systems, such as low surface brightness galaxies mentioned earlier. Such discrepancies prompted proposals to modify the properties of dark matter particles, to make them self-interacting, warm *etc.* Most of such proposals appear to create more problems than they solve and will not be discussed here.

Today, the situation appear less problematic, in particular after the analysis of Hayashi *et al.* [291]. Our approach, given the uncertainties regarding observed and simulated halo profiles, will be to consider the central slope of the galactic density profile as a free parameter and discuss the prospects of indirect detection of dark matter for the different models proposed in literature.

2.5 The Case of the Milky Way

Since the Milky Way is prototypical of the galaxies that contribute most to the cosmic luminosity density, it is natural to ask how the results discussed in the previous section compare with the wide range of observational data available for our galaxy.

One way to probe the nature of matter in our neighborhood is to study microlensing events in the direction of the galactic center. In fact, such events can only be due to compact objects, acting as lenses of background sources, and

it is commonly believed that dark matter is simply too weakly interacting to clump on small scales².

Binney and Evans (BE) [104] recently showed that the number of observed microlensing events implies an amount of baryonic matter within the Solar circle greater than about $3.9 \times 10^{10} M_{\odot}$. Coupling this result with estimates of the local dark matter density, they exclude cuspy profiles with power-law index $\gamma \gtrsim 0.3$.

Nevertheless, Klypin, Zhao and Somerville (KZS) [334] find a good agreement between NFW profiles ($\gamma = 1$) and observational data for our galaxy and M31. The main difference between these analyses is the value of the microlensing optical depth towards the Galactic center used. Observations of this quantity disagree by a factor of ~ 3 and a low value within this range permits the presence of a dark matter cusp. Another difference arises from the modeling of the galaxy: KZS claim to have taken into account dynamical effects neglected by BE and to have a “more realistic” description of the galactic bar.

An important addition is adiabatic compression of the dark matter by baryonic dissipation. This results in a dark matter density that is enhanced in the core by an order of magnitude. This result can be reconciled with modelling of the rotation curve if the lower value of the microlensing optical depth found by the EROS collaboration is used rather than that of the MACHO collaboration. In the latter case, little dark matter is allowed in the central few kpc. The microlensing result constrains the stellar contribution to the inner rotation curve, and hence to the total allowed density.

2.5.1 The Galactic center

The dark matter profile in the inner region of the Milky Way is even more uncertain. Observations of the velocity dispersion of high proper motion stars suggest the existence of a Super Massive Black Hole (SMBH) lying at the center of our galaxy, with a mass, $M_{\text{SMBH}} \approx 2.6 \times 10^6 M_{\odot}$ [252]³.

Recently, near-infrared high-resolution imaging and spectroscopic observations of individual stars, as close as a few light days from the galactic center, were carried out at Keck [251] and ESO/VLT telescopes (see Ref. [445], for an excellent and updated discussion of the stellar dynamics in the galactic center, based on the most recent observations at ESO/VLT). The analysis of the orbital parameters of such stars suggest that the mass of the SMBH could possibly be a factor of two larger with respect to the above cited estimate from the velocity dispersion. In Fig. 7 we show a plot of the enclosed mass as a function of the galactocentric distance, along with a best-fit curve, which corresponds to a dark object with a mass of $2.87 \pm 0.15 \times 10^6 M_{\odot}$.

²It was noticed by Berezinsky *et al.* [76] that if microlensing was due to neutralino stars (see the definition of “neutralino” in the chapter on dark matter candidates), *i.e.* self-gravitating systems of dark matter particles, then the gamma-ray radiation originated by annihilations in these object would exceed the observed emission.

³The existence of a SMBH at the center of the galaxy is not surprising. There is, in fact, mounting evidence for the existence of 10^6 – $10^8 M_{\odot}$ black holes in the centers of most galaxies with mass amounting to approximately 0.1% of the stellar spheroid (see, *e.g.* Ref. [342]).

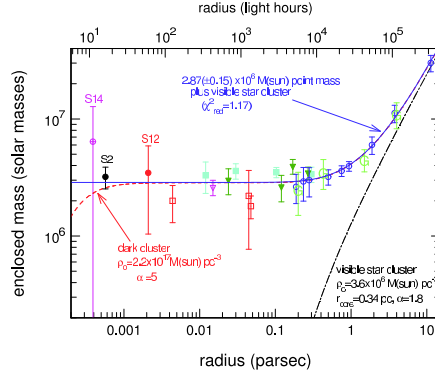


Figure 7: The mass distribution in the galactic center, as derived by different observations, down to a 10^{-4} pc scale. Lines represent fits under different assumptions, as specified by the text in the figure. In particular, the solid line is the overall best fit model: a $2.87 \pm 0.15 \times 10^6 M_\odot$ central object, plus a stellar cluster distributed with a power-law of index 1.8. For more details see Ref. [445].

It has long been argued (see *e.g.* Peebles, Ref. [412]) that if a SMBH exists at the galactic center, the process of adiabatic accretion of dark matter on it would produce a “spike” in the dark matter density profile. Gondolo and Silk [261] have recently applied such a process to study the enhancement of the the annihilation signal from the galactic center.

If we consider an initial power-law type profile of index γ , similar to those discussed in Sec. 2.4, the corresponding dark matter profile, $\rho'(r)$, after this accretion process is, following Ref. [261],

$$\rho' = \left[\alpha_\gamma \left(\frac{M}{\rho_D D^3} \right)^{3-\gamma} \right]^{\gamma_{sp}-\gamma} \rho_D g(r) \left(\frac{D}{r} \right)^{\gamma_{sp}}, \quad (47)$$

where $\gamma_{sp} = (9 - 2\gamma)/(4 - \gamma)$, $D \simeq 8$ kpc is the solar distance from the Galactic center and $\rho_D \simeq 0.3 \text{ GeV}/c^2/\text{cm}^3$ is the density in the solar neighborhood. The factors α_γ and $g_\gamma(r)$ cannot be determined analytically (for approximate expressions and numerical values see Ref. [261]). Eq. 47 is only valid in a central region of size $R_{sp} = \alpha_\gamma D (M/\rho_D D^3)^{1/(3-\gamma)}$, where the central black hole dominates the gravitational potential.

It is easy to understand the basics of adiabatic accretion under the assumptions of circular orbits. Assuming an initial power-law distribution, $\rho \propto r^{-\gamma}$, and a final distribution, $\rho \propto r^{-\gamma_{sp}}$, the equations of conservation of mass and angular momentum can be expressed, respectively, as

$$\rho_i r_i^2 dr_i = \rho_f r_f^2 dr_f \quad (48)$$

and

$$r_i M_i(r) = r_f M_f(r) \approx r_f M_{BH}, \quad (49)$$

which imply, respectively,

$$r_i \propto r_f^{(3-\gamma_{sp})/(3-\gamma)} \quad (50)$$

and

$$r_i \propto r_f^{1/(4-\gamma)}. \quad (51)$$

The final distribution will thus have a power-law index

$$\gamma_{sp} = \frac{9-2\gamma}{4-\gamma}, \quad (52)$$

which assumes values in the range of 2.25 to 2.5 as γ varies in the interval of 0 to 2.

If we take into account the annihilation of dark matter particles, the density cannot grow to arbitrarily high values, the maximal density being fixed by the value

$$\rho_{core} = \frac{m}{\sigma v t_{BH}}, \quad (53)$$

where $t_{BH} \approx 10^{10}$ yr is the age of the central black hole. The final profile, resulting from the adiabatic accretion of annihilating dark matter on a massive black hole is

$$\rho_{dm}(r) = \frac{\rho'(r)\rho_{core}}{\rho'(r) + \rho_{core}} \quad (54)$$

following a power-law for large values of r , and with a flat core of density, ρ_{core} , and dimension,

$$R_{core} = R_{sp} \left(\frac{\rho(R_{sp})}{\rho_{core}} \right)^{(1/\gamma_{sp})}. \quad (55)$$

We will use these equations when discussing the prospects for indirect detection of dark matter in the presence of a spike. We recall, nevertheless, that they have been derived under the simplifying assumption that the SMBH formed at a position coinciding exactly with the center of the galactic potential well, and neglecting all dynamical effects.

It was shown by Ullio, Zhao and Kamionkowski [481] that if the black hole forms from a low-mass seed, then its spiral-in to reach the exact center of the galaxy could take a length of time longer than the age of the galaxy. If, conversely, the seed black hole is massive, the back-reaction to the spiral-in of the black hole leads to the formation of a weak-density cusp, with $\rho \propto r^{-0.5}$. Fig. 8 shows the modification of an NFW dark matter profile due to the off-center formation of the seed black hole. The solution found by Gondolo and Silk would be indistinguishable from the case of an initial light seed of roughly $10^{-2} M_{SMBH}$, starting its growth very near to the galactic center.

The spike could also be destroyed by hierarchical mergers, as discussed by Merritt *et al.* [381], but such mergers are unlikely to have occurred in the recent history of the Milky Way. What can be stated with considerable confidence is

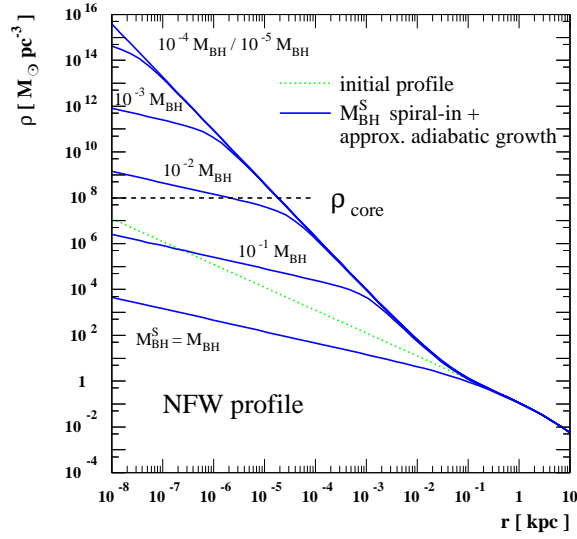


Figure 8: Modification of an NFW profile due to the off-center formation of a black-hole seed of mass M_{BH}^{S} , its spiral-in the center of the dark matter system and its adiabatic growth to the present-day mass, M_{SMBH} (called M_{SM} in the figure). From Ref. [481].

that the Milky Way galaxy underwent one significant merger about 12 billion years ago. This resulted in the formation of the bulge, and therefore presumably of the SMBH, and of the thick disk. The chemical evidence for a unique merger origin in the case of our Milky Way's thick disk is compelling [254, 500], as the continuity between thin disk, thick disk, and bulge would have been destroyed had anything significant happened more recently in the way of a merger (see also the discussion of Bertone, Sigl and Silk [92]).

Furthermore, the scattering of dark matter particles by stars in the dense stellar cusp observed around the SMBH could substantially lower the dark matter density near the Galactic center over 10^{10} years, due both to kinetic heating, and to capture of dark matter particles by the SMBH [380].

The existence of such spikes would produce a dramatic enhancement of the annihilation radiation from the galactic center. The implications for indirect detection of dark matter particles have been discussed in Refs. [261, 262, 91, 92].

2.5.2 The local density

Very important to the prospects for direct and indirect detection is the density of dark matter in the region of our solar system. Although this quantity is considerably more well known than the density near the galactic center, there are still uncertainties associated with the local density, which we will discuss here.

The local density of dark matter is determined by observing the rotation curves of the Milky Way. This is somewhat difficult to do from our location within the galaxy. Furthermore, rotation curves measure the total mass within an orbit, thus the density distributions of the galactic bulge and disk are needed to accurately calculate the dark matter profile.

In addition to the local density, the velocity distribution of dark matter in the local region is needed to accurately calculate direct and indirect detection rates. This is also best inferred from observed rotation curves.

Different groups have come to somewhat different conclusions regarding the local density and velocity distribution of dark matter. For example, Bahcall *et al.* finds a best-fit value of $\rho_0 = 0.34 \text{ GeV/cm}^3$ [53], Caldwell and Ostriker find $\rho_0 = 0.23 \text{ GeV/cm}^3$ [136] while Turner calculates $\rho_0 = 0.3 - 0.6 \text{ GeV/cm}^3$ [473]. In figure 9 we show the range of local dark matter densities found to be acceptable by Bergstrom, Ullio and Buckley [80] for various choices of halo profile and galactocentric distance. They find local dark matter densities acceptable in the range of about $0.2 - 0.8 \text{ GeV/cm}^3$.

The velocity distribution of dark matter is typically described only by its average velocity, $\bar{v} = \langle v^2 \rangle^{1/2} \cong 270 \text{ km/s}$.

For more discussion on the local dark matter distribution, see section 2.4 of Ref. [319].

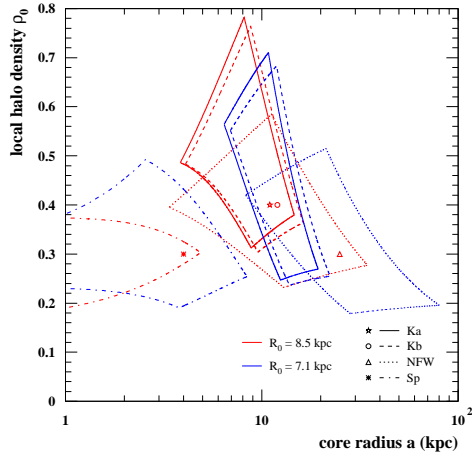


Figure 9: The range of local dark matter densities acceptable with observations of rotation curves for a variety of halo profiles and galactocentric distances. Densities in the range of $0.2 - 0.8 \text{ GeV/cm}^3$ are shown to be acceptable. From Ref. [80].

3 Candidates

As we have seen in the previous section, the evidence for non-baryonic dark matter is compelling at all observed astrophysical scales. It is therefore natural to ask *what is the dark matter made of?* In this section, we present some of the candidates discussed in the literature, and focus our attention especially on two popular candidates: the supersymmetric *neutralino*, probably the most widely studied candidate, and the $B^{(1)}$ particle, the first Kaluza–Klein excitation of the B boson in theories with universal extra dimensions. We will also briefly discuss “superheavy” candidates, also referred to as *wimpzillas*.

3.1 The Non-Baryonic Candidate Zoo

There is no shortage of candidates for non-baryonic dark matter. In this section we briefly describe some of these candidates.

- *Standard Model neutrinos*

Neutrinos have been considered, until recently, excellent dark matter candidates for their “undisputed virtue of being known to exist” [86]. However, a simple calculation shows that, if we call m_i the mass of the i -th neutrino, their total relic density is predicted to be

$$\Omega_\nu h^2 = \sum_{i=1}^3 \frac{m_i}{93 \text{ eV}} . \quad (56)$$

The best laboratory constraint on neutrino masses comes from tritium β -decay experiments at Troitsk and Mainz [496], pointing to the following upper limit on the neutrino mass

$$m_\nu < 2.05 \text{ eV (95\% C.L.)}, \quad (57)$$

while next-generation experiments are expected to reach a sensitivity of approximately 0.2 eV (see Ref. [496] and references therein). The above upper limit applies to all three mass eigenvalues [73], since the mass differences among them must be very small to explain solar ($\Delta m^2 \approx 7 \cdot 10^{-5} \text{ eV}^2$) and atmospheric ($\Delta m^2 \approx 3 \cdot 10^{-3} \text{ eV}^2$) neutrino anomalies (see *e.g.* Ref. [265]). This implies an upper bound on the total neutrino relic density of

$$\Omega_\nu h^2 \lesssim 0.07, \quad (58)$$

which means that neutrinos are simply not abundant enough to be the dominant component of dark matter. A more stringent constraint on the neutrino relic density comes from the analysis of CMB anisotropies, combined with large-scale structure data, suggesting $\Omega_\nu h^2 < 0.0067$ (95% confidence limit). For three degenerate neutrino species this implies $m_\nu < 0.23 \text{ eV}$. If extra neutrino interactions are allowed, *e.g.*, the coupling of neutrinos to a light boson, the neutrino mass limits arising from large scale structure can be evaded [74].

Being relativistic collisionless particles, neutrinos erase (moving from high to low density regions) fluctuations below a scale of $\sim 40 \text{ Mpc}$ ($m_\nu/30 \text{ eV}$), called the *free-streaming* length [122]. This would imply a *top-down* formation history of structure in the Universe, where big structures form first. The fact that our galaxy appears to be older than the Local Group [413], and the discrepancy between the predicted late formation of galaxies, at redshift $z \lesssim 1$, against observations of galaxies around $z > 4$ [123], is a further argument against neutrinos as a viable dark matter candidate.

- *Sterile neutrinos*

These hypothetical particles are similar to Standard Model neutrinos, but without Standard Model weak interactions, apart from mixing. They were proposed as dark matter candidates in 1993 by Dodelson and Widrow [191]. Stringent cosmological and astrophysical constraints on sterile neutrinos come from the analysis of their cosmological abundance and the study of their decay products (see Ref. [1] and references therein).

Light neutrinos, with masses below a few keV, would be ruled out as dark matter candidates. In fact, if the WMAP result for the reionization optical depth is correct, then dark matter structures were in place to form massive stars prior to redshift $z > 20$, which is simply not possible if the dark matter particle mass is smaller than $\sim 10 \text{ keV}$ [504]. An alternative explanation for the WMAP optical depth is reionization by decaying particles, such as sterile neutrinos (see Ref. [287] and references

therein). Sterile neutrinos could also be cold dark matter, if there is a very small lepton asymmetry, in which case they are produced resonantly with a non-thermal spectrum [448].

- *Axions*

Introduced in an attempt to solve the problem of CP violation in particle physics, axions have also often been discussed as a dark matter candidate. Laboratory searches, stellar cooling and the dynamics of supernova 1987A constrain axions to be very light ($\lesssim 0.01$ eV). Furthermore, they are expected to be extremely weakly interacting with ordinary particles, which implies that they were not in thermal equilibrium in the early universe.

The calculation of the axion relic density is uncertain, and depends on the assumptions made regarding the production mechanism. Nevertheless, it is possible to find an acceptable range where axions satisfy all present-day constraints and represent a possible dark matter candidate (see *e.g.* Ref. [428]).

- *Supersymmetric candidates*

- *Neutralinos*

Neutralinos in models of R-parity conserving supersymmetry are by far the most widely studied dark matter candidates. We devote Sec. 3.2 to their presentation.

- *Sneutrinos*

The superpartners of the Standard Model neutrinos in supersymmetric models have long been considered as dark matter candidates. It has been shown that sneutrinos will have a cosmologically interesting relic density if their mass is in the range of 550 to 2300 GeV. However, the scattering cross section of a sneutrino with nucleons is easily calculated and is much larger than the limits found by direct dark matter detection experiments [226].

- *Gravitinos*

Gravitinos are the superpartners of the graviton in supersymmetric models. In some supersymmetric scenarios, gauge mediated supersymmetry for example, gravitinos can be the lightest supersymmetric particle and be stable. Gravitinos are thus very strongly theoretically motivated. With only gravitational interactions, however, gravitinos are very difficult to observe [234].

It has been known for some time that long lived gravitinos can pose problems for cosmology [214, 216, 390, 409, 494, 505]. In particular, their presence can destroy the abundances of primordial light elements in some scenarios [385, 170, 219, 233]. Gravitinos may also be overproduced in the early universe if the temperature of the reheating epoch is not sufficiently low [385]. In some scenarios, however, these problems can be circumvented [132, 152, 249].

– *Axinos*

Axinos, the superpartner of the axion, were believed until recently to only be capable of acting as a warm, or hot, dark matter candidate [124, 268]. It has been shown, however, that for quite low reheating temperatures, cold axino dark matter may be possible [164, 165, 166, 366]. In many ways, axinos and gravitinos share similar phenomenological properties.

- *Light scalar dark matter*

Considering fermionic dark matter candidates with standard Fermi interactions, Lee and Weinberg concluded that relic density arguments preclude such a WIMP with a mass less than a few GeV [355] (see also Hut 1977 [314]). If the dark matter is made up other types of particles, however, this limit could be evaded. For example, a 1-100 MeV scalar candidate has been proposed [117, 118].

Such a candidate, although somewhat ad hoc from a particle physics perspective, has recently become experimentally motivated. In Ref. [120], it has been suggested that the 511 keV gamma-ray line emission observed by the INTEGRAL satellite from the galactic bulge could be the product of light dark matter particles annihilating into positrons which then annihilate producing the observed gamma-ray line. To confirm this hypothesis, more tests are needed. In particular, a similar signature could be expected from dwarf spheroidal galaxies [304].

Very recently, light decaying dark matter particles such as axinos with R-parity violation [311] or sterile neutrinos [416] have been suggested as the source of the observed 511 keV emission.

- *Dark matter from Little Higgs models*

As an alternative mechanism (to supersymmetry) to stabilize the weak scale, the so-called “little Higgs” models have been proposed and developed [38, 39, 40, 41]. In these models, the Standard Model Higgs is a pseudo-Goldstone boson with its mass protected by approximate non-linear global symmetries. The divergences to the Higgs mass which remain are present only at the two-loop level and, therefore, the weak scale can be stabilized in an effective field theory which is valid up to ~ 10 TeV. Recall that in supersymmetry, the divergences to the Higgs mass are exactly cancelled at all orders.

At least two varieties of little Higgs models have been shown to contain possible dark matter candidates. One of these classes of models, called “theory space” little Higgs models, provide a possibly stable, scalar particle which can provide the measured density of dark matter [110]. In Ref. [105], the detection prospects for such a candidate were found to be not dissimilar to WIMPs predicted in models of supersymmetry or universal extra dimensions.

Cheng and Low [147] have developed another variety of little Higgs model, motivated by the problem of the hierarchy between the electroweak scale and the masses of new particles constrained by electroweak precision measurements. They solve this problem by introducing a new symmetry at the TeV scale which results in the existence of a stable WIMP candidate with a \sim TeV mass.

For a potential dark matter candidate from a little Higgs model to be stable, we must assume that the discrete symmetry which protects it from decay is fundamental and is not broken by the operators in the UV completion.

- *Kaluza-Klein states*

Kaluza-Klein excitations of Standard Model fields which appear in models of universal extra dimensions have also been discussed a great deal recently as a candidate for dark matter. They are discussed in Sec. 3.3. Additionally, a dark matter candidate has been proposed in the framework of “warped” universal extra-dimensions: an exotic particle with gauge quantum numbers of a right-handed neutrino, but carrying fractional baryon-number [15].

- *Superheavy dark matter*

Superheavy dark matter particles, sometimes called *Wimpzillas*, have interesting phenomenological consequences, including a possible solution to the problem of cosmic rays observed above the GZK cutoff. These are discussed in Sec. 3.4.

- *Q-balls [351, 350], mirror particles [298, 237, 315, 383, 238], CHarged Massive Particles (CHAMPs) [182], self interacting dark matter [458, 173], D-matter [449], cryptons [215, 212], superweakly interacting dark matter [234], brane world dark matter [141], heavy fourth generation neutrinos [431, 321], etc.*

Although some of these candidates or classifications present some intriguing features we will not discuss them here. We refer the interested reader to the wide literature on the subject, *e.g.* the reviews of non-baryonic candidates by Ellis [208] and Bergstrom [86].

We stress that it is by no means assured that the dark matter is made of a single particle species. On the contrary, we already know that Standard Model neutrinos contribute to dark matter, but cannot account for all of it. Even in supersymmetry models for dark matter, $N = 2$ supersymmetry allows the possibility of two stable dark matter relics (see, for example, Ref. [119]).

In what follows, we will assume that the abundance of our candidates satisfy the limits provided by the analysis of the CMB discussed in Sec.2.3, but we stress that, although the upper bound is a strict limit, the lower bound can be relaxed, assuming that our candidate is a sub-dominant component of dark matter. The interested reader will find in Ref. [201] a detailed discussion on the detection prospects of a subdominant density component of dark matter.

3.2 Supersymmetry

It would be impossible to review in only a few pages the history and theory of Supersymmetry (SUSY). Instead, we prefer here to review the motivations that led to its introduction and to briefly present the concepts and the notations that we will use in the following chapters. Furthermore, we present a few of the supersymmetric models discussed in the literature (we reserve the word “scenario” for a specific choice of parameters in the framework of a given model) and discuss the consequences of various assumptions, involved in the process of model-building, on SUSY phenomenology. For further discussions of supersymmetry, we refer the interested reader to Refs. [101, 157, 497, 190, 319, 372, 403, 153].

3.2.1 Basics of supersymmetry

As we saw in Sec.1.3, in the Standard Model of particle physics there is a fundamental distinction between bosons and fermions: while bosons are the mediators of interactions, fermions are the constituents of matter. It is therefore natural to ask whether a symmetry exists which relates them, thus providing a sort of “unified” picture of matter and interactions.

Another way to state the problem is to ask whether a Lie group exists mixing internal (Isospin, *etc.*) and space-time (Lorentz) symmetries [282]. Although apparently uncorrelated to the differing behaviour of bosons and fermions, this problem led to the study of the same algebraic structures. Early attempts to find a broad Lie group including the Poincaré and internal symmetry groups had to face the limitations imposed by the so-called *no-go* theorem of Coleman and Mandula. Such limitations were finally circumvented with the introduction of *graded* Lie algebras, *i.e.* algebras involving fermionic generators satisfying anticommutation relations (see below).

For those who are not convinced by these symmetry arguments, there are other major reasons for interest in supersymmetry. One reason is its role in understanding the *hierarchy problem*. The hierarchy problem is linked to the enormous difference between the electroweak and Planck energy scales. This problem arises in the radiative corrections to the mass of the Higgs boson.

All particles get radiative corrections to their mass, but while fermion masses increase only logarithmically, scalar masses increase quadratically with energy, giving corrections at 1-loop of

$$\delta m_s^2 \sim \left(\frac{\alpha}{2\pi}\right) \Lambda^2, \quad (59)$$

where Λ is a high-energy cut-off where new physics is expected to play an important role. The radiative corrections to the Higgs mass (which is expected to be of the order of the electroweak scale $M_W \sim 100$ GeV) will destroy the stability of the electroweak scale if Λ is higher than \sim TeV, *e.g.* if Λ is near the Planck mass.

An appealing, though not the only, solution to this problem is to postulate the existence of new particles with similar masses but with spin different by one

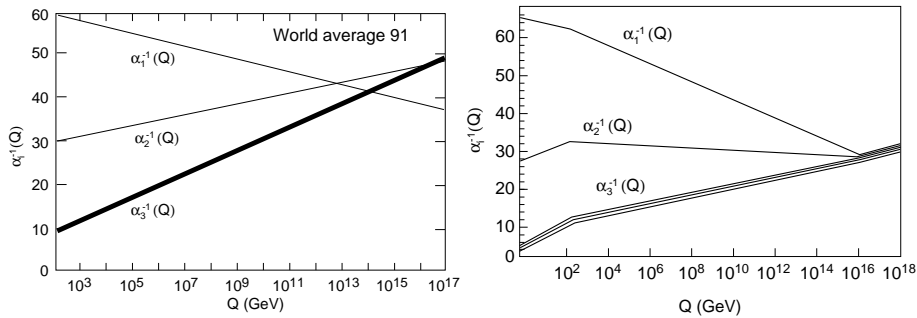


Figure 10: The measurements of the gauge coupling strengths at LEP do not (left) evolve to a unified value if there is no supersymmetry but do (right) if supersymmetry is included [29, 220].

half. Then, since the contribution of fermion loops to δm_s^2 have opposite sign to the corresponding bosonic loops, at the 1-loop level, Eq. 59 becomes

$$\delta m_s^2 \sim \left(\frac{\alpha}{2\pi}\right) (\Lambda^2 + m_B^2) - \left(\frac{\alpha}{2\pi}\right) (\Lambda^2 + m_F^2) = \left(\frac{\alpha}{2\pi}\right) (m_B^2 - m_F^2). \quad (60)$$

Furthermore, the supersymmetric algebra insures that (provided $|m_B^2 - m_F^2| \lesssim 1$ TeV) the quadratic divergence to the Higgs mass is cancelled at all orders of perturbation theory. The algebra of supersymmetry naturally guarantees the existence of new particles, with the required properties, associating to all of the particles of the Standard Model superpartners with the same mass and opposite spin-type (boson or fermion).

Another reason for interest in supersymmetric theories comes from the unification of gauge couplings at a scale $M_U \sim 2 \times 10^{16}$ GeV (see Fig. 10). Although extrapolation of the coupling constants using only Standard Model particles fails to unify them to a common value (left frame of Fig. 10), by introducing supersymmetry at the TeV scale, it was shown [29] that these forces naturally unify at a scale $M_U \sim 2 \times 10^{16}$ GeV (right frame of Fig. 10). This has been taken as a strong hint in favor of a Grand Unified Theory (GUT) which predicts gauge coupling unification below the Planck scale.

The new generators introduced with supersymmetry change fermions into bosons and vice versa, *i.e.*

$$Q|\text{fermion}\rangle = |\text{boson}\rangle; \quad Q|\text{boson}\rangle = |\text{fermion}\rangle. \quad (61)$$

Because of their fermionic nature, the operators Q must carry spin 1/2, which implies that supersymmetry must be a spacetime symmetry. The question then arises of how to extend the Poincaré group of spatial translations and Lorentz transformations to include this new boson/fermion symmetry. The structure of such a group is highly restricted by the Haag-Lopuszanski-Sohnius extension

of the Coleman and Mandula theorem cited above. For realistic theories, the operators, Q , which we choose by convention to be Majorana spinors, must satisfy

$$\{Q_a, \bar{Q}_b\} = 2\gamma_{ab}^\mu P_\mu \quad (62)$$

$$\{Q_a, P_\mu\} = 0 \quad (63)$$

$$[Q_a, M^{\mu\nu}] = \sigma_{ab}^{\mu\nu} Q^b \quad (64)$$

where

$$\bar{Q}_a \equiv (Q^\dagger \gamma_0)_a \quad (65)$$

and

$$\sigma^{\mu\nu} = \frac{i}{4} [\gamma^\mu, \gamma^\nu] \quad (66)$$

are the structure constants of the theory.

Just as Lorentz invariance is manifest in Minkowski space-time, supersymmetry is manifest in the so-called *superspace* formalism, where a superspace is defined as a set of coordinates $\{x, \theta, \bar{\theta}\}$, where $x = x^\mu$ are the usual coordinate of Minkowski spacetime, and $\theta, \bar{\theta}$ are anti-commuting Weyl spinors.

A *superfield* is then a function, $\Phi(x, \theta, \bar{\theta})$, defined on a superspace; it is common to introduce *chiral fields* representing matter and *vector fields* representing gauge fields.

3.2.2 Minimal supersymmetric Standard Model

To continue our brief introduction to SUSY, we consider the *minimal* supersymmetric extension of the Standard Model (MSSM, for Minimal Supersymmetric Standard Model). The MSSM is minimal in the sense that it contains the smallest possible field content necessary to give rise to all the fields of the Standard Model. This can be done as follows:

- We associate fermionic superpartners to all gauge fields. Gluons, W^\pm and B bosons then get fermionic partners called *gluinos* (\tilde{g}), *winos* (\tilde{W}^i) and *binos* (\tilde{B}), respectively. The common name for all partners of gauge fields is the *gaugino*.
- We associate scalar partners to the fermions, *i.e.* quarks and leptons get scalar partners called *squarks* and *sleptons*.
- We introduce one additional Higgs field (for a total of two Higgs doublets, corresponding to five physical Higgs states) and associate one spin 1/2 *Higgsino* to each Higgs boson. This is done to give masses to both up and down-type quarks upon electroweak symmetry breaking and also preserve supersymmetry (therefore, we cannot use the conjugate of the Higgs as is done in Standard Model). Introducing another Higgs doublet also makes the theory anomaly free.

The resulting particle content of the theory is shown in tables 3 and 4.

Superfield	SM particles	Spin	Superpartners	Spin
Q	$\begin{pmatrix} u_L \\ d_L \end{pmatrix}$	1/2	$\begin{pmatrix} \tilde{u}_L \\ \tilde{d}_L \end{pmatrix}$	0
U^c	\bar{u}_R	1/2	\tilde{u}_R^*	0
D^c	\bar{d}_R	1/2	\tilde{d}_R^*	0
L	$\begin{pmatrix} \nu_L \\ e_L \end{pmatrix}$	1/2	$\begin{pmatrix} \tilde{\nu}_L \\ \tilde{e}_L \end{pmatrix}$	0
E^c	\bar{e}_R	1/2	\tilde{e}_R^*	0
H_1	H_1	0	\tilde{H}_1	1/2
H_2	H_2	0	\tilde{H}_2	1/2
G^a	g	1	\tilde{g}	1/2
W_i	W_i	1	\tilde{W}_i	1/2
B	B	1	\tilde{B}	1/2

Table 3: Field content of the MSSM.

The MSSM is then specified through the *superpotential*, defined as

$$W = \epsilon_{ij} [y_e H_1^j L^i E^c + y_d H_1^j Q^i D^c + y_u H_2^i Q^j U^c] + \epsilon_{ij} \mu H_1^i H_2^j \quad (67)$$

where i and j are SU(2) indices, and y are Yukawa couplings. Color and generation indices have been suppressed in the above expression. The superpotential represents a supersymmetrization of the Standard Yukawa couplings plus a bilinear Higgs term. The superpotential enters the Lagrangian of the theory through the terms

$$\mathcal{L}_{\text{SUSY}} = -\frac{1}{2} (W^{ij} \psi_i \psi_j + W_{ij}^* \psi^{i\dagger} \psi^{j\dagger}) - W^i W_i^* \quad (68)$$

where we have used $W^i \equiv \partial W / \partial \phi_i$, $W_i^* \equiv \partial W / \partial \phi^{i*}$, and $W^{ij} \equiv \partial^2 W / \partial \phi_i \partial \phi_j$. ϕ_i and ψ_i are scalar and fermion fields, respectively.

One additional ingredient of the MSSM is the conservation of R -parity. R -parity is a multiplicative quantum number defined as

$$R \equiv (-1)^{3B+L+2s} . \quad (69)$$

All of the Standard Model particles have R -parity $R = 1$ and all sparticles (*i.e.* superpartners) have $R = -1$. Thus, as a consequence of R -parity conservation, sparticles can only decay into an odd number of sparticles (plus Standard Model particles). The lightest sparticle (dubbed the LSP, for Lightest Supersymmetric Particle) is, therefore, stable and can only be destroyed via pair annihilation, making it an excellent dark matter candidate [256, 213]. Note that this not the original motivation for R -parity. In fact, R -parity was first introduced to suppress the rate of proton decay [228, 183, 495, 436, 185].

The nature of the LSP in the MSSM is constrained by many observations. It cannot have a non-zero electric charge or color, or it would have condensed with baryonic matter to produce heavy isotopes, in conflict with observations.

Standard Model particles and fields		Supersymmetric partners			
Symbol	Name	Interaction eigenstates	Mass eigenstates	Symbol	Name
$q = d, c, b, u, s, t$	quark	\tilde{q}_L, \tilde{q}_R	squark	\tilde{q}_1, \tilde{q}_2	squark
$l = e, \mu, \tau$	lepton	\tilde{l}_L, \tilde{l}_R	slepton	\tilde{l}_1, \tilde{l}_2	slepton
$\nu = \nu_e, \nu_\mu, \nu_\tau$	neutrino	$\tilde{\nu}$	sneutrino	$\tilde{\nu}$	sneutrino
g	gluon	\tilde{g}	gluino	\tilde{g}	gluino
W^\pm	W -boson	\tilde{W}^\pm	wino	}	$\tilde{\chi}_{1,2}^\pm$ chargino
H^-	Higgs boson	\tilde{H}_1^-	higgsino		
H^+	Higgs boson	\tilde{H}_2^+	higgsino		
B	B -field	\tilde{B}	bino	}	$\tilde{\chi}_{1,2,3,4}^0$ neutralino
W^3	W^3 -field	\tilde{W}^3	wino		
H_1^0	Higgs boson	\tilde{H}_1^0	higgsino		
H_2^0	Higgs boson	\tilde{H}_2^0	higgsino		
H_3^0	Higgs boson				

Table 4: Standard Model particles and their superpartners in the MSSM (adapted from Ref. [203]).

Among the neutral candidates, a possible LSP could be the sneutrino. Sneutrino LSPs have, however, been excluded by direct dark matter detection experiments (see sections 4.1 and 5). Although axinos and gravitinos cannot be *a priori* excluded, they arise only in a subset of supersymmetric scenarios and have some unattractive properties (see section 3.1). In particular, gravitinos and axinos have very weak interactions and would be practically impossible to detect, making them less interesting from a phenomenological perspective. The lightest *neutralino* remains an excellent dark matter candidate, and is further discussed in the next section.

To determine the identity of the LSP (or other characteristics) in a given supersymmetric scenario, we have to specify how supersymmetry is *broken*. If supersymmetry were not broken, then each superpartner would have a mass identical to its Standard Model counterpart, which is clearly not the case. Thus, new terms which break supersymmetry must be added to the Lagrangian. These terms, however, should be added carefully, in order not to destroy the hierarchy between Planck and electroweak scales. The possible forms for such terms are

$$\begin{aligned}
\mathcal{L}_{soft} = & -\frac{1}{2}M_\lambda^a \lambda^a \lambda^a - \frac{1}{2}(m^2)_j^i \phi_i \phi_j^* \\
& -\frac{1}{2}(BM)^{ij} \phi_i \phi_j - \frac{1}{6}(Ay)^{ijk} \phi_i \phi_j \phi_k + h.c., \quad (70)
\end{aligned}$$

where the M_λ^a are gaugino masses, m^2 are soft scalar masses, B is a bilinear mass term, and A is a trilinear mass term. We will discuss some specific supersymmetry breaking scenarios later in this section.

3.2.3 The lightest neutralino

In the MSSM, the superpartners of the B , W_3 gauge bosons (or the photon and Z , equivalently) and the neutral Higgs bosons, H_1^0 and H_2^0 , are called binos (\tilde{B}), winos (\tilde{W}_3), and higgsinos (\tilde{H}_1^0 and \tilde{H}_2^0), respectively. These states mix into four Majorana fermionic mass eigenstates, called neutralinos. The four neutralino mass eigenstates are typically labelled $\tilde{\chi}_1^0$, $\tilde{\chi}_2^0$, $\tilde{\chi}_3^0$ and $\tilde{\chi}_4^0$, ordered with increasing mass. In the following we will refer to $\tilde{\chi}_1^0$, *i.e.* the lightest of the four neutralinos, as *the* neutralino, and denote it simply as, $\chi \equiv \tilde{\chi}_1^0$.

In the basis $(\tilde{B}, \tilde{W}_3, \tilde{H}_1^0, \tilde{H}_2^0)$, the neutralino mass matrix can be expressed as

$$\mathcal{M}_N = \begin{pmatrix} M_1 & 0 & -M_Z \cos \beta \sin \theta_W & M_Z \sin \beta \sin \theta_W \\ 0 & M_2 & M_Z \cos \beta \cos \theta_W & -M_Z \sin \beta \cos \theta_W \\ -M_Z \cos \beta \sin \theta_W & M_Z \cos \beta \cos \theta_W & 0 & -\mu \\ M_Z \sin \beta \sin \theta_W & -M_Z \sin \beta \cos \theta_W & -\mu & 0 \end{pmatrix}, \quad (71)$$

where M_1 and M_2 are the bino and wino mass parameters, respectively, θ_W is the Weinberg angle and $\tan \beta$ is the ratio of the vacuum expectation values of the Higgs bosons. μ is the higgsino mass parameter. As we have seen, the (lightest) neutralino is a linear combination of \tilde{B} , \tilde{W}_3 , \tilde{H}_1^0 and \tilde{H}_2^0 ,

$$\chi = N_{11} \tilde{B} + N_{12} \tilde{W}_3 + N_{13} \tilde{H}_1^0 + N_{14} \tilde{H}_2^0. \quad (72)$$

We then define the *gaugino fraction*, f_G , and the *higgsino fraction*, f_H , as

$$f_G = N_{11}^2 + N_{12}^2 \quad (73)$$

and

$$f_H = N_{13}^2 + N_{14}^2. \quad (74)$$

For the analytic expressions used to diagonalize the neutralino mass matrix, see Appendix A.

The neutralino interactions most relevant for the purposes of dark matter are self annihilation and elastic scattering off of nucleons. Neutralinos are expected to be extremely non-relativistic in the present epoch, allowing us to safely keep only the a -term in the usual expansion of the annihilation cross section,

$$\sigma v = a + bv^2 + \mathcal{O}(v^4). \quad (75)$$

The b -term must be included in performing calculations of the neutralino relic density, however.

At low velocities, the leading channels for neutralino annihilation are annihilations to fermion-antifermion pairs (primarily heavy fermions, such as top, bottom and charm quarks and tau leptons), gauge bosons pairs (W^+W^- and Z^0Z^0) and final states containing Higgs bosons. In appendix B, we give the most important neutralino annihilation diagrams, amplitudes and cross sections (in the low velocity limit). For a complete list of all tree level processes, diagrams, amplitudes and cross sections, see the excellent review of Jungman, Kamionkowski and Griest [319].

3.2.4 Supersymmetric models

Although relatively simple in many respects, the MSSM has a huge number of free parameters. Most of these parameters represent masses and mixing angles, much as in the case of the Standard Model. To allow for the practical phenomenological study of the MSSM, the number of parameters which are considered must be reduced. This can be done by making (theoretically well motivated) assumptions which reduce the free parameters from more than 100 to a more tractable quantity. Depending on the assumptions used, one obtains different supersymmetric models. In the following section, we will describe a few of the most widely considered supersymmetric scenarios, including mSUGRA (often called the constrained MSSM) and a phenomenologically simplified MSSM (called the phenomenological, or, pMSSM). We also discuss the phenomenological features of the MSSM in anomaly, gauge and gaugino mediated scenarios.

mSUGRA The mSUGRA, or constrained MSSM, scenario is a simple phenomenological model based on a series of theoretical assumptions (see *e.g.* Kane *et al.* [327]). The number of free parameters is reduced in this scenario by assuming that the MSSM parameters obey a set of boundary conditions at the Grand Unification scale:

- Gauge coupling unification

$$\alpha_1(M_U) = \alpha_2(M_U) = \alpha_3(M_U) \equiv \alpha_U \quad (76)$$

with $\alpha_i = g_i^2/4\pi$

- Unification of the gaugino masses

$$M_1(M_U) = M_2(M_U) = M_3(M_U) \equiv m_{1/2} \quad (77)$$

- Universal scalar [sfermion and Higgs boson] masses

$$\begin{aligned} M_{\tilde{Q}}(M_U) = M_{\tilde{u}_R}(M_U) = M_{\tilde{d}_R}(M_U) = M_{\tilde{L}}(M_U) = M_{\tilde{t}_R}(M_U) \\ = M_{H_u}(M_U) = M_{H_d}(M_U) \equiv m_0 \end{aligned} \quad (78)$$

- Universal trilinear couplings:

$$A_u(M_U) = A_d(M_U) = A_t(M_U) \equiv A_0 \quad (79)$$

By requiring the minimization of the Higgs potential (in order to recover electroweak symmetry breaking), we are left with five (four continuous and one discrete) free parameters:

$$\tan \beta, m_{1/2}, m_0, A_0, \text{sign}(\mu), \quad (80)$$

where $\tan \beta$ is the ratio of the vacuum expectation values of the two Higgs fields and μ is the higgsino mass parameter.

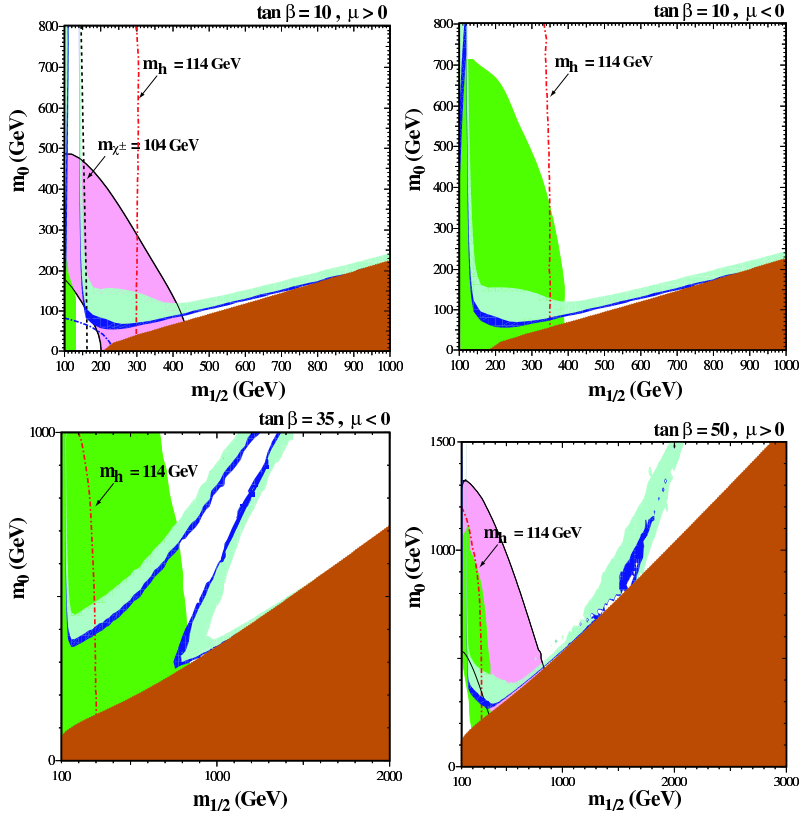


Figure 11: The $(m_{1/2}, m_0)$ planes for mSUGRA with (a) $\tan\beta = 10, \mu > 0$, (b) $\tan\beta = 10, \mu < 0$, (c) $\tan\beta = 35, \mu < 0$, and (d) $\tan\beta = 50, \mu > 0$. In each panel, the region allowed by the older cosmological constraint $0.1 \leq \Omega_\chi h^2 \leq 0.3$ has cyan shading, and the region allowed by the newer cosmological constraint $0.094 \leq \Omega_\chi h^2 \leq 0.129$ has dark blue shading. For more details, see Ref. [217].

A recent study of mSUGRA parameter space in light of the WMAP measurement of the dark matter relic density can be found in Ref. [217]. We show in Fig. 11 and Fig. 12 the regions of the $(m_{1/2}, m_0)$ plane consistent with CMB and accelerator data. It is worth mentioning that neutralino models with relic densities lower than the WMAP measurement are not ruled out, although evidently they cannot make up all the dark matter.

In addition to constraints on models in mSUGRA which come from the WMAP measurements, strong constraints can also be placed by collider data. In particular, constraints arise from the absence of new particles at LEP below ≈ 100 GeV and the agreement of $b \rightarrow s\gamma$ decays with predictions of the Standard Model. Measurements of the anomalous magnetic momentum of the muon, $g_\mu - 2$, also provide a possible constraint. These constraints have been studied in the

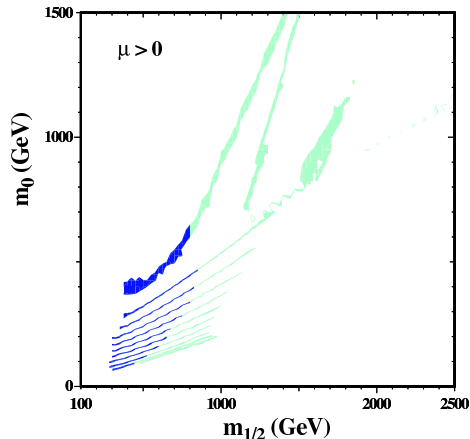


Figure 12: Regions of the $(m_{1/2}, m_0)$ plane in mSUGRA that are compatible with $0.094 < \Omega_\chi h^2 < 0.129$ and laboratory constraints for $\mu > 0$ and $\tan\beta = 5, 10, 15, 20, 25, 30, 35, 40, 45, 50, 55$. The parts of the strips compatible with $g_\mu - 2$ at the $2\text{-}\sigma$ level have darker shading. From Ref. [217].

context of mSUGRA in great detail [47, 218, 430]. The interested reader will find a discussion of mSUGRA parameters and the definition of SUSY *benchmarks* points in Ref. [65]. For more on collider constraints, see section 3.5.

The phenomenological MSSM The scenario we present in this section is not necessarily motivated by any theoretical arguments, but rather is justified by focusing on the aspects of supersymmetric phenomenology which are the most interesting for neutralino dark matter. The phenomenological MSSM, or pMSSM, is an adaptable framework which can be described by as many as tens of parameters, or as few as five or seven. It is NOT a model, but rather a convenient description of the phenomenology most relevant to supersymmetric dark matter. Common choices in defining a phenomenological MSSM include a) no new sources of CP violation (all the phases in the SUSY breaking terms are set to zero), b) no flavor-changing neutral currents and c) first and second generation universality.

One example of a phenomenological MSSM is used in the DarkSusy program package [264]. In this scheme, in addition to the common features described above, gaugino unification is assumed (similar to Eq. 77). The remaining inputs are defined by seven free parameters:

$$\mu, M_2, \tan\beta, M_A, m_0, A_b \text{ and } A_t \quad (81)$$

where M_A is the mass of the pseudo-scalar Higgs boson, m_0 is the common scalar mass, and $A_{b,t}$ are trilinear couplings appearing in SUSY breaking terms. Unlike in the case of the mSUGRA scenario, the input parameters are chosen at

the electroweak scale without making use of renormalization group equations. The inputs used in DarkSusy can be expanded beyond these seven to include other parameters, thus representing a more general MSSM.

We note that these scenarios are less theoretically motivated in comparison to mSUGRA. Various combinations of theoretically and phenomenologically-based descriptions for supersymmetry are often considered in the literature, often maintaining some of the theoretically motivated constraints of mSUGRA while relaxing other requirements (for example, see Refs. [90, 109]).

The focus point region of mSUGRA In most of the parameter space of mSUGRA or other similar scenarios, the lightest neutralino is a gaugino-like neutralino with a mass of a couple hundred GeV or less. In the so-called “focus point” region of mSUGRA, however, the lightest neutralino can have a considerable higgsino content, and be significantly more heavy [194, 198, 229, 230, 231].

In the focus point region, very large scalar masses are possible without violating naturalness constraints. This occurs because the soft masses squared of the Higgs boson, $m_{H_u}^2$, have pseudo fixed-point behavior, and can start with a wide range of input values and run to a similar negative value at the low scale. This is interesting because it indicates that, in the focus point region, electroweak symmetry breaking does not require fine-tuning in the high energy input values.

A typical feature of the focus point region are large scalar masses (usually \sim TeV). The main reason for a larger higgsino content in the LSP is the larger input value of the soft scalar mass. The tree level electroweak symmetry breaking condition gives

$$\frac{1}{2}m_Z^2 \sim -m_{H_u}^2 - \mu^2. \quad (82)$$

In the typical mSUGRA scenarios, $m_{H_u}^2$ is driven to some large negative value due to the running of the renormalization group equations. This requires a large value of μ to give the correct Z mass. In the focus point region, however, it is possible that the large input value of the scalar soft mass makes $m_{H_u}^2$ less negative. Hence, a smaller value of μ is possible, which leads to a larger higgsino content in the LSP.

Anomaly mediated SUSY breaking Anomaly Mediated Supersymmetry Breaking (AMSB) is an attractive alternative to general gravity mediated scenarios as it provides an elegant solution to the so-called flavor problem through an elegant decoupling mechanism. The resulting soft parameters are “UV insensitive”. In this scenario, the SUSY parameters can all be expressed in terms of low energy parameters such as the Yukawa and gauge couplings. Although the details of AMSB are quite technical, and are beyond the scope of this work, we will here describe some of the phenomenological features of this scenario which are most relevant for dark matter.

In AMSB, the gaugino spectrum is given by

$$M_{\lambda^a} = \frac{\beta_{g_a}}{g_a} m_{3/2}, \quad (83)$$

where β are beta-functions computed in the supersymmetric limit [424, 255, 250]. The proportionality of the β -function to the low energy masses leads to a specific relationship between the gaugino masses: $M_1 : M_2 : M_3 = 2.8 : 1 : 7.1$. This is very different than would be predicted by the GUT relations used in mSUGRA, for example, with the wino and bino mass hierarchy reversed. When the neutralino mass matrix is diagonalized in AMSB, these ratios result in an LSP which is almost purely (neutral) wino [367, 479]. Additionally, a charged wino, with a mass only a few hundred MeV heavier than the LSP, is predicted. This leads to a long lived chargino with distinctive collider signatures. Also, in AMSB, with such large values of M_3 , the gluino and squarks are predicted to be considerably heavier than in mSUGRA or other similar scenarios.

The heterotic orbifold model The weakly coupled heterotic string with orbifold compactification is among the earliest and best understood string models that can accommodate in four dimensions the Standard Model gauge group, three generations of squarks and a coherent mechanism of supersymmetry breaking. These models show a behavior that interpolates between the phenomenology of mSUGRA and models dominated by superconformal anomalies (AMSB) [100].

Recently, the full one loop soft supersymmetry breaking terms in a large class of superstring effective theories have been calculated [102] based on orbifold compactifications of the weakly coupled heterotic string (including the so-called anomaly mediated contributions). The parameter space in this class of models has already been severely constrained by taking into account accelerator and relic density constraints, as well as direct and indirect searches (see Refs. [95, 100, 99, 326, 108]).

Gauge mediated SUSY breaking Another alternative SUSY breaking mechanism is mediated by gauge interactions [186, 391, 28, 187, 188, 189]. In Gauge Mediated Supersymmetry Breaking (GMSB), we have the following approximate relationship between the low energy SUSY masses and the gravitino mass

$$\frac{m_{3/2}}{m_{\text{SUSY}}} \sim \frac{1}{\alpha_a} \frac{M_S}{M_{Pl}} \ll 1, \quad (84)$$

where M_S is some typical supersymmetry breaking scale. Therefore, generically, we will have a very light gravitino as the LSP [184]. Such a scenario provides a dark matter candidate which is very difficult to observe. We will not discuss gravitino dark matter or GMSB further for this reason.

Gaugino mediated SUSY breaking Gaugino mediated supersymmetry breaking [330, 146] represents another class of SUSY breaking mediation motivated by the brane-world scenario. In this scenario, unwanted supersymmetry

breaking effects, such as the flavor violating couplings, are suppressed by the separation of the observable and hidden sectors via the separation of their respective branes. Gauginos are allowed to propagate off of the branes (in the bulk) in this scenario, communicating SUSY breaking from the hidden sector.

The most important phenomenological feature of this mechanism is that the sfermion masses are suppressed relative to the gaugino masses. This is because sfermion masses can only be generated from the 1-loop diagrams in which a gaugino is emitted, travels through the bulk to the supersymmetry breaking brane, gets the information of SUSY breaking and then returns to join the sfermion propagator again. Generically, these masses are suppressed relative to the gaugino mass by a loop factor, $m_{\tilde{f}}^2 \sim M_\lambda^2/(16\pi^2)$.

3.3 Extra Dimensions

Although our world appears to consist of 3+1 (three space and one time) dimensions, it is possible that other dimensions exist and appear at higher energy scales.

From the physics point-of-view, the concept of extra dimensions received great attention after the idea of Kaluza, in 1921, to unify electromagnetism with gravity by identifying the extra components of the metric tensor with the usual gauge fields. More recently, it has been realized that the hierarchy problem (see section 3.2.1) could be addressed, and possibly solved, by exploiting the geometry of spacetime.

In many extra-dimensional models, the 3+1 dimensional spacetime we experience is a structure called a *brane*, which is embedded in a $(3 + \delta + 1)$ spacetime called the *bulk*. The hierarchy problem can then be addressed by postulating that all of the extra dimensions are compactified on circles (or other topology) of some size, R , as has been done in the Arkani-Hamed, Dimopoulos and Dvali (ADD) scenario [42], thus lowering the fundamental Planck scale to an energy near the electroweak scale. Alternatively, this could be accomplished by introducing extra dimensions with large curvature (warped extra dimensions) as has been suggested by Randall and Sundrum [423]. The extra dimensional scenario which we will focus on throughout the remainder of this review (universal extra dimensions) does not share the features of the ADD or RS scenarios. Rather, it introduces flat extra dimensions which are much smaller than those in the ADD framework.

In addition to the hierarchy problem, motivation for the study of theories with extra dimensions comes from *string theory* and *M-theory*, which today appear to be the best candidates for a consistent theory of quantum gravity and a unified description of all interactions. It appears that such theories may require the presence of six or seven extra-dimensions.

A general feature of extra-dimensional theories is that upon compactification of the extra dimensions, all of the fields propagating in the bulk have their momentum quantized in units of $p^2 \sim 1/R^2$. The result is that for each bulk field, a set of Fourier expanded modes, called Kaluza–Klein (KK) states, appears. From our point of view in the four dimensional world, these KK states

appear as a series (called a tower) of states with masses $m_n = n/R$, where n labels the mode number. Each of these new states contains the same quantum numbers, such as charge, color, etc.

In many scenarios, the Standard Model fields are assumed to be confined on the brane, with only gravity allowed to propagate in the bulk. Nevertheless, if the extra-dimensions are small, it would be possible for all fields to freely propagate in the extra dimensions. Such is the case in models with universal extra dimensions, which we discuss in the next section.

3.3.1 Universal extra dimensions

Scenarios in which all fields are allowed to propagate in the bulk are called Universal Extra Dimensions (UED) [35]. Following Ref. [446], we note that there is significant phenomenological motivation to have all Standard Model fields propagate in the bulk, including:

- Motivation for three families from anomaly cancellation
- Attractive dynamical electroweak symmetry breaking
- Prevention of rapid proton decay
- *Provides a viable dark matter candidate.*

In the case of one extra dimension, the constraint on the compactification scale in UED models from precision electroweak measurements is as low as $R^{-1} \gtrsim 300$ GeV [35]. Recently, it was shown that this bound can be weakened to $R^{-1} \gtrsim 280$ GeV if one allows a Higgs mass as heavy as $m_H \gtrsim 800$ GeV [36]. This is to be contrasted with another class of models where Standard Model bosons propagate in extra dimensions while fermions are localized in 4 dimensions. In such cases, the constraint on the compactification scale is much stronger, requiring $R^{-1} \gtrsim$ several TeV [151].

The prospect of UED models providing a viable dark matter candidate is indeed what motivates us in our discussion here. The existence of a viable dark matter candidate can be seen as a consequence of the conservation of momentum in higher dimensional space. Momentum conservation in the compactified dimensions leads to the conservation of KK number. This does not stabilise the lightest KK state, however. To generate chiral fermions at the zero mode, the extra dimensions must be moded out by an orbifold, such as S/Z_2 for one extra dimension or T^2/Z_2 for two. This orbifolding results in the violating of KK number, but can leave a remnant of this symmetry called KK-parity (assuming that the boundary terms match). All odd-level KK particles are charged under this symmetry, thus ensuring that the lightest (first level) KK state is stable. In this way, the Lightest Kaluza-Klein Particle (LKP) is stabilized in a way quite analogous to the LSP in R-parity conserving supersymmetry.

In the next section, we will discuss some of the characteristics of the LKP in models of UED.

3.3.2 The lightest Kaluza–Klein particle

The study of the Lightest Kaluza-Klein Particle (LKP) as a dark matter candidate dates back to the work of Kolb and Slansky in 1984 [338], where the KK excitations were referred to as *pyrgons*, from the Greek $\pi\nu\rho\gamma\omicron\varsigma$ for “scale” or “ladder”. The LKP has since been reconsidered in the framework of universal extra dimensions, in which it is likely to be associated with the first KK excitation of the photon, or more precisely the first KK excitation of the hypercharge gauge boson [149]. We will refer to this state as $B^{(1)}$.

A calculation of the $B^{(1)}$ relic density was performed by Servant and Tait [446], who found that if the LKP is to account for the observed quantity of dark matter, its mass (which is inversely proportional to the compactification radius R) should lie in the range of 400 to 1200 GeV, well above any current experimental constraint.

We show in Fig. 13 the relic density of the $B^{(1)}$ particle versus its mass, including coannihilations (see section 1.5) with the next-to-lightest KK particle, which in the case shown is $e_R^{(1)}$, the first KK excitation of the right-handed electron. This figure is a new version of Fig. 3 in Ref. [446], updated to include the new WMAP constraints on the cold dark matter relic density ⁴.

Note that the results of the LKP relic density calculation can vary depending on the spectrum of other first level KK states. Unlike in the case of supersymmetry, the density of KK dark matter is *increased* through coannihilations with other KK particles.

This is due to the fact that in the case of neutralinos, the cross section for the interaction between neutralinos and the NLSP is much larger than the neutralino self-annihilation cross section, which implies that DM particles are kept longer in thermodynamic equilibrium, thus decoupling with a lower relic density. In contrast, the interactions between the $B^{(1)}$ and $e_R^{(1)}$ are comparable with the $B^{(1)}$ self-interaction. Decoupling in presence of coannihilations thus happens essentially at the same time as in the case with no coannihilations, and the $B^{(1)}$ relic density becomes larger since the $e_R^{(1)}$, after decoupling at the same time, decays in the $B^{(1)}$.

The spectrum of first level KK states has been calculated to one loop by Cheng, Matchev and Schmaltz [149], although higher dimensional operators localized at the boundary may change the details of the spectrum (without affecting KK parity). Variations in this spectrum can result in variations for the predicted LKP relic abundance.

The $B^{(1)}$ annihilation cross section has been studied in Ref. [446], and is given by

$$\sigma v = \frac{95g_1^4}{324\pi m_{B^{(1)}}^2} \simeq \frac{0.6 \text{ pb}}{m_{B^{(1)}}^2 [\text{TeV}]} . \quad (85)$$

The branching ratios for $B^{(1)}$ annihilation (see table 5) are almost independent of the particle mass. Unlike in the case of supersymmetry, the bosonic nature of the LKP means that there will be no chirality suppression in its annihilations,

⁴see section 2.3 for a discussion of the CMB and, in particular, the recent WMAP data

Channel	Branching ratio
quark pairs	35%
charged lepton pairs	59%
neutrino pairs	4%
Higgs bosons	2%

Table 5: Branching ratios for the annihilation of the $B^{(1)}$ particle. Note that small variations from these results can occur with variation in the KK spectrum.

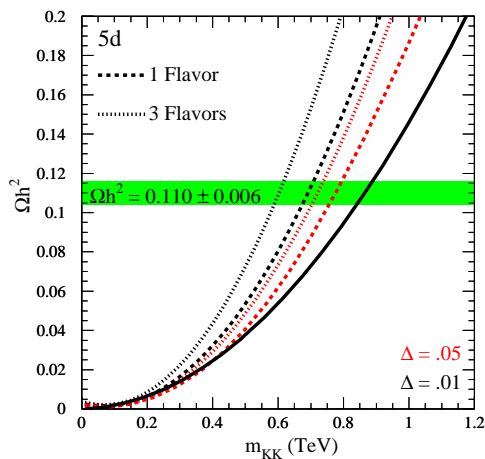


Figure 13: Relic density versus mass of the $B^{(1)}$. The solid line is the case for $B^{(1)}$ alone, dashed and dotted lines are for one (three) flavors of nearly degenerate $e_R^{(1)}$. For each case, black curves (upper of each pair) are for $\Delta = 0.01$ and red curves (lower of each pair) for $\Delta = 0.05$. Figure kindly provided by G. Servant.

and thus can annihilate efficiently to fermion-fermion pairs. In particular, since the annihilation cross section is proportional to hypercharge⁴ of the final state, a large fraction of LKP annihilations produce charged lepton pairs.

Direct detection of the LKP via its elastic scattering with nuclei was investigated in Refs. [150, 447]. It was emphasized in Ref. [447] that a one-ton detector is needed to probe the expected heavy masses as indicated by the relic density calculation [446] of the LKP. One must, therefore, wait for the next generation of direct detection experiments such as GENIUS [333] or XENON [37] (see section 4.1). Simultaneously, the LHC should probe most of the relevant KK mass parameter space (up to $R^{-1} \sim 1.5$ TeV [148]) and confirm or rule out UED at the TeV scale.

3.4 Superheavy Candidates

Dark matter particles are usually assumed to be relatively “light”, meaning lighter than a few hundred TeV. This “limit” is a consequence of the existence of a maximum annihilation cross section, σv , for a particle of a given mass, m_{DM} , set by the so-called *unitarity bound* (see *e.g.* Ref. [493]). Griest and Kamionkowski [277] applied this bound and the constraint on the relic density to infer an upper limit on the dark matter particle mass:

$$m_{DM} \lesssim 340 \text{ TeV} . \quad (86)$$

We note that nowadays, using the WMAP constraint on $\Omega_{DM}h^2$, such a constraint can be made ten times stronger,

$$m_{DM} \lesssim 34 \text{ TeV} . \quad (87)$$

The assumption behind this argument is that the dark matter particle is a thermal relic of the early Universe, otherwise we could not have applied the relation between $\Omega_{DM}h^2$ and σv . In this section, we consider superheavy dark matter candidates, defined as candidates with mass $m_{DM} > 10^{10}$ GeV, that we call generically *wimpzillas* [339, 144]. Thus the first condition for this scenario is that *wimpzillas must not have been in thermal equilibrium during freeze-out*. Since they are not in thermal equilibrium during freeze-out, their relic abundance does not depend on their annihilation cross section, but rather is a function of the wimpzilla’s production cross section. Furthermore, we want them to be sufficiently stable against decay and annihilation to significantly contribute to the present day matter density.

There are many ways to produce wimpzillas in the early Universe. Among the most studied is *gravitational production* at the end of inflation, resulting from the expansion of the background spacetime (for details on this and other scenarios see *e.g.* Ref. [339] and references therein).

Natural mass scales for wimpzillas include the inflaton or grand unified masses, which are usually assumed to be roughly 10^{11} GeV or 10^{16} GeV, respectively. Alternatively, D-matter provides a good candidate for wimpzillas with a somewhat larger mass [449]. The interaction cross sections with ordinary matter for such particles can vary from very weak to strong (in the latter case supermassive particles are sometimes called *simpzillas*).

A common motivation for superheavy dark matter comes from the observation of cosmic rays at ultra-high energies[16], above the so-called GZK (Greisen-Zatsepin-Kuzmin) cutoff [273, 506]. Above this cutoff, which occurs at $\sim 5 \times 10^{19}$ eV, protons interact at resonance with CMB photons with a center-of-mass energy nearly equal to the mass of the Δ -hadron (1.232 GeV). The cross section for this interaction is quite large, thus making the Universe opaque to ultra-high energy protons over cosmological distances ($\gtrsim 50$ Mega-parsecs). Since no astrophysical sources of ultra-high energy protons are known within this range, more exotic scenarios have been developed to account for these observed events. Such scenarios include ultra-high energy cosmic-ray production via

the decay or annihilation of superheavy dark matter particles, called top-down cosmic-ray models (see, for example, Refs. [113, 78, 444, 442, 111, 508, 161, 451]).

3.5 Collider Constraints

The constraints which can be placed on a dark matter candidate from collider experiments are highly model dependent in nature. It is, unfortunately, impossible to completely or simply describe the reach of colliders in their search for dark matter in any kind of general way. We will here, rather, review several of the most important collider searches which have been carried out for dark matter particles and for particles associated with a dark matter candidate.

3.5.1 Current collider constraints

- *Invisible Z width*

If a dark matter candidate is sufficiently light, Z bosons may decay invisibly to such particles with a non-zero branching fraction. Of course, there is a substantial background to such events, namely $Z \rightarrow \nu\bar{\nu}$ decays. Presently, to contribute less than one standard deviation to the measured neutrino contribution, the analysis of LEP2 finds that a decay width of $\Gamma_{Z \rightarrow XX} < 4.2$ MeV is required (X denotes a dark matter particle).

Similarly, single photon events can be an interesting search channel for light dark matter particles. At LEP2, the Standard Model background process for this signature is $e^+e^- \rightarrow Z \rightarrow \nu\bar{\nu}$ with an additional photon radiated off of the initial state. The total cross section for γZ production at LEP2 is less than 31 pb with a minimum 1 GeV transverse momentum cut for the photon. The contribution to this final state (single photon) from particle dark matter, in addition to $Z \rightarrow XX$ with an additional photon radiated off of the initial state, are t-channel dark matter producing processes in which a photon is radiated off of a charged propagator (a selectron in supersymmetry, for example).

- *Searches for new charged particles*

LEP2 has placed very stringent bounds on charged particles lighter than about 100 GeV. In e^+e^- colliders, cross sections for the direct pair production of charged particles are quite large, allowing for limits to be placed at or slightly below half of the center-of-mass energy of the collision. For LEP2, which reached a center-of-mass energy of 209 GeV, limits of 87-103 GeV have been placed for such particles; in particular for charginos ($m_{\chi^\pm} > 103$ GeV) and charged sleptons ($m_{\tilde{e}} > 99$ GeV, $m_{\tilde{\mu}} > 96$ GeV, $m_{\tilde{\tau}} > 87$ GeV) in supersymmetric models. If the LSP is only slightly less massive than the charged particle, however, this limit may be substantially lower [60, 3, 11, 293].

Limits on charged particles can only indirectly constrain dark matter, however. In supersymmetry, chargino masses and neutralino masses are,

in some models, related by the unification of gaugino masses. Although such a relationship is often assumed, it is quite possible that the pattern of gaugino masses is not so simple. If gaugino mass unification is assumed chargino limits can translate to neutralino mass limits of about half of the chargino mass limit ($m_{\chi^0} \gtrsim 50$ GeV). Without such a relationship, the LSP could be much lighter [308, 126].

- *Sneutrino limits*

Limits for charged sleptons can be used to indirectly limit the possible masses for sneutrinos beyond the invisible Z width constraints. Such a bound is the result of a basic SU(2) symmetry between the supersymmetry breaking masses of the left handed slepton and the sneutrino of a given lepton flavor. Limits somewhat lower than for charged particles ($m_{\tilde{\nu}} \gtrsim 85$ GeV) can be placed on sneutrinos if such theoretical assumptions are made [3, 11, 293].

- *Searches for colored particles*

Hadron colliders, such as the Tevatron, can place the strongest limits on colored particles (squarks and gluinos in supersymmetry or KK excitations of quarks and gluons in models with universal extra dimensions, for example). Such particles would most likely undergo a series of cascades upon decaying, possibly producing dark matter candidates among other particles. Combinations of squarks and gluinos are searched for using jets and missing energy signatures. This leads to exclusion contours in the squark and gluino mass plane.

In supersymmetry, the spectrum of neutralinos, charginos and sleptons lighter than the decaying squark/gluino is very important in placing limits on squark and gluino masses. Similar ambiguities are present in other models as well, such as universal extra dimensions, etc. Typically, limits of ~ 200 GeV are obtained for new colored particles, unless there exists an invisible final state particle with a mass close to the new colored particle's mass [4, 5, 6, 9, 419].

- *New gauge bosons*

Heavy gauge bosons appear in many models of particle physics beyond the Standard Model. Heavy charged gauge bosons (called W' 's) and heavy neutral gauge bosons (called Z' 's) have been excluded below about 600-800 GeV, depending on the details of the analysis [14, 8]. These limits assume that these particles have couplings equal to their Standard Model counterparts. If their couplings were smaller, the resulting limits could be considerably weaker. Electroweak precision measurements can also constrain heavy gauge bosons considerably (see below).

- *Higgs searches*

In supersymmetric models, the Higgs mass is increased from its tree level mass (below m_Z) by loop processes involving superparticles, most importantly top squarks. Current bounds on the (lightest) Higgs mass, therefore, constrain the masses of top squarks and other superparticles. Furthermore, if supersymmetry is manifest below 1 TeV, as is normally expected, the Higgs mass must be less than about 130 GeV, not very far above current limits from LEP2 ($m_h < 114.1$ GeV) [356, 357, 294, 295, 2, 10]. Note that this bound is somewhat lower for cases with very large values of $\tan\beta$.

Searches for charged Higgs bosons can also provide constraints on models of physics beyond the Standard Model. More sensitive, however, may be the impact of charged Higgs bosons in the branching fraction of $b \rightarrow s\gamma$.

- *Flavor changing neutral currents*

Many models of physics beyond the Standard Model introduce flavor changing neutral currents, often at tree level. To avoid the corresponding flavor constraints, either the masses of new particles involved must be quite large, or symmetries must be imposed to solve the “flavor problem”. For example, the squark and slepton mass matrices are flavor diagonal in the constrained MSSM (mSUGRA) scenario, thus suppressing such processes. Flavor changing neutral currents in models with universal extra dimensions have also been explored [134].

- $b \rightarrow s\gamma$

The branching fraction for $b \rightarrow s\gamma$ [133, 22, 7, 359, 45], measured at CLEO and BELLE, is of particular interest for supersymmetry and other beyond the Standard Model phenomenology. In many scenarios, the contributions to this process from new physics can add substantially to the Standard Model prediction. In particular, light charged Higgs bosons and/or charginos can be quite important for this decay [138, 401, 402]. In supersymmetry, the constraint is considerably stronger if $\mu < 0$, but also relevant for $\mu > 0$, especially for large values of $\tan\beta$. $b \rightarrow s\gamma$ is also an important constraint in models of universal extra dimensions [134].

- $B_s \rightarrow \mu^+\mu^-$

The branching fraction for $B_s \rightarrow \mu^+\mu^-$ is quite small in the Standard Model ($\simeq 3.5 \times 10^{-9}$) [34]. The contribution from supersymmetry scales as $\tan^6\beta$, and thus becomes quite large for models with large values of $\tan\beta$. In run I of the Tevatron, a value consistent with the Standard Model was found. The sensitivity of run II of the Tevatron to this quantity will be considerably greater.

- *The anomalous magnetic moment of the muon, $g_\mu - 2$*

In 2001, the E821 experiment at the Brookhaven National Laboratory reported a measurement of the muon’s magnetic moment which was 2.6 standard deviations from the Standard Model prediction [130]. Since then,

however, an important error in the theoretical calculation was discovered which reduced the significance of this anomaly to about 1.6 standard deviations [336, 337, 290, 115, 116]. With the reduction of statistical error which has been achieved more recently, the deviation from the Standard Model prediction of this measurement is again about 3σ using e^+e^- data (although the significance is somewhat less using τ decay data) [70, 174, 283, 316]. These measurements, although somewhat difficult to interpret, can be used to constrain TeV-scale particle physics beyond the Standard Model.

- *Electroweak precision measurements*

In addition to the useful direct particle searches at LEP2, the Tevatron and other experiments, impressively accurate electroweak measurements have been made. Various limits on the scale of new physics and associated particle masses have been inferred from these measurements. Given these constraints, models with universal extra dimensions are limited to the scale ~ 300 GeV or higher [35]. These measurements also yield particularly important bounds for models without a custodial SU(2) symmetry, such as many little Higgs models [169].

Together, these constraints can be very powerful, often providing very tight bounds for specific models. For example, in Fig. 14, we show the impact of collider and cosmological constraints on the constrained Minimal Supersymmetry Standard Model (or mSUGRA). We find that over the parameter space shown, constraints from LEP2 searches (Higgs, charginos and selectrons), along with $g_\mu - 2$ and relic density constraints, leave only a small region near $m_{1/2} \cong 300 - 400$ GeV and $m_0 \cong 80 - 150$ GeV. Although the power of these and other constraints is quite model dependent, they are often very useful in supersymmetry and other classes of models.

3.5.2 The reach of future collider experiments

- *Future reach of the Tevatron*

The reach of the Tevatron extends to higher energies than any other accelerator until the time at which the Large Hadron Collider (LHC) becomes operational. The range of masses which can be searched for colored particles (squarks, gluinos and KK quarks, for example), heavy gauge bosons and other new physics will be increased significantly at the Tevatron IIb [325, 9].

- *The Large Hadron Collider*

The Large Hadron Collider (LHC) is expected to begin operation around 2007 with proton-proton collisions at 14 TeV center-of-mass energy. A luminosity of 300 inverse femtobarns is expected to be achieved, making the prospects for discovering new physics at the LHC excellent. Numerous classes of models which provide interesting dark matter candidates will be

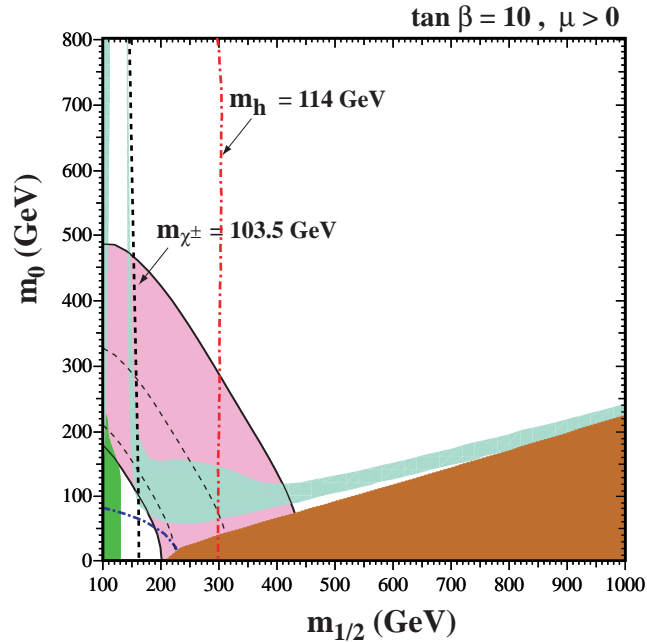


Figure 14: An example of the impact of collider (and cosmological) constraints on a model of particle dark matter [403]. The model shown is the constrained Minimal Supersymmetric Standard Model (cMSSM or mSUGRA) with $\tan \beta = 10$, $\mu > 0$ and $A_0 = 0$. The almost vertical lines represent the limits on chargino (left) and Higgs (right) masses from LEP2. The blue dot-dash curve in the bottom left corner follows the 99 GeV selectron mass contour, excluded by LEP2. In the dark red region in the lower right, the LSP is a stau and is not, therefore, a viable dark matter candidate. The green region in the lower left corner is excluded by the $b \rightarrow s\gamma$ constraint. The long and often narrow turquoise region provides a relic density of $0.1 \leq \Omega h^2 \leq 0.3$, near the observed quantity. The pink region extending over much of the lower left is the region within the 2σ range for $g_\mu - 2$. The two dashed curves within this region are the 1σ bounds.

tested at this very important experiment, searching at scales of up to several TeV. In addition to the Higgs boson(s), the LHC will be sensitive to most supersymmetry scenarios, models with TeV-scale universal extra dimensional, little Higgs models, etc.

For a few examples of studies which discuss the sensitivity of the LHC to new physics, see Refs.[44, 155, 176, 25, 26, 49, 297, 420, 107]. In Fig. 15, an example of such a study is shown [49]. It is interesting to note that in the region of the MSSM which is the most difficult to probe at the LHC, direct dark matter detection rates are very high [48].

- *Beyond the LHC*

After the LHC, other collider experiments are likely to follow. Although no specific post-LHC program is certain at this time, a 500-1000 GeV linear collider is a possibility, perhaps followed by a Very Large Hadron Collider (VLHC). These or other post-LHC colliders will, of course, have great value to particle dark matter studies [492, 67].

4 Experiments

4.1 Direct Detection Experiments

Direct detection experiments appear today as one of the most promising techniques to detect particle dark matter. The idea is very simple: if the galaxy is filled with WIMPs, then many of them should pass through the Earth, making it possible to look for the interaction of such particles with matter, e.g. by recording the recoil energy of nuclei, as WIMPs scatter off them [200, 266, 487].

The key ingredients for the calculation of the signal in direct detection experiments are the density and the velocity distribution of WIMPs in the solar neighborhood and the WIMP-nucleon scattering cross section. With this information, it is then possible to evaluate the rate of events expected in an experiment (*i.e.* WIMP-nucleon scattering events) per unit time, per unit detector material mass.

The rate is approximately given by

$$R \approx \sum_i N_i n_\chi \langle \sigma_{i\chi} \rangle, \quad (88)$$

where the index, i , runs over nuclei species present in the detector

$$N_i = \frac{\text{Detector mass}}{\text{Atomic mass of species } i}$$

is the number of target nuclei in the detector,

$$n_\chi \equiv \frac{\text{WIMP energy density}}{\text{WIMP mass}}$$

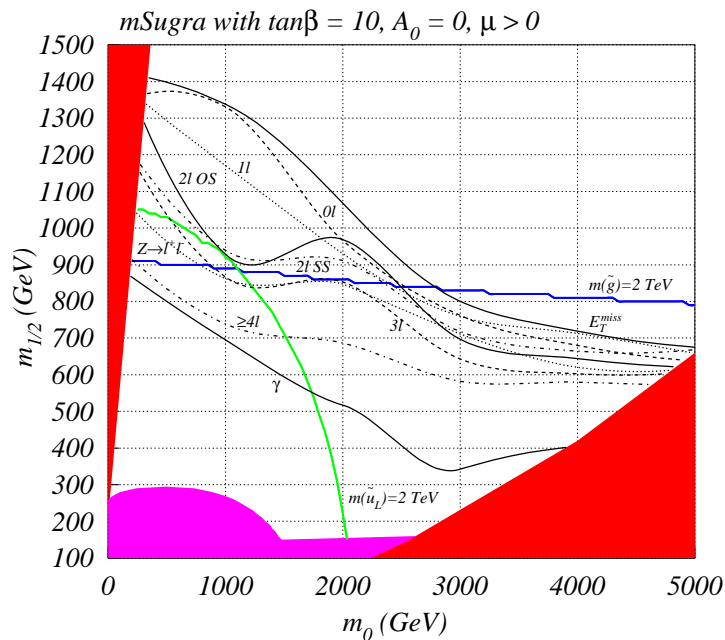


Figure 15: An example of the reach of the Large Hadron Collider (LHC) to new TeV-scale physics [49]. As a function of m_0 and $m_{1/2}$ in the mSUGRA (or constrained MSSM) scenario, with $\tan\beta = 10, A_0 = 0$ and positive μ , the reach is shown for a variety of channels: zero leptons ($0l$), one lepton ($1l$), leptons with opposite charge (OS), leptons with the same charge (SS), three leptons ($3l$), four or more leptons ($\geq 4l$), any number of leptons plus a photon (γ), at least two opposite sign leptons with the invariant mass within an optimized interval around the Z mass ($Z \rightarrow l^+ l^-$) and an “inclusive” missing transverse energy channel. Also shown are the 2 TeV up squark and 2 TeV gluino mass contours. The red regions are excluded by theoretical constraints, while the magenta region is excluded experimentally. 100fb^{-1} of integrated luminosity is assumed.

is the local WIMP density and $\langle \sigma_{i\chi} \rangle$ is the cross section for the scattering of WIMPs off nuclei of species i , averaged over the relative WIMP velocity with respect to the detector. For a more through discussion see, *e.g.*, Ref. [319].

4.1.1 Scattering classifications

The type of scattering processes considered can be classified by two important characteristics: elastic or inelastic scattering and spin-dependent or spin-independent scattering.

- Elastic and Inelastic Scattering

The elastic scattering of a WIMP off of a nucleus in a detector is simply the interaction of the WIMP with a nucleus as a whole, causing it to recoil, ideally often enough to measure the recoil energy spectrum in the target. With a Boltzman velocity distribution of WIMPs, centered at 270 km/s, the spectrum of recoils is exponential with typical energies of $\langle E \rangle \sim 50$ keV. Current experiments can detect recoils of considerably lower energy, as low as 1-10 keV.

Inelastic scattering, on the other hand, is not observed by the recoil of a target nuclei. Instead, the WIMP interacts with orbital electrons in the target either exciting them, or ionizing the target. Alternatively, the WIMP could interact with the target nuclei leaving it in an excited nuclear state. This process leaves the signature of a recoil followed by the emission of a photon a nanosecond, or so, later [210]. Such signatures have to compete with backgrounds of natural radioactivity, however.

- Spin-Dependent and Spin-Independent Scattering

WIMP scattering off of nuclei is commonly discussed in the context of two classes of couplings. First, axial-vector (spin dependent) interactions result from couplings to the spin content of a nucleon. The cross sections for spin-dependent scattering are proportional to $J(J+1)$ rather than the number of nucleons, so little is gained by using heavier target nuclei. For scalar (spin-independent) scattering, however, the cross section increases dramatically with the mass of the target nuclei, and typically dominates over spin-dependent scattering in current experiments which use heavy atoms as targets.

It should be pointed out that a WIMP which is not a Majorana particle could also scatter by vector interactions. Heavy Dirac neutrinos or MSSM sneutrinos are examples of particles which would scatter in this way. Neutralinos and Kaluza-Klein dark matter do not have such couplings, however.

For more on scalar, axial-vector and vector WIMP-nucleon scattering, see Appendix C.

4.1.2 Experimental Efforts

More than 20 direct dark matter detection experiments are either now operating or are currently in development. In these many experiments, numerous techniques have been developed to measure the nuclear recoil produced by dark matter scattering. Some of these methods include the observation of scintillation (used by DAMA, ZEPLIN-I, NAIAD, LIBRA), photons (used by CREST and CUORICINO) and ionization (used by HDMS, GENIUS, IGEX, MAJORANA and DRIFT). Some experiments use multiple techniques, such as CDMS and Edelweiss which use both ionization and photon techniques, CRESST-II and ROSEBUD which use both scintillation and photon techniques and XENON, ZEPLIN-II, ZEPLIN-III and ZEPLIN-MAX, which use both scintillation and ionization techniques.

The use of such a large array of techniques and technologies is important not only to accelerate the progress of the field, but also to vary the systematic errors from experiment to experiment, allowing for a critical assessment of a positive signal.

Some experiments are also attempting to separate WIMP signatures from background by looking for an annual modulation in their rate. Such an effect would arise due to the Earth's annual motion around the Sun, resulting in a relative velocity relative to the galaxy's frame of reference [199]. Under this effect, the Earth's velocity is given by

$$v_E = 220 \text{ km/s} \left(1.05 + 0.07 \cos(2\pi(t - t_m)) \right), \quad (89)$$

where t_m is roughly the beginning of June and the times are in units of years. The result of this effect is a $\cong 7\%$ variation in the WIMP flux and direct detection rate over the course of the year. Since this variation is quite small, many events are needed to identify such a signature. For more on this technique and the status of direct detection techniques, see section 5.

4.2 Gamma-Ray Experiments

In addition to detecting WIMPs directly, efforts are underway to attempt to observe the products of WIMP annihilations in the galactic halo, the center of the Sun or other regions. These annihilation products include neutrinos, positrons, anti-protons and gamma-rays.

To observe cosmic gamma-rays directly, observations must be made from space. This is because in the energy range we are most interested (GeV to TeV), photons interact with matter via e^+e^- pair production, which leads to an interaction length of approximately 38 g cm^{-2} , which is much shorter than the thickness of the Earth's atmosphere (1030 g cm^{-2}). Thus, at the energies we are considering, gamma-rays cannot reach ground based telescopes. Efforts have been developed, nevertheless, to observe gamma-rays indirectly with ground based experiments. In this section, we discuss the status of both ground and space-based gamma-ray telescopes.

4.2.1 Ground-based telescopes

When photons interact in the atmosphere, they produce an electromagnetic cascade and thus a shower of secondary particles, allowing ground-based telescopes to *indirectly* observe gamma-rays through the detection of secondary particles and the Cerenkov light originating from their passage through the Earth’s atmosphere.

It was P. Blackett (winner of the Nobel prize in 1948) who first realized the possibility of detecting Cerenkov light from cosmic air showers. This realization was experimentally confirmed by W. Galbraith and J. Jelley (1953). Cosmic gamma-rays can be difficult to observe in this way, however, as most of the observed Cerenkov light is due to cosmic-ray induced showers with isotropic arrival directions. For detecting gamma-ray showers, an excess above the isotropic background of cosmic rays must be seen in the direction of a source. To accomplish this, the rejection of cosmic ray showers is of crucial importance.

To distinguish between cosmic ray and gamma-ray induced air showers, the observed Cerenkov light is compared with numerical simulations of atmospheric showers (see Fig. 16). Apart from the difficulties in the treatment of interactions at very high energies, numerical simulations are complicated by uncertainties associated with the density profile of the atmosphere and the Earth’s magnetic field. Nevertheless, reliable codes for simulating atmospheric showers exist on the market, for example CORSIKA and AIRES (see *e.g.* Knapp *et al.* [335]).

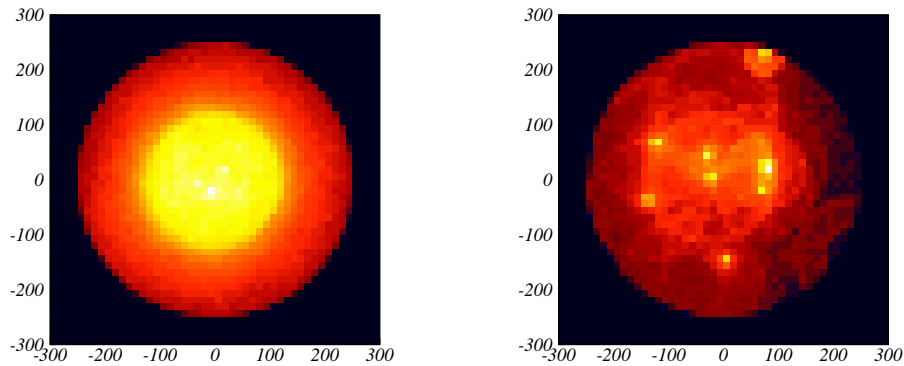


Figure 16: Simulations of Cerenkov light from electromagnetic cascades initiated by a 1 TeV photon (left) and a 1 TeV proton (right). The figures show the distribution of light to the ground in a $600 \times 600 \text{ m}^2$ area. Figures kindly provided by I. Perez.

The methods of collecting Cerenkov light are quite varied, ranging from telescopes (and array of telescopes) to converted solar arrays. We show in table 6 a list of existing ground based experiments for the detection of gamma-rays. These include imaging and non-imaging Air Cerenkov telescopes, reconverted

VHE Gamma-Ray Sources

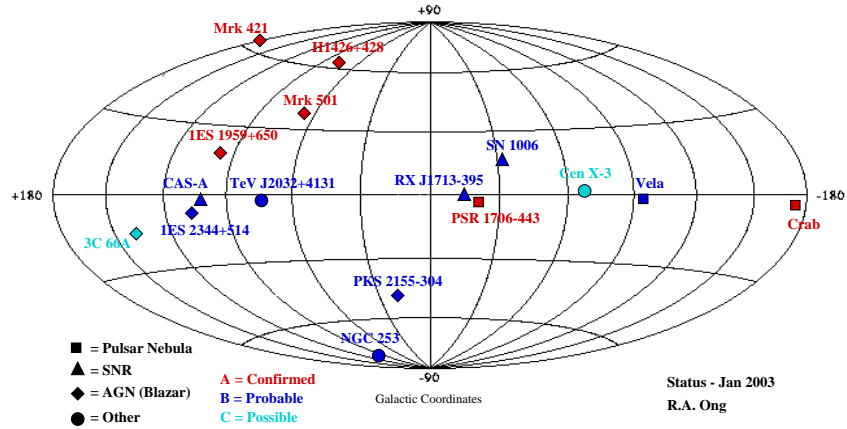


Figure 17: Sky Map for sources of very high-energy (TeV) gamma-rays, as of January 2003 (Ref. [406]).

solar arrays as well as experiments which detect secondary particles produced in showers.

The first observation of Cerenkov light due to gamma-ray emission from an astrophysical source was the detection of the Crab Nebula (which today is regarded as the “standard candle” at these energies) with the Whipple Observatory 10m reflector [490]. Currently, only six TeV gamma-ray sources have been *confirmed*, above 10 GeV, having been detected by multiple experiments at a high significance level (red symbols in Fig. 17). Eight sources are *probable*, *i.e.* detected at high significance by at least one group (blue symbols), and two are “possible” (light blue symbols, see Ref. [406] for more details).

Although only a few TeV gamma-ray sources have been confirmed, many more could be detected in next generation experiments. Among these experiments:

- MAGIC is a 17m imaging air Cerenkov telescope recently completed on the island of La Palma [511]. It has already started taking data.
- CANGAROO-III is an array of four 10 m Cerenkov telescopes being constructed in Woomera, Australia [512]. It should start taking data in 2004.
- HESS consists of four 12m diameter Cerenkov telescopes, at a site in the Gamsberg area of Namibia [513]. The telescopes are operational and started taking data.

<i>Imaging</i>				
Group	Location	Telescope(s) Num. \times Apert.	Threshold (TeV)	Ref.
Whipple	Arizona, USA	10 m	0.4	[140]
Crimea	Ukraine	6 \times 2.4 m	1	[484]
SHALON	Tien Shen, Ru	4 m	1.0	[398]
CANG-II	Woomera, Au	10 m	0.5	[289]
HEGRA	La Palma, Es	5 \times 5 m	0.5	[172]
CAT	Pyrenées, Fr	4.5 m	0.25	[267]
TACTIC	Mt. Abu	10 m	0.3	[97]
Durham	Narrabri	3 \times 7 m	0.25	[143]
7TA	Utah, USA	7 \times 2 m	0.5	[501]

<i>Non-Imaging</i>				
Group	Location	Type	Telescopes	Ref.
Potchefstroom	South Africa	Lateral Array	4	[180]
Pachmarhi	India	Lateral Array	25	[98]
Beijing	China	Double	2	[502]

<i>Solar Arrays</i>				
Group	Location	Heliostats Now (future)	Threshold GeV	Ref.
STACEE	Albuq., USA	32 (48)	180	[407]
CELESTE	Themis, Fr	40 (54)	50 \pm 10	[181]
Solar-2	Barstow, USA	32 (64)	20	[509]

<i>Non - air Cerenkov</i>				
Group	Location	Telescope	Threshold TeV	Ref.
Milagro	Fenton Hill, US	Water Cher.	0.5-1.0	[503]
Tibet HD	Tibet	Scintillators	3	[30]

Table 6: Atmospheric Cerenkov Imaging Observatories *circa* September 2003.

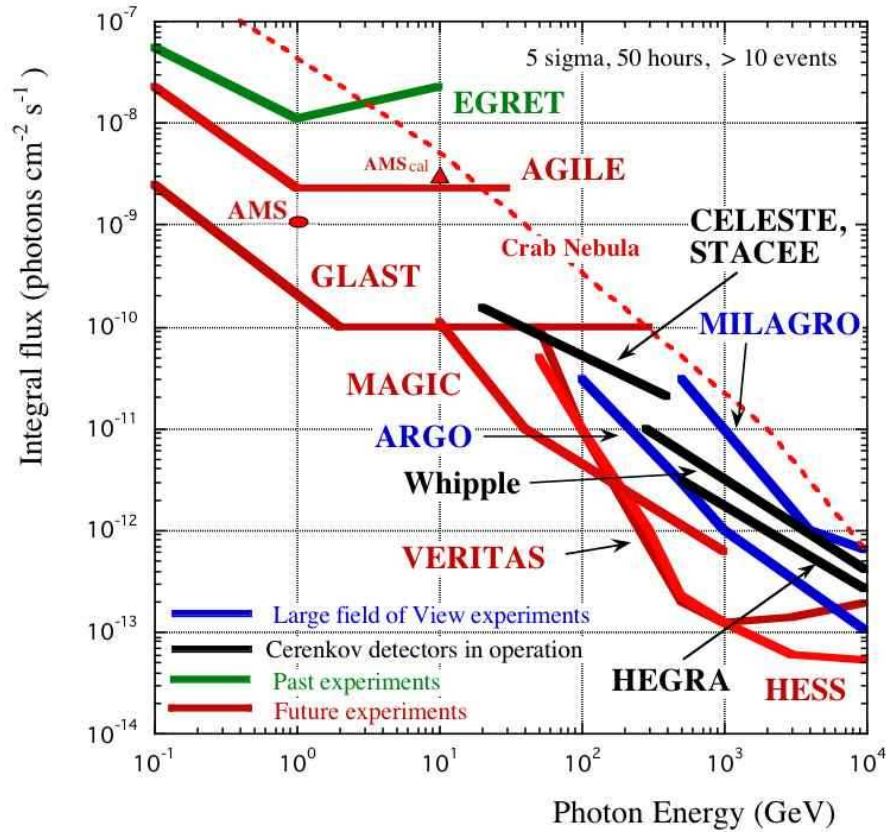


Figure 18: Sensitivity of present and future detectors in gamma-ray astrophysics (from Ref. [386]).

- VERITAS is an array of 7 telescopes in construction on Kitt Peak in Arizona, USA [514]. A preliminary version, VERITAS-4, with 4 telescopes should be operative around 2006.

4.2.2 Space-based telescopes

The first high-energy (above GeV) gamma-ray space telescopes was EGRET (the Energetic Gamma-Ray Experiment Telescope), onboard the Compton gamma-ray observatory. Launched in 1991, EGRET has observed the universe in a range of energies extending up to approximately 30 GeV, amassing a large catalog of observed gamma-ray sources, although around 60% of these sources remain unidentified.

The next space-based gamma-ray observatory will be GLAST (Gamma-ray Large Area Space Telescope), which is scheduled for launch in 2007. As for its predecessor, GLAST will detect gamma-rays by recording the characteristics of

e^+e^- pairs produced in the interaction of the incident gamma-ray with a dense layer of tungsten. GLAST's effective area to gamma-rays will be a full square meter, considerably larger than with EGRET. GLAST will have an angular resolution on the order of arcminutes, compared to the degree level with EGRET (energy resolution varies with energy for both experiments). Unlike EGRET, GLAST will be sensitive to gamma-rays up to several hundred GeV in energy.

GLAST is expected to be complementary to ground-based telescopes due to the lower range of energies observed, larger field of view, and higher duty cycle. We show in Fig.18 the sensitivity of some of the present and next generation ground-based and space-based gamma-ray experiments. We will use such information when discussing the prospects for indirect detection of particle dark matter.

4.3 Neutrino Telescopes

In addition to gamma-rays, neutrinos can be produced in the annihilations of dark matter particles. In this section, we review the status of high-energy neutrino telescopes, in particular, large volume Cerenkov detectors such as AMANDA, ANTARES and IceCube.

Neutrinos are considerably more difficult to observe than gamma-rays due to their weak interactions with ordinary matter. Neutrinos are not easily absorbed, however, allowing for their observation in underground, low background, experiments. In the GeV-TeV energy range, neutrinos are most easily observed by their “muon tracks” produced in charged current interactions inside of or nearby the detector volume. These muons travel through the detector emitting Cerenkov light which allows their trajectory to be reconstructed.

For a cosmic neutrino flux, $d\Phi_\nu/dE_\nu$, the rate of muon tracks in a detector is given by

$$\text{rate} = \int_{E_\mu^{\text{thr}}} dE_\nu \int_0^{1 - \frac{E_\mu^{\text{thr}}}{E_\nu}} dy A(E_\mu) P_\mu(E_\nu, y; E_\mu^{\text{thr}}) \frac{d\Phi_\nu}{dE_\nu}, \quad (90)$$

where E_μ^{thr} is the muon threshold energy of the experiment (generally between 10 and 100 GeV), $A(E_\mu)$ is the effective area of the detector, typically in the range of 0.01 to 1.0 square kilometers (for further details and numerical values, see *e.g.* Ref. [54]) and $P_\mu(E_\nu, y; E_\mu^{\text{thr}})$ is the probability that a neutrino of energy E_ν interacts with a nucleon producing a muon of energy $E_\mu \equiv (1 - y)E_\nu$ above the detector threshold energy. As one would expect, this probability depends on the muon range, $R(E_\mu, E_\mu^{\text{thr}})$, *i.e.* the distance travelled by muons before their energy drops below E_μ^{thr} . The function $P_\mu(E_\nu, y; E_\mu^{\text{thr}})$ is thus given by

$$P_\mu(E_\nu, y; E_\mu^{\text{thr}}) = N_A R(E_\mu, E_\mu^{\text{thr}}) \frac{d\sigma_{CC}^{\nu N}(E_\nu, y)}{dy} \quad (91)$$

where $N_A = 6.022 \times 10^{23} g^{-1}$ is Avogadro's number and $d\sigma_{CC}^{\nu N}(E_\nu, y)/dy$ is the differential cross section for neutrino–nucleon charged–current scattering.

The cross-section used in Eq. 91 is described in high-energy physics textbooks, but carries uncertainties due to our limited knowledge of parton densities. It can be expressed as

$$\sigma^{(\bar{\nu})N}(s) = \int_0^1 dx \int_0^1 dy \frac{d^2\sigma^{(\bar{\nu})N}}{dxdy} \quad (92)$$

with

$$\frac{d^2\sigma^{(\bar{\nu})N}}{dxdy} = \frac{G_F^2 s}{2\pi} (1 + xys/M_W^2)^{-2} [(1-y)F_2^{(\bar{\nu})} + y^2 x F_1^{(\bar{\nu})} \pm y(1-\frac{y}{2})x F_3^{(\bar{\nu})}] \quad (93)$$

where $F_i = F_i(x, Q^2 = xys)$ are the structure functions, $s = 2M_N E_{\bar{\nu}}$ and $G_F = 1.1663 \times 10^{-5} \text{ GeV}^{-2}$. For details regarding the calculation of high-energy neutrino-nucleon interactions including structure functions, see Ref. [246].

The muon range, $R(E_\mu, E_\mu^{\min})$, appearing in Eq. 91 follows from the energy-loss equation [281]

$$-dE_\mu/dX = \alpha_\mu(E_\mu) + \beta_\mu(E_\mu) E_\mu, \quad (94)$$

with X being the thickness of matter traversed by the muon, and the quantities $\alpha_\mu(E_\mu)$ and $\beta_\mu(E_\mu)$ are the ionization loss and the fractional energy loss coefficients, respectively. Integrating this result, we get the muon range

$$R(E_\mu, E_\mu^{\min}) \equiv X(E_\mu^{\min}) - X(E_\mu) = \frac{1}{\beta_\mu} \ln \frac{\alpha_\mu + \beta_\mu E_\mu}{\alpha_\mu + \beta_\mu E_\mu^{\min}}. \quad (95)$$

We adopt here the following values for the coefficients: $\alpha_\mu = 2.0 \times 10^{-3} \text{ GeV (cm we)}^{-1}$ ($\text{cmwe} \equiv g/\text{cm}^2$) and $\beta_\mu = 6.0 \times 10^{-6} \text{ (cm we)}^{-1}$ [253].

We pass now to a brief description of existing and future neutrino telescopes, focusing on kilometer-scale experiments. The key idea is to detect muons, originating from neutrino fluxes as discussed above, building large arrays of photo-multipliers deep in the ice, in a lake or in the sea, to search for the Cerenkov light they are expected to emit as they move through these media.

The early pioneering effort made by the DUMAND collaboration [274] was followed by the deployment of the Lake Baikal experiment [56] and of AMANDA [32, 33] at the South Pole. Although these experiments have observed neutrinos produced in the Earth's atmosphere, they have not, thus far, identified any extra-terrestrial neutrinos.

AMANDA, with approximately 50,000 square meters of effective area (at trigger level) and a 30 GeV muon energy threshold, has been taking data for several years in its current configuration. ANTARES [43, 112], currently under construction in the Mediterranean, will have a similar effective area and a lower

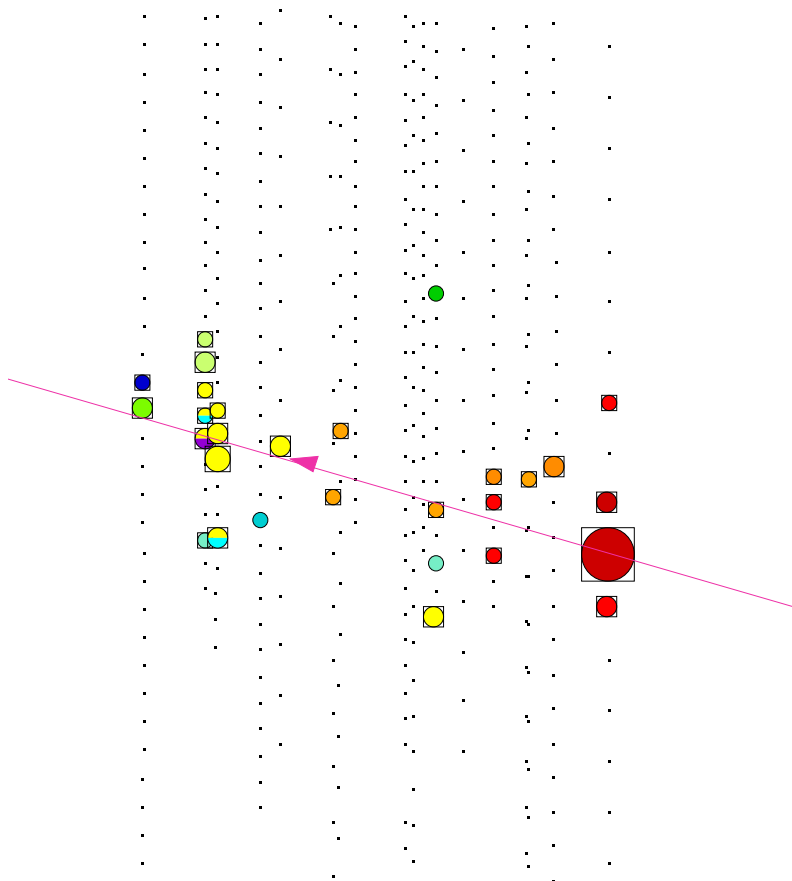


Figure 19: A muon neutrino event in AMANDA. Shown is the central part of the detector. The colorscale and symbol size correspond to hit time and amplitude [499].

energy threshold of about 10 GeV. Unlike with experiments at the South Pole, ANTARES will be sensitive in the direction of the galactic center.

IceCube[18, 19], beginning construction in 2005, and scheduled for completion in 2010, will be the first kilometer scale high-energy neutrino telescope. Using technology similar to AMANDA, IceCube will be considerably more sensitive to dark matter annihilations than current experiments. Even larger, and perhaps lower threshold, experiments may be needed beyond IceCube to further search for evidence of dark matter annihilations. For a review of high-energy neutrino astronomy, see Refs. [284, 353].

4.4 Positron and Anti-Proton Experiments

Evidence for dark matter annihilations may also be observed in the spectra of cosmic positrons or anti-protons. Unlike gamma-rays and neutrinos, however, these charged particles do not point to their source due to the presence of galactic magnetic fields. Here we describe some of the experiments most important to these measurements.

The HEAT (High-Energy Antimatter Telescope) experiment made its first balloon flight in 1994-1995, measuring the spectrum of positrons between 1 and 30 GeV [64]. The results of this flight were very interesting, as they indicated an excess in the positron flux peaking at about 9 GeV and extending to higher energies. This excess could be a signature of dark matter annihilation in the local galactic halo (see section 6.5). A second HEAT flight in 2000 confirmed this observation [162, 163].

The BESS (Balloon borne Experiment Superconducting Solenoidal spectrometer) experiment has had several successful balloon flights since 1993, providing the most detailed measurements of the cosmic anti-proton spectrum to date in the range of about 200 MeV to 3 GeV [408, 370]. Above this energy, up to about 40 GeV, the CAPRICE experiment provides the best anti-proton measurements [121]. There appears to be a mild excess in the anti-proton spectrum in the hundreds of MeV range, although it is very difficult to assess this result with any certainty.

In the future, the experimental sensitivity to the cosmic positron and anti-proton spectra is likely to improve a great deal. Perhaps as early as 2005, the satellite borne PAMELA experiment, will begin its mission, measuring the spectra of both cosmic positrons and anti-protons with considerably improved precision. The primary objective of PAMELA is to measure the cosmic anti-proton spectrum in the range of 80 MeV to 190 GeV and the cosmic positron spectrum in the range of 50 MeV to 270 GeV, far beyond the energies measured by HEAT, BESS or CAPRICE. In Fig. 20, we show the projected sensitivity of PAMELA to cosmic positrons (left) and anti-protons (right). The results are shown assuming a contribution from annihilating neutralino dark matter. It is clear that PAMELA will measure these spectra to far greater precision than previous experiments, especially at high energies (above ~ 10 GeV).

AMS (the Alpha Magnetic Spectrometer) will considerably refine the measurement of the positron spectrum in its next manifestation, called AMS-02,

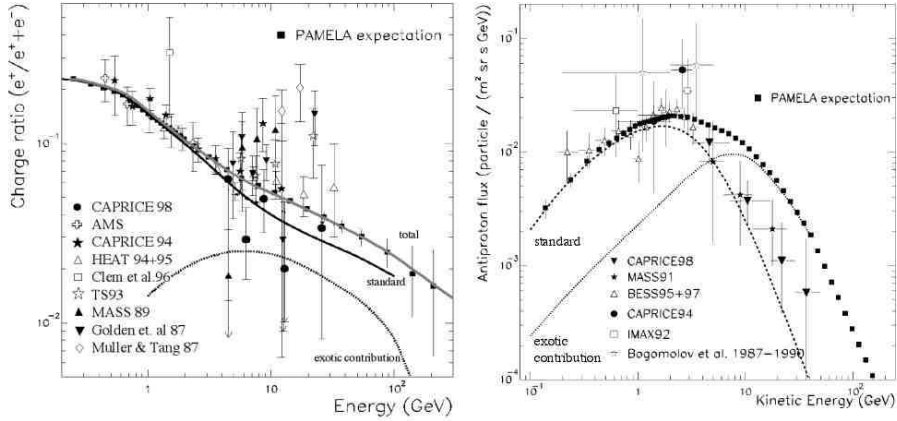


Figure 20: The projected ability of the PAMELA experiment to measure the spectra of cosmic positrons (left) and anti-protons (right). A contribution from annihilating neutralino dark matter is included in the spectra shown. Notice, in comparison to the measurements made by HEAT, CAPRICE, BESS and other experiments, the dramatic improvement in precision. Also note the reach to higher energies made possible with PAMELA. From Ref. [417].

onboard the International Space Station [66]. AMS-02, with a $5000 \text{ cm}^2 \text{ sr}$ aperture and a 1000 day duration, will provide exceptional precision in measuring the spectrum of cosmic positrons.

4.5 Observations at Radio Wavelengths

Observations at radio wavelengths belong to the realm of “classical” astronomy. Radio emission from the galactic halo, particularly from the galactic center, can provide a valuable probe of particle dark matter.

Electrons and protons produced in dark matter annihilations in the Galactic Center region will emit synchrotron radiation (at radio wavelengths) as they propagate through the galactic magnetic fields (see section 6.2).

The observed Sgr A* (Galactic Center) radio emission could be explained in terms of synchrotron radiation emitted by shock-accelerated electrons (for more details see Ref. [360] and references therein).

Rather than reviewing the subject of radio observations of the galactic halo, we refer to Cane (Ref. [137]) and to Brown (Ref. [131]), which also includes an interesting discussion of the absorption of radio emission at different wavelengths. A complete catalog of observations of the Galactic center at all frequencies, and in particular at radio wavelengths, can be found in Ref. [392]. Additional information on specific measurements can be found in Refs. [175, 31, 352].

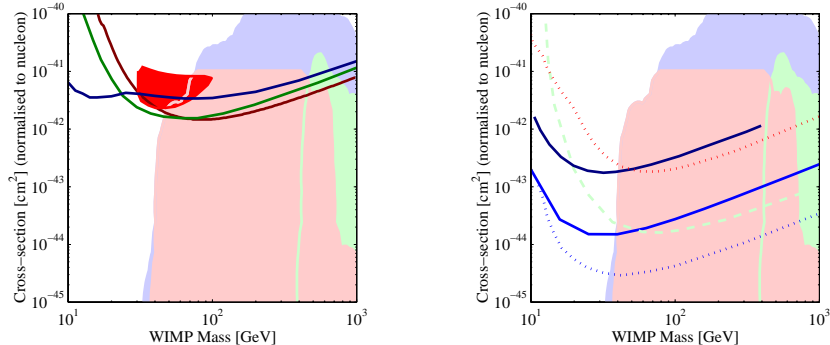


Figure 21: Current (left) and future (right) sensitivities of direct detection experiments. In the left frame, from top to bottom along the right side of the figure, the current limits from the CDMS, ZEPLIN-I and Edelweiss experiments are shown. The filled region near 30-100 GeV and 10^{-41} cm^2 is the parameter space favored by the DAMA experiment. In the right frame, from top to bottom along the right side of the figure, the projected reach of the GENIUS test facility (solid), CRESST-II (dots), CDMS-Soudan (solid), Edelweiss-II (dashed) and ZEPLIN-MAX (dots) are shown. In each frame, as filled regions, the space of models predicted by supersymmetry are shown [258]. The narrow region along the right side of the figure represents higgsino-like models, the region that reaches to the top of the figure represents mixed higgsino-gaugino models and the largest region represents gaugino-like models. These figures were made using the interface found at <http://dendera.berkeley.edu/plotter/entryform.html>.

5 Direct Detection

Many direct detection experiments have already produced quite strong limits on the elastic scattering cross section with protons or neutrons of potential dark matter candidates. Furthermore, experiments in the coming years will improve on current limits by several orders of magnitude making the prospects for discovery very great.

Presently, the best direct detection limits come from the CDMS, Edelweiss and ZEPLIN-I experiments, shown in the left frame of Fig. 21. These limits are for spin-independent (scalar) interactions. With modern experiments, which use very heavy target nuclei, spin-dependent scattering experiments are not as sensitive to most dark matter candidates.

Also shown in the left frame of Fig. 21 is the region in which the DAMA experiment claims a discovery (see *e.g.* Ref. [88] for a recent review). DAMA, located at the INFN laboratories under the Gran Sasso mountain in Italy and consisting of high purity NaI crystals, has reported an annual modulation of their event rate consistent with the detection of a WIMP with a mass of approximately 60 GeV and a scattering cross section on of the order of 10^{-41} cm^2 .

Other experiments, such as EDELWEISS [71] and CDMS [21] have explored the parameter space favored by DAMA without finding any evidence of dark matter. A recent model independent analysis has shown that it is difficult to reconcile the DAMA result with other experiments [349] (see also Ref. [478]) although it may still be possible to find exotic particle candidates and halo models which are able to accommodate and explain the data from all current experiments (for example, see Refs. [422, 247, 456, 472]).

Theoretical and experimental results on direct detection are usually obtained under some simplifying assumptions on the dark matter profile. In particular, an isothermal profile is often assumed, with $\rho \propto r^{-2}$ (thus, with a flat rotation curve), a local density of $\rho_0 = 0.3 \text{ GeV cm}^{-3}$, and a Maxwell-Boltzmann velocity distribution with a characteristic velocity of $v_0 = 270 \text{ km s}^{-1}$. Uncertainties in the density and velocity distribution of dark matter lead to the enlargement of the allowed region in the cross section-mass plane shown in Fig. 21, however, extending the mass range up to $\sim 250 \text{ GeV}$ and the cross section range down to $\sigma_{\chi-n} \sim 10^{-7} \text{ pb}$ [69, 129]. If this results were confirmed, it could explain the discrepancy between the observational findings of different experiments. Unfortunately, subsequent analyses lead to different results (see in particular Refs. [160, 272]), leaving the experimental situation unclear.

Nevertheless, the DAMA collaboration (whose raw data are not publicly available) insists on the compatibility of their result with null searches of other experiments [88], questioning specific experimental issues like rejection procedures and energy scale determination.

Next generation experiments should clarify the experimental situation, thanks to the large improvement expected in sensitivity, around two orders of magnitude in scattering cross section for EDELWEISS II and even more for ZEPLIN-MAX (See Fig. 21, generated using the *dark matter limit plot generator* at <http://dendera.berkeley.edu/plotter/entryform.html>).

In Fig. 22 we show the current constraints on neutralino dark matter in different supersymmetric scenarios. Shades paler than in the legend denote a value of the muon anomalous magnetic moment outside of the 2σ range [283] $8.1 \times 10^{-10} < \delta_\mu^{\text{susy}} = \delta_\mu^{\text{exp}} - \delta_\mu^{\text{SM}} < 44.1 \times 10^{-10}$ (see Ref. [94] for more details). Future generation detectors will probe a wide portion of the supersymmetric parameter space and will give important insights into the nature of dark matter particles. The $B^{(1)}$ particle (KK dark matter) should have a scattering cross section with nucleons in the range of 10^{-10} – 10^{-12} pb , depending on its mass and on the mass difference with KK quark states [447].

6 Indirect Detection

Indirect detection of dark matter is the technique of observing the radiation produced in dark matter annihilations. The flux of such radiation is proportional to the annihilation rate, which in turn depends on the square of the dark matter density, $\Gamma_A \propto \rho_{DM}^2$. Therefore, the “natural” places to look at, when searching for significant fluxes, are the regions where large dark matter densities

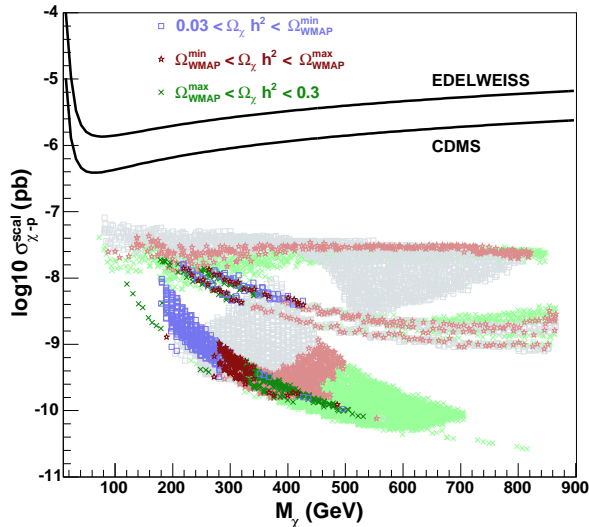


Figure 22: Current experimental sensitivity of WIMP direct detection experiments. Shown are the upper limits set by EDELWEISS [71] and CDMS at Soudan [20]. For comparison we also show predictions for different supersymmetric scenarios (see text). Figure kindly provided by E. Nezri.

accumulate. We will also refer to these regions or objects as *amplifiers*.

Dense regions of the galactic halo, such as the galactic center, may be excellent amplifiers for the purposes of detecting gamma-rays or neutrinos. Other astrophysical objects, such as the Sun or the Earth, could also act as amplifiers for dark matter annihilations by capturing dark matter particles as they lose energy through scattering with nucleons in the interiors of these objects. Only neutrinos can escape these dense objects, however. Annihilation products which are charged move under the influence of magnetic fields making it impossible to consider point sources of such radiation. Despite this, observations of cosmic positrons and anti-protons can be valuable tools in searching for particle dark matter.

In this section, we compare the predictions for gamma-ray, synchrotron, neutrino, positron and anti-proton fluxes from dark matter annihilation with current experimental data and with the expected sensitivities of future experiments. We will show that by using these techniques, it is possible to constrain dark matter models and, in the future, potentially detect the presence of particle dark matter.

6.1 Gamma-rays and neutrinos from the Galactic center

One of the most interesting regions for the indirect detection of dark matter is the galactic center, where, according to the results of numerical simulations, the dark matter density profile is expected to grow as a power-law, $\rho \propto r^{-\alpha}$. The possible values of α , as well as alternative density profiles, have been discussed in chapter 2. Also recall from chapter 2 that an additional enhancement of the density in this region could result from the process of adiabatic accretion onto the supermassive black hole at the galactic center.

Gamma-ray emission from the Galactic center has been discussed in the past by numerous authors (see *e.g.* Bouquet, Salati and Silk [128], Stecker [461], Berezhinsky *et al.* [75], Bergstrom, Ullio and Buckley [80] for neutralinos, Bertone, Servant and Sigl [93] for $B^{(1)}$ particles, Bertone and Sigl and Silk [92] for the case of a density spike at the galactic center). Here, we will review these calculations and arguments for evaluating the prospects for the indirect detection of dark matter near the Galactic center with present and next-generation experiments.

The flux of dark matter annihilation products is proportional to the number of annihilations per unit time, per unit volume, $\propto \sigma v n^2(r) \equiv \sigma v \rho^2(r)/m_{\text{DM}}^2$, where $n(r)$ and $\rho(r)$ are the number and the mass density of a dark matter particle, respectively. m_{DM} is the dark matter particle's mass and σv is its annihilation cross section multiplied by velocity. r is the distance from the galactic center. The flux is also proportional to the spectrum of secondary particles of species, i , per annihilation, dN_i/dE . The flux observed is found by integrating the the density squared along the line-of-sight connecting the observer (the Earth) to the Galactic center . Including all factors, the observed flux can be written as

$$\Phi_i(\psi, E) = \sigma v \frac{dN_i}{dE} \frac{1}{4\pi m_{\text{DM}}^2} \int_{\text{line of sight}} ds \rho^2(r(s, \psi)), \quad (96)$$

where the index i denotes the secondary particle observed (in this section, γ -rays and neutrinos) and the coordinate s runs along the line of sight, in a direction making an angle, ψ , from the direction of the galactic center. If the dark matter particle is not its own anti-particle (particle-antiparticle annihilation), Eq. 96 is reduced by a factor of 2.

In order to separate the factors which depend on the halo profile from those which depend only on particle physics, we introduce, following Ref. [80], the quantity $J(\psi)$:

$$J(\psi) = \frac{1}{8.5 \text{ kpc}} \left(\frac{1}{0.3 \text{ GeV/cm}^3} \right)^2 \int_{\text{line of sight}} ds \rho^2(r(s, \psi)). \quad (97)$$

We define $\bar{J}(\Delta\Omega)$ as the average of $J(\psi)$ over a spherical region of solid angle, $\Delta\Omega$, centered on $\psi = 0$. The values of $\bar{J}(\Delta\Omega = 10^{-3} \text{ str})$ are shown in the last column of table 7 for the respective density profiles.

We can then express the flux from a solid angle, $\Delta\Omega$, as

$$\Phi_i(\Delta\Omega, E) \simeq 5.6 \times 10^{-12} \frac{dN_i}{dE} \left(\frac{\sigma v}{\text{pb}} \right) \left(\frac{1 \text{ TeV}}{m_{\text{DM}}} \right)^2 \bar{J}(\Delta\Omega) \Delta\Omega \text{ cm}^{-2} \text{ s}^{-1}. \quad (98)$$

	α	β	γ	R (kpc)	$\bar{J}(10^{-3})$
Kra	2.0	3.0	0.4	10.0	2.166×10^1
NFW	1.0	3.0	1.0	20	1.352×10^3
Moore	1.5	3.0	1.5	28.0	1.544×10^5
Iso	2.0	2.0	0	3.5	2.868×10^1

Table 7: Parameters of some widely used density profiles and corresponding value of $\bar{J}(10^{-3} \text{ str})$. For more on halo profiles, see chapter 2.

6.1.1 Prospects for Neutralinos

To study the detectability of gamma-ray fluxes from neutralino annihilations, extensive scans of the MSSM are conducted, retaining only the small minority of models which are consistent with accelerator and cosmological constraints. We show in Fig. 23 the expected gamma-ray fluxes from the Galactic center for neutralino dark matter, considering an NFW halo profile. To adapt this spectrum to another profile, simply scale the flux by the value of $\bar{J}(\Delta\Omega = 10^{-3} \text{ str})$ found in table 7. In Fig. 23, all continuum processes are included (typically dominated by annihilations to heavy quarks and gauge bosons for neutralino annihilation). Shown for comparison are the limit from EGRET and the projected reach of GLAST. For fairly heavy neutralinos, ACTs can also be effective.

In addition to continuum gamma-ray emission, neutralinos can annihilate to mono-energetic gamma-ray lines via the processes $\chi\chi \rightarrow \gamma\gamma$ and $\chi\chi \rightarrow \gamma Z$ [433]. Such a line, if observed, would be a clear signature for dark matter annihilation (a “smoking gun”). The flux of gamma-rays from such process is quite small, however, as no tree level feynman diagrams contribute to the process. For the loop-level feynman diagrams which lead to gamma-ray line emission, see appendix B.4.

The gamma-ray fluxes predicted from the Galactic center can be considerably enhanced if a density spike is considered. In Fig. 25, the (continuum) gamma-ray flux from the Galactic center is shown for four different values of γ , the slope of the inner halo profile, in the presence of a density spike. For most of the models, a value of γ between 0.05 and 0.1 can reproduce the scale of the gamma-ray flux observed by EGRET.

6.1.2 Prospects for Kaluza-Klein dark matter

Using the expression for the $B^{(1)}$ annihilation cross section found in Sec. 3.3.2, the flux of annihilation products from the Galactic center can be simplified to

$$\Phi_i(\Delta\Omega) \simeq 3.4 \times 10^{-12} \frac{dN_i}{dE} \left(\frac{1 \text{ TeV}}{m_{B^{(1)}}} \right)^4 \bar{J}(\Delta\Omega) \Delta\Omega \text{ cm}^{-2} \text{ s}^{-1}. \quad (99)$$

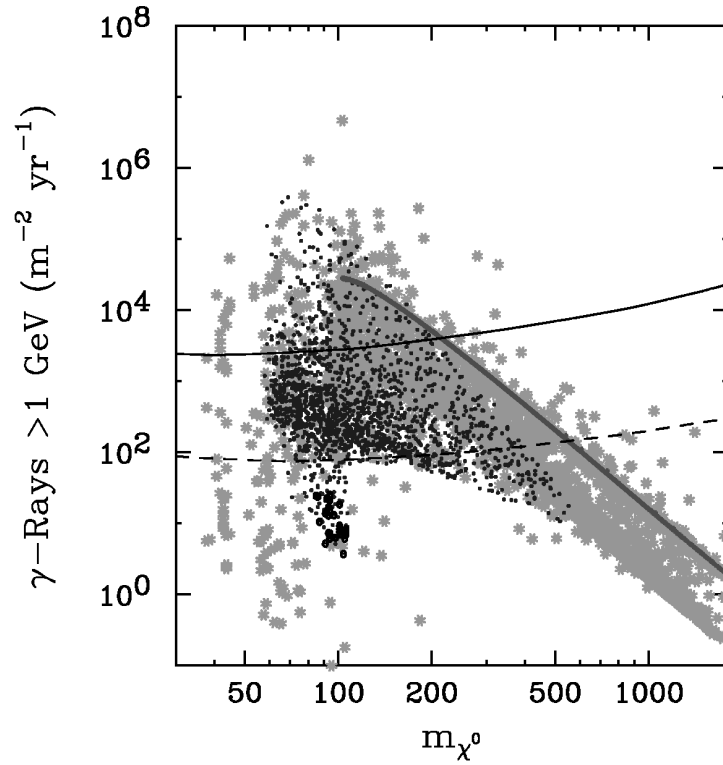


Figure 23: The flux of gamma-rays above 1 GeV per square meter per year from the Galactic center from annihilations of neutralino dark matter. A NFW halo profile has been used. For each point, the thermal relic density is below the maximum value allowed by WMAP. The solid and dashed lines are the limit from the EGRET experiment and predicted sensitivity for GLAST, respectively [302]. The various shadings refer to different scenarios of supersymmetry breaking. For more information, see Ref. [310].

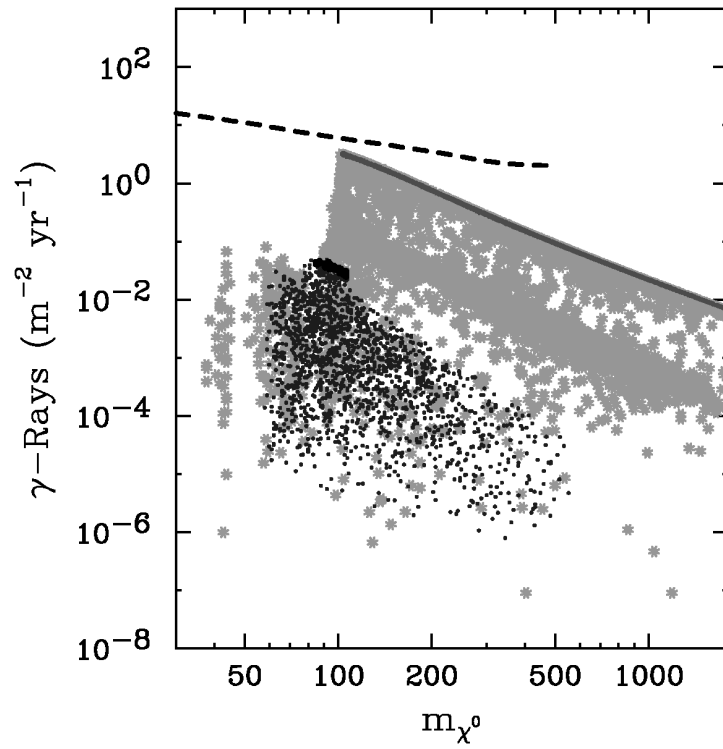


Figure 24: As in the previous figure, but from the annihilation of neutralino dark matter to a $\gamma\gamma$ line. The dashed line represents the predicted sensitivity for GLAST. The flux for neutralino annihilation to γZ is similar. For more information, see Ref. [310].

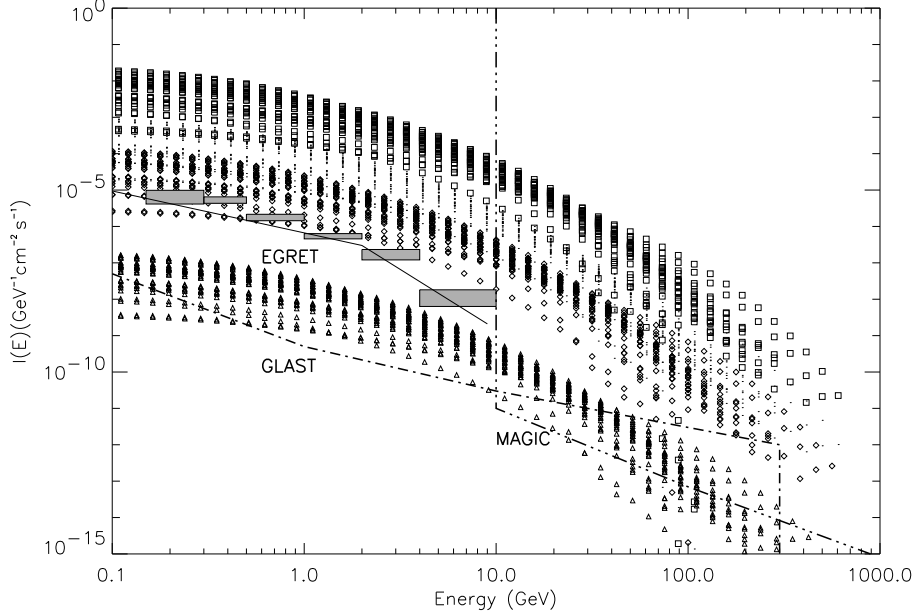


Figure 25: Predicted gamma-ray fluxes for a large set of supersymmetric models and halo profiles: $\gamma=0.05$ (triangles), $\gamma=0.12$ (diamonds), $\gamma=0.2$ (dots), $\gamma=1.0$ (squares). The flux observed by EGRET [392] is shown as grey boxes. Also shown are the projected sensitivities of for GLAST (1 month observation time) and MAGIC (50 hours).

In Fig. 26, the predicted γ -ray flux from KK dark matter annihilations in the Galactic center is shown. Results for LKP masses of 0.4, 0.6, 0.8, and 1 TeV are shown. A halo profile with $\bar{J}(10^{-3}) = 500$ has been used, although the effect of this choice is easily scaled with the values shown in table 7.

Unlike in the case of supersymmetry, with Kaluza-Klein dark matter, there are few free parameters in calculating the gamma-ray spectrum from the Galactic center ($m_{B^{(1)}}$ and $\bar{J}(\Delta\Omega)$). We can, therefore, easily place limits on the halo profile as a function of the LKP mass. We show in Fig. 27 the constraints on these parameters based on the expected sensitivity of GLAST, MAGIC and HESS. For example, with an NFW profile, LKP masses below about 600 GeV will be excluded if MAGIC does not observe any radiation from the galactic center.

Neutrino telescopes will also be capable of searching for signals of dark matter annihilation in the Galactic center (see Sec. 4.3), although these prospects are considerably poorer. In Fig. 28, we plot the integral flux of muon neutrinos above 50 GeV (solid line) as a function of the $B^{(1)}$ mass. This result is obtained by adding the neutrino fluxes from three different channels:

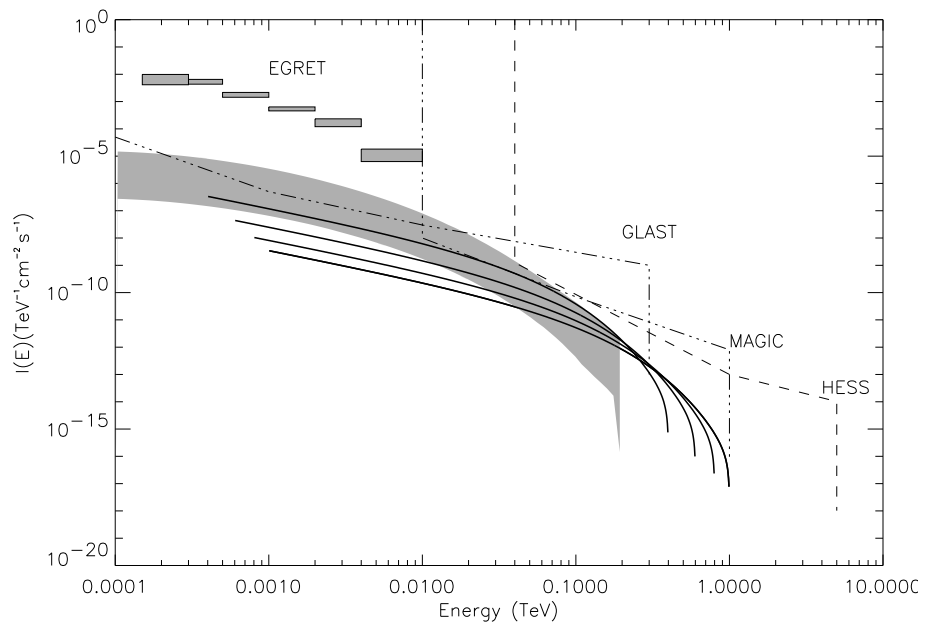


Figure 26: Expected γ -ray fluxes for (top to bottom) $m_{B(1)} = 0.4, 0.6, 0.8,$ and 1 TeV and $\bar{J}(10^{-3}) = 500$. For comparison shown are typical γ -ray fluxes predicted for neutralinos of mass $\simeq 200$ GeV, (shadowed region) as well as EGRET [377] data and expected sensitivities of the future GLAST[435], MAGIC[415] and HESS[485] experiments.

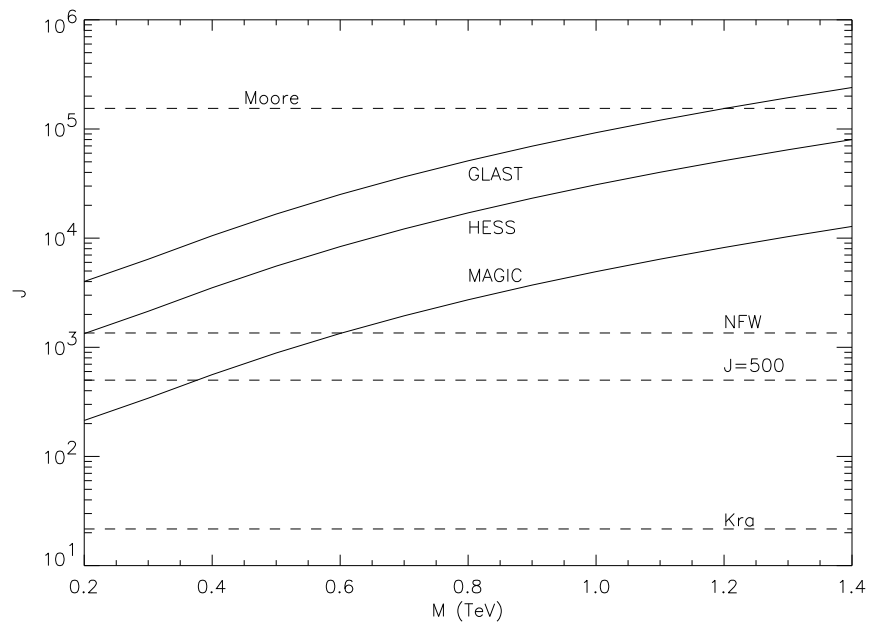


Figure 27: Value of $J = \bar{J}(10^{-3})$ required to produce γ fluxes observable by the future GLAST, MAGIC and HESS experiments, as a function of the $B^{(1)}$ mass. For comparison we show the values of J for some profiles discussed in the text.

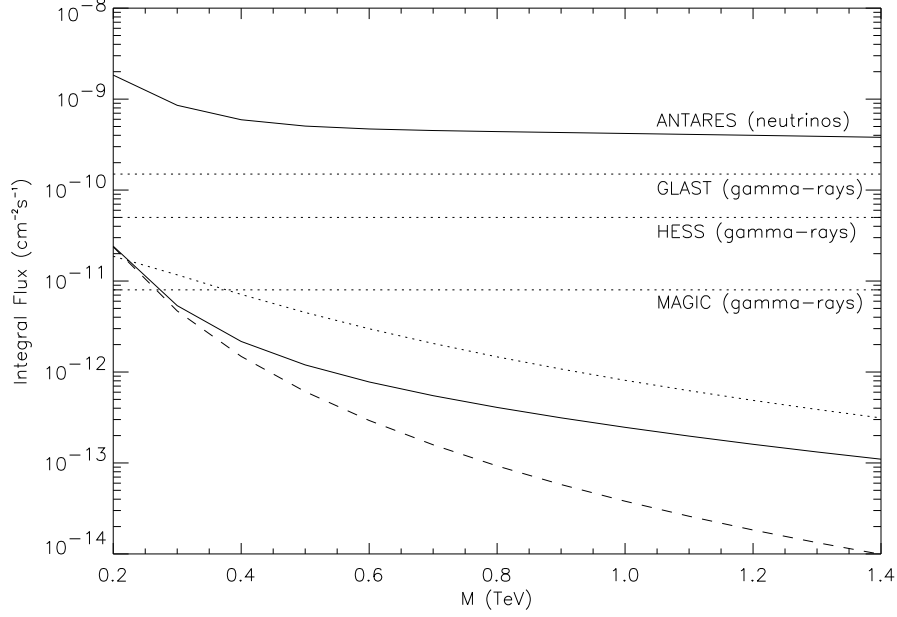


Figure 28: Integral flux of γ -rays (sloped dotted line) and muon neutrinos (solid) above 50 GeV, for $\bar{J} (10^{-3}) = 500$. The dashed line shows the contribution of direct $B^{(1)}$ annihilation into neutrinos. Horizontal lines are sensitivities of present and future experiments for γ -rays (dotted horizontal lines) and neutrinos (upper solid line).

- Neutrinos produced directly in $B^{(1)}$ annihilations (dashed line), their spectrum being a line at energy $E_\nu = m_{B^{(1)}}$.
- Secondary neutrinos from decay of charged pions. This spectrum can be evaluated using the expressions for the charged pion decay found in Ref. [354].
- Secondary neutrinos from “prompt” semi-leptonic decay of heavy quarks (solid line). This spectrum is given, for example, in Ref. [318].

We show in the same figure an estimate of the sensitivity of the neutrino telescope ANTARES (upper solid line). To estimate this sensitivity, we first evaluated the rate of muons in ANTARES from the direction of the galactic center, which depends (see Eq. 90) on specific experimental quantities, such as the detector effective area and the threshold energy for the detection of muons. The rate is higher for more energetic neutrinos, being proportional to the muon range and to the neutrino-nucleon cross section, which are both increasing functions of energy. See Sec. 4.3 for a discussion of neutrino telescopes.

Of these neutrino producing channels, ANTARES is most sensitive to those neutrinos produced directly in $B^{(1)}B^{(1)} \rightarrow \nu\nu$ annihilations. Although the

branching ratio for this channel is an order of magnitude smaller than that into quark pairs, the neutrinos produced are emitted at the highest available energy, $E_\nu = m_{B^{(1)}}$, increasing their probability of being detected. Neutralinos, which do not annihilate directly to neutrinos, are more difficult to observe with neutrino telescopes.

In Fig. 28, the integral flux of gamma-rays is shown for comparison, along with the projected sensitivity of future experiments GLAST, MAGIC and HESS.

6.1.3 The gamma-ray source at the Galactic center

The EGRET experiment (see Sec. 4.2.2) has reported an excess of gamma-rays in the region of the galactic center, in an error circle of 0.2 degree radius including the position $l=0(\text{deg})$ and $b=0(\text{deg})$ [377]. The name for this source, in the language of high-energy astrophysicists, is 3EG J1746-2851. The radiation is well above the gamma-ray emission which would be expected from interactions of primary cosmic rays with the interstellar medium (see, *e.g.*, Refs. [464, 142]).

It is intriguing to imagine that such excess emission could be the product of dark matter annihilations near the Galactic center. However, it should be noted that some difficulties exist, related to this interpretation. In fact, as shown in Refs. [302, 303], the EGRET source is not exactly coincident with the galactic center. This makes the interpretation of the EGRET signal as dark matter annihilation in a density spike (see Sec.2.5.1) problematic.

Furthermore there is some evidence, though weak, that the source could be variable. Such a result could rule out completely the interpretation of the excess emission as due to annihilation radiation from the galactic center. The variability of 3EG J1746-2851 has been recently discussed in Ref. [399].

We briefly note here that multiple Atmospheric Cerenkov Telescopes (ACTs) have recently reported an excess of gamma-rays from the Galactic center region. The VERITAS collaboration, using the Whipple telescope, have reported a flux of $1.6 \pm 0.5 \pm 0.3 \times 10^{-8} \text{ m}^{-2} \text{ s}^{-1}$ above 2.8 TeV [343]. The CANGAROO collaboration has reported a flux of approximately $2 \times 10^{-6} \text{ m}^{-2} \text{ s}^{-1}$ from this region in the range of 250 GeV to 1 TeV [471]. We eagerly await the results of HESS, which should be the most sensitive to the Galactic center region.

It is certainly too soon to determine whether the fluxes observed by these experiments are the product of dark matter annihilations or are the result of another process, most likely astrophysical [307]. Improvements in the measurement of the gamma-ray spectrum, and improved angular resolution will be needed to resolve this issue.

6.1.4 Upper Limit for the Neutrino Flux from the GC

Despite the large uncertainties associated with the distribution of dark matter in the innermost regions of our galaxy, it is possible to set an upper limit on the neutrino flux by requiring that the associated gamma-ray emission does not exceed the flux observed by EGRET (see previous section) [94].

The maximum neutrino flux is obtained by normalizing the associated flux of gamma-rays to the EGRET data. This corresponds to fixing, for each model, the product, $\sigma v N_\gamma$, with $N_\gamma = \sum_i N_i R_i$. Here R_i is the branching ratio of all the channels, i , contributing N_i gamma-rays above a given threshold energy.

Having fixed the particle physics contents of our dark matter candidate, the ratio between the number of photons and the number of neutrinos emitted per annihilation is known.

The rescaled flux of muons, $\phi_\mu^{\text{norm}}(> E_{th})$, will thus be given by

$$\phi_\mu^{\text{norm}}(> E_{th}) = \frac{\phi_\mu^{\text{NFW}}(> E_{th}) \phi_\gamma^{\text{EGRET}}(E_*)}{\phi_\gamma^{\text{NFW}}(E_*)}, \quad (100)$$

where the label NFW indicates that NFW profiles have been used to compute profile-independent flux ratios and E_* is the energy at which we decide to normalize the flux to the gamma-ray data (in our case, $E_* = 2$ GeV).

The results are shown in Fig. 29, where shades paler than in the legend denote a low value for the muon's magnetic moment (see Ref. [94] for more details). The neutrino induced muon flux normalized to the EGRET data represents an upper limit, as the observed gamma-ray emission certainly could be due to processes other than dark matter annihilation. The comparison with the sensitivity of ANTARES shows that only the highest mass neutralinos can possibly be detected with neutrino from the galactic center. In this case, conservatively assuming that the gamma-ray emission observed by EGRET is entirely due to neutralino annihilation, the upper limit on the neutrino flux is barely above the minimum signal observable by ANTARES in 3 years.

If neutrinos are nevertheless observed above the given fluxes, then their interpretation as due to neutralino annihilation is problematic and would actually require either the adoption of other dark matter candidates annihilating dominantly into neutrino pairs or a different explanation, e.g. in terms of astrophysical sources.

6.2 Synchrotron Radiation from the Galactic Center

Another interesting means of indirect detection of dark matter is observing the synchrotron radiation originating from the propagation of secondary e^\pm 's in the galactic magnetic fields. We will focus on what happens at the center of our galaxy, where most of the annihilation signal comes from.

The magnetic field around the Galactic center is thought to be at *equipartition*, *i.e.* there is equipartition of magnetic, gravitational and kinetic energy of the plasma surrounding the central supermassive black hole (see Sec. 2.5.1).

It is easy to derive the strength of the magnetic field under a few simplifying assumptions. Let us consider the existence of a galactic wind of particles with velocity, v_{gw} . These particles will be captured by the gravitational potential well of the black hole at the center of the galaxy within the accretion radius, $r_a \equiv 2GM/v_{gw}^2$, where M is the mass of the central object. Under the assumption of

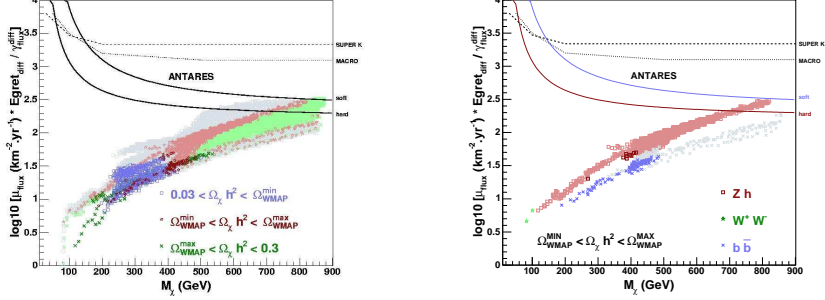


Figure 29: Neutrino-induced muon flux from the Galactic center normalized to EGRET. Models are sorted by relic density (left) and leading annihilation channel (right). Shades paler than in the legend denote a low $\delta_{\mu}^{\text{susy}}$ value.

purely radial infall, the radial dependence of the particle velocity is simply

$$v(r) = -c \left(\frac{r_S}{r} \right)^{1/2}, \quad (101)$$

where $r_S \equiv GM/c^2$ is the Schwarzschild radius of the black hole. For a steady flow, the number of plasma particles through a sphere of radius, r , around the black hole is

$$\dot{N} \equiv \frac{dN}{dt} = -4\pi r^2 n(r) v(r), \quad (102)$$

where $n(r)$ is the plasma number density. Solving for $n(r)$ we find

$$n(r) = \frac{\dot{N}}{4\pi c r_S^2} \left(\frac{r_S}{r} \right)^{3/2}. \quad (103)$$

The accretion rate can be parametrised as follows

$$\dot{N} m_p \approx 10^{22} \text{g s}^{-1} \mathcal{W} M_6^2, \quad (104)$$

where m_p is the proton mass, M_6 is the mass of the central black hole in units of $10^6 M_{\odot}$, and $\mathcal{W} \sim 1$ parameterizes the uncertainties of the physical parameters around the black hole, namely the velocity and mass-loss rate of the circumnuclear wind (see Ref. [379] for more details).

We now note that the infalling plasma is expected to be highly ionized, and its energy density will reach equipartition with kinetic and gravitational energies. After simple calculations, we find that the magnetic field under equipartition evaluates to [379, 450]

$$B = 324 \mu\text{G} \left(\frac{r}{\text{pc}} \right)^{-5/4}. \quad (105)$$

Far from the galactic center, the equipartition does not apply anymore and we assume a flat profile for the magnetic field. More specifically, the profile we adopt is

$$B(r) = \max \left[324\mu\text{G} \left(\frac{r}{\text{pc}} \right)^{-5/4}, 6\mu\text{G} \right] \quad (106)$$

which means that the magnetic field is assumed to be in equipartition with the plasma out to a galactocentric distance $r_c = 0.23$ pc and equal to a typical value observed throughout the galaxy at larger distances.

If the actual value of the magnetic field away from the central region was smaller than the value we considered, this would imply a shift of the radio spectrum toward lower energies and thus, in the range of frequencies we are interested in, a higher flux for a given frequency. This would also translate into stronger constraints for the mass and annihilation cross section. Nevertheless, we prefer to be conservative and consider a quite high value of B . Note that magnetic fields stronger than equipartition values are physically unlikely.

The mechanism of synchrotron emission is well known. We will now estimate the synchrotron luminosity produced by the propagation of secondary e^\pm 's originating from dark matter annihilation in the galactic magnetic field

We recall that the critical synchrotron frequency, $\nu_c(E)$, *i.e.* the frequency around which the synchrotron emission of an electron of energy, E , in a magnetic field of strength B , peaks, can be expressed as

$$\nu_c(E) = \frac{3}{4\pi} \frac{eB}{m_e c} \left(\frac{E}{m_e c^2} \right)^2, \quad (107)$$

where m_e is the electron mass. Inverting this relation, we determine the energy of the electrons which give the maximum contribution at that frequency,

$$E_m(\nu) = \left(\frac{4\pi}{3} \frac{m_e^3 c^5}{e} \frac{\nu}{B} \right)^{1/2} = 0.25 \left(\frac{\nu}{\text{MHz}} \right)^{1/2} \left(\frac{r}{\text{pc}} \right)^{5/8} \text{ GeV}. \quad (108)$$

To compute the synchrotron luminosity we also need to know their energy distribution, which in our case can be expressed as (see, *e.g.*, Ref. [262])

$$\frac{dn}{dE} = \frac{\Gamma Y_e(> E)}{P(E)} f_e(r), \quad (109)$$

where Γ is the annihilation rate,

$$\Gamma = \frac{\sigma v}{m_{\text{DM}}^2} \int_0^\infty \rho_{sp}^2 4\pi r^2 dr. \quad (110)$$

The function $f_e(r)$ is given by

$$f_e(r) = \frac{\rho_{sp}^2}{\int_0^\infty \rho_{sp}^2 4\pi r^2 dr} \quad (111)$$

and

$$P(E) = \frac{2e^4 B^2 E^2}{3m_e^4 c^7} \quad (112)$$

is the total synchrotron power spectrum. Note that the general expression for $f_e(r)$ would have to take into account spatial redistribution by diffusion (see, *e.g.*, Ref. [262]), but this is typically negligible [91].

The quantity $Y_e(> E)$ is the number of e^\pm 's with energy above E produced per annihilation, which depends on the annihilation modes, and can be equivalently expressed as a function of the particle mass, m_{DM} , and the frequency considered, ν . Actually, Eq. (108) shows that for the frequencies we are interested in, $E_m(\nu) \ll m_{\text{DM}}$, and thus the energy dependence of $Y_e(> E)$ can be neglected. We estimate $Y_e(> E)$ by the number of charged particles produced in quark fragmentation (see below for further details).

For each electron the total power radiated in the frequency interval between ν and $\nu + d\nu$ is given by

$$P(\nu, E) = \frac{\sqrt{3}e^3}{m_e c^2} B(r) \frac{\nu}{\nu_c(E)} \int_0^\infty K_{5/3}(y) dy = \frac{\sqrt{3}e^3}{m_e c^2} B(r) F\left(\frac{\nu}{\nu_c(E)}\right), \quad (113)$$

where $K_n(y)$ are the modified Bessel functions of order n (for definitions see *e.g.* [434]) and

$$F\left(\frac{\nu}{\nu_c(E)}\right) = \frac{\nu}{\nu_c(E)} \int_0^\infty K_{5/3}(y) dy. \quad (114)$$

Integrating this formula over the dark matter distribution, we obtain the total synchrotron luminosity

$$L_\nu = \int_0^\infty dr 4\pi r^2 \int_{m_e}^{m_{\text{DM}}} dE \frac{dn_e}{dE} P(\nu, E), \quad (115)$$

which by substitution becomes

$$L_\nu = \frac{\sqrt{3}e^3 \Gamma}{m_e c^2} \int_0^\infty dr 4\pi r^2 f_e(r) B(r) \int_{m_e}^{m_{\text{DM}}} dE \frac{Y_e(> E)}{P(E)} F\left(\frac{\nu}{\nu_c(E)}\right). \quad (116)$$

It is possible to simplify this formula by introducing the following approximation (see Rybicki & Lightman [434]):

$$F\left(\frac{\nu}{\nu_c(E)}\right) \approx \delta(\nu/\nu_c(E) - 0.29). \quad (117)$$

The evaluation of the integral then gives

$$L_\nu(\psi) \simeq \frac{1}{4\pi} \frac{9}{8} \left(\frac{1}{0.29\pi} \frac{m_e^3 c^5}{e} \right)^{1/2} \frac{\sigma v}{m_{\text{DM}}^2} Y_e(m_{\text{DM}}, \nu) \nu^{-1/2} I(\psi), \quad (118)$$

where

$$I(\psi) = \int_0^\infty ds \rho^2(r(s, \psi)) B^{-1/2}(r(s, \psi)) \quad (119)$$

and s is the coordinate running along the line-of-sight.

For frequencies around 400 MHz, used below, and for the lowest value of the magnetic field, we find that $E_m(400 \text{ MHz}) \lesssim 2 \text{ GeV}$. In reality, for dark matter profiles with central cusps, e.g. the NFW, Kravtsov, and Moore profiles, most of the annihilation signal comes from the inner region of the galaxy, where the magnetic field is probably higher. For $\nu = 400 \text{ MHz}$ and $r < r_c$,

$$E_m(\nu) \simeq 0.3 \left(\frac{\nu}{400 \text{ MHz}} \right)^{1/2} \left(\frac{r}{\text{pc}} \right)^{5/8} \text{ GeV}, \quad (120)$$

which at the inner edge of the profile, corresponding to the Schwarzschild radius of the supermassive black hole at the galactic center, $R_S = 1.3 \times 10^{-6} \text{ pc}$, takes the value of $E_m(400 \text{ MHz}) = 2.2 \times 10^{-5} \text{ GeV}$. We thus always have $E_m(400 \text{ MHz}) \ll m_{\text{DM}}$, which means that most of the secondary electrons are produced above this energy and contribute to the radio flux.

For a particle of mass m_{DM} , the average electron multiplicity per annihilation, $Y_e(m_{\text{DM}})$, is evaluated by adding the contribution of each annihilation channel with cross section $(\sigma v)_i$, producing $Y_e^i(m_{\text{DM}})$ electrons:

$$\sigma v Y_e(m_{\text{DM}}) = \sum_i (\sigma v)_i Y_e^i(m_{\text{DM}}), \quad (121)$$

where σv is the total annihilation cross section.

The main channels contributing to this flux are direct production of leptons and annihilation into quarks. The calculations are easily performed for Kaluza-Klein dark matter. For direct production of leptons,

$$Y_e^{e^\pm}(M) = Y_e^{\mu^\pm}(M) \simeq 2 \quad (122)$$

in the relevant range of masses. In the quark channel, to count the number of electrons, $Y_e^{q\bar{q}}(M)$, we integrate the fragmentation functions for e^\pm 's from π^\pm 's. This results in

$$\sigma v Y_e(1 \text{ TeV}) \simeq 6 \times 10^{-3} \text{ TeV}^{-2} \quad (123)$$

and

$$Y_e(1 \text{ TeV}) \simeq 4.5, \quad (124)$$

for $m_{\text{DM}} = 1 \text{ TeV}$. The electron multiplicity in the hadronic channel alone would be much larger, roughly 20.

The case of neutralinos is much more complicated, as the dominating annihilation modes can vary from model to model (a discussion of branching ratios in the framework of the mSUGRA models can be found in Ref. [89]). Such calculations must, therefore, be conducted on a model-by-model basis.

One more step is necessary to calculate the observed radiation. We must multiply the synchrotron luminosity, L_ν , with the synchrotron self-absorption coefficient, which we calculate next.

Synchrotron emission is accompanied by absorption, in which a photon loses its energy due to the interaction with a charge in a magnetic field. The

synchrotron self-absorption coefficient is by definition (see Rybicki and Lightman [434])

$$A_\nu = \frac{1}{a_\nu} \int_0^\infty (1 - e^{-\tau(b)}) 2\pi b db, \quad (125)$$

where $\tau(b)$ is the optical depth as a function of the cylindrical coordinate b ,

$$\tau(b) = a_\nu \int_{d(b)}^\infty f_e(b, z) dz, \quad (126)$$

and the coefficient, a_ν , is given by

$$a_\nu = \frac{e^3 \Gamma B(r)}{9m_e \nu^2} \int_{m_e}^m E^2 \frac{d}{dE} \left[\frac{Y_e(> E)}{E^2 P(E)} \right] F \left(\frac{\nu}{\nu_c} \right) dE. \quad (127)$$

The final luminosity is obtained by multiplying Eq. (115) with A_ν , given by Eq. (125). It is evident that in the limit of small optical depth, the coefficient $A_\nu \rightarrow 1$, as can be seen by expanding the exponential.

The lower limit of integration of Eq. (126) is

$$d(b) = 0 \quad \text{for} \quad b^2 + z^2 > (4Rs)^2, \quad (128)$$

$$d(b) = \sqrt{(4Rs)^2 - b^2} \quad \text{elsewhere.}$$

Using the approximation introduced in Eq. (117), we find

$$a_\nu = \frac{\Gamma Y c^2}{4\pi \nu^3}, \quad (129)$$

which can in turn be used to evaluate $\tau(b)$ in Eq. (126) and A_ν in Eq. (125).

If a density spike exists at the galactic center, the self-absorption coefficient cannot be neglected and can lead to a significant reduction of the observed synchrotron flux by up to several orders of magnitude. The results of synchrotron emission in presence of a spike has been discussed in Ref. [91]. If a spike exists at the galactic center, and if neutralinos are the dark matter particle, only small values of γ are compatible with radio observations. Kaluza-Klein dark matter has annihilation cross section typically larger than neutralinos. Thus Kaluza-Klein dark matter is very problematic in a scenario with a density spike.

Note that Eqs. 125–127 are valid, strictly speaking, only for position independent quantities. A rigorous treatment of synchrotron emission and self-absorption would require the solution of the radiative transport equation. Recently, Aloisio *et al.* 2004 Ref. [27] have derived the equilibrium distribution of electrons and positrons from neutralino annihilation at the Galactic center, and the resulting radiation considering adiabatic compression in the accretion flow, inverse Compton scattering of synchrotron photons (synchrotron self-Compton scattering), and synchrotron self-absorption. Such a detailed analysis allows a more precise estimate of the radio emission and confirms that neutralino annihilation in a NFW profile with a spike would exceed the observed radio emission from the Galactic center.

If there is no spike at the galactic center, the optical depth is negligible and the self-absorption coefficient is of the order of unity. In fact, using Eq. 129, the optical depth in Eq. 126 can be expressed as

$$\tau \simeq \frac{\sigma v}{m_{\text{DM}}^2} \frac{Y_e(M)}{4\pi} \frac{1}{\nu^3} \int_0^{d_\odot} ds \rho^2(s), \quad (130)$$

where $d_\odot \simeq 8 \text{ kpc}$ is the distance of the Sun from the galactic center. Using $m_{\text{DM}} = 1 \text{ TeV}$, $\sigma v = 1.6 \times 10^{-4} \text{ TeV}^{-2}$ (for the cross section for annihilation into right-handed up quarks) and a NFW halo profile, we find

$$\tau = 1.78 \times 10^{-4} \left(\frac{\nu}{100 \text{ MHz}} \right)^{-3}. \quad (131)$$

We can thus neglect self-absorption unless the frequency considered is very small. The absorption on relativistic electrons from other sources is also negligible. Using

$$n(E) \lesssim 10^{-2} \text{ GeV}^{-1} \text{ cm}^{-2} \text{ s}^{-1} \text{ sr}^{-1} \quad (132)$$

for the locally observed differential electron flux (see Ref. [387]) in the relevant energy range given by Eq. (120), one obtains an absorption coefficient per length

$$\alpha_\nu \lesssim 6 \times 10^{-16} \text{ pc}^{-1} \left(\frac{B}{\mu\text{G}} \right) \left(\frac{\nu}{\text{GHz}} \right)^{-2}. \quad (133)$$

Even if the relativistic electron flux due to non-acceleration processes close to the Galactic center is orders of magnitude larger, this effect would still be negligible. However, for frequencies below a few MHz, free-free absorption is important (see e.g. Ref. [137]).

To compare with observations, we integrate over the relevant solid angle. The comparison between predicted and observed fluxes can constrain the cross sections and masses of annihilating dark matter particles for a given halo profile. In particular, this method can be used to provide a lower bound on the mass of a Kaluza-Klein dark matter particle. In Fig. 30 we show predicted and observed fluxes for Kaluza-Klein particles, for a NFW profile, as a function of the particle mass. Three cases are shown (see Ref. [92] for more details). For each case the predicted and observed fluxes are plotted, the latter being represented by a horizontal line. The three cases are represented by solid, dashed and dotted lines. Case 1 is the most constraining, implying a lower bound on the mass of about 0.3 TeV (assuming an NFW halo profile).

The fluxes predicted at high latitudes can also be compared with observations (see Ref. [137]). The strongest constraints result from the lowest frequencies at which free-free and synchrotron self-absorption are not yet important, i.e. $\sim 10 \text{ MHz}$. Here, the observed background emission between 0° and 90° from the galactic anti-center is $\simeq 6 \times 10^6 \text{ Jy}$. Comparing with the predicted emission results in the limit

$$\sigma v \lesssim 10^{-22} \left(\frac{m_{\text{DM}}}{\text{TeV}} \right)^2 \frac{Y_e(1 \text{ TeV})}{Y_e(m_{\text{DM}})} \text{ cm}^3 \text{ s}^{-1}. \quad (134)$$

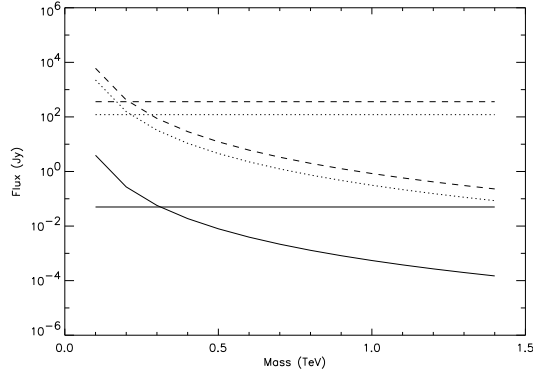


Figure 30: Predicted (curves) and observed (horizontal lines) radio flux from annihilating Kaluza-Klein dark matter from regions close to the galactic center. An NFW profile has been assumed. Three cases for the radio frequency and observed region are shown.

While this is considerably weaker than the constraints above, it is largely independent of the unknown halo profile near the galactic center.

The argument can also be turned the other way round and interpreted as a measure of the galactic magnetic field. One can in fact decide to select the values of γ reproducing the normalization of the observed gamma-ray emission and look for the values of the magnetic field that reproduce the correct normalization of the observed radio emission. Due to the uncertainties in the particle physics models, the precision obtained is unfortunately poor (see Ref. [92]).

A comparison between the prospects for indirect detection at different wavelengths shows that constraints from synchrotron emission are more stringent than those obtained from gamma-ray and neutrino fluxes (from current experiments), although they are less robust, being derived under the additional assumptions made about the strength of the magnetic field at equipartition. In the future, however, the strongest constraints will likely result from gamma-ray experiments.

6.3 Annihilation Radiation from External or Dwarf Galaxies

It also might be possible to observe annihilation radiation from galaxies outside of the Milky Way. In this case, although such galaxies are far more distant than the galactic center, the observed emitting region is much larger. Dwarf galaxies within the Milky Way may also be observable regions of dark matter annihilation.

Baltz *et al.* [57] studied the expected flux of gamma-rays from M87 and several local dwarf spheroidal galaxies. The predicted fluxes are calculated using the same formulae for indirect detection of secondary particles described above.

Using a profile with a central core for the sources, they conclude that predicted fluxes are below the sensitivities of next-generation experiments, unless the annihilation signal is boosted by a significant amount of dense clumps. A similar analysis was carried on for the prospect of observing M31 with CELESTE (see Falvard *et al.* [227]).

Tasitsiomi, Gaskins and Olinto [466] focused on gamma-ray and synchrotron emission from the Large Magellanic Cloud (LMC). Fitting the LMC rotation curve with different profiles, they determined that although present data do not constrain SUSY parameters, future experiments like GLAST (gamma-rays), and LOFAR (low frequencies emission), could probe a significant portion of the SUSY parameter space. Similar, though more optimistic, conclusions have been obtained by Pieri and Branchini [418].

Finally, particularly interesting are the prospects for dark matter observations in the Draco and Sagittarius dwarf galaxies [224, 475].

6.4 High-Energy Neutrinos from the Sun or Earth

In addition to gamma-rays, neutrinos can be produced in dark matter annihilations. Unlike gamma-rays, however, neutrinos can escape from dense media in which such annihilations may take place. For example, WIMPs which are captured in deep gravitational wells such as the Sun or Earth, can annihilate at great rates. Although gamma-rays cannot escape these objects, neutrinos often can, providing an interesting signature to search for with high-energy neutrino telescopes [452, 285, 232, 63, 72, 82, 239, 345, 244]

6.4.1 Capture and annihilation in the Sun

In order to provide an observable flux of neutrinos, dark matter particles must be gathered in high concentrations. In the following calculation, we will focus on WIMP capture in the Sun, as these prospects are more promising than for capture in the Earth.

The rate at which WIMPs are captured in the Sun depends on the nature of the interaction the WIMP undergoes with nucleons in the Sun. For spin-dependent interactions, the capture rate is given by [269, 319]

$$C_{\text{SD}}^{\odot} \simeq 3.35 \times 10^{20} \text{ s}^{-1} \left(\frac{\rho_{\text{local}}}{0.3 \text{ GeV/cm}^3} \right) \left(\frac{270 \text{ km/s}}{\bar{v}_{\text{local}}} \right)^3 \left(\frac{\sigma_{\text{H,SD}}}{10^{-6} \text{ pb}} \right) \left(\frac{100 \text{ GeV}}{m_{\text{DM}}} \right)^2, \quad (135)$$

where ρ_{local} is the local dark matter density, $\sigma_{\text{H,SD}}$ is the spin-dependent, WIMP-on-proton (hydrogen) elastic scattering cross section, \bar{v}_{local} is the local rms velocity of halo dark matter particles and m_{DM} is the dark matter particle's mass.

The analogous formula for the capture rate from spin-independent (scalar) scattering is [269, 319]

$$C_{\text{SI}}^{\odot} \simeq 1.24 \times 10^{20} \text{ s}^{-1} \left(\frac{\rho_{\text{local}}}{0.3 \text{ GeV/cm}^3} \right) \left(\frac{270 \text{ km/s}}{\bar{v}_{\text{local}}} \right)^3 \left(\frac{100 \text{ GeV}}{m_{\text{DM}}} \right)^2 \times \left(\frac{2.6 \sigma_{\text{H,SI}} + 0.175 \sigma_{\text{He,SI}}}{10^{-6} \text{ pb}} \right). \quad (136)$$

Here, $\sigma_{\text{H,SI}}$ is the spin-independent, WIMP-on-proton elastic scattering cross section and $\sigma_{\text{He,SI}}$ is the spin-independent, WIMP-on-helium, elastic scattering cross section. Typically, $\sigma_{\text{He,SI}} \simeq 16.0 \sigma_{\text{H,SI}}$. The factors of 2.6 and 0.175 include information on the solar abundances of elements, dynamical factors and form factor suppression.

Although these two rates appear to be comparable in magnitude, the spin-dependent and spin-independent cross sections can differ radically. For example, for Kaluza-Klein dark matter, the spin-dependent cross section is typically three to four orders of magnitude larger than the spin-independent cross section [446, 150] and solar accretion by spin-dependent scattering dominates. Spin-dependent capture also dominates for most neutralino models. On the other hand, for scalar dark matter candidates (such as sneutrinos, or candidates from theory space little Higgs models), the spin-independent cross section can dominate.

If the capture rates and annihilation cross sections are sufficiently high, equilibrium may be reached between these processes. For N WIMPs in the Sun, the rate of change of this quantity is given by

$$\dot{N} = C^{\odot} - A^{\odot} N^2, \quad (137)$$

where C^{\odot} is the capture rate and A^{\odot} is the annihilation cross section times the relative WIMP velocity per volume. C^{\odot} was given in Eq. 135, while A^{\odot} is

$$A^{\odot} = \frac{\langle \sigma v \rangle}{V_{\text{eff}}}, \quad (138)$$

where V_{eff} is the effective volume of the core of the Sun determined roughly by matching the core temperature with the gravitational potential energy of a single WIMP at the core radius. This was found in Refs. [280, 270] to be

$$V_{\text{eff}} = 5.7 \times 10^{27} \text{ cm}^3 \left(\frac{100 \text{ GeV}}{m_{\text{DM}}} \right)^{3/2}. \quad (139)$$

The present WIMP annihilation rate is given by

$$\Gamma = \frac{1}{2} A^{\odot} N^2 = \frac{1}{2} C^{\odot} \tanh^2 \left(\sqrt{C^{\odot} A^{\odot}} t_{\odot} \right), \quad (140)$$

where $t_{\odot} \simeq 4.5$ billion years is the age of the solar system. The annihilation rate is maximized when it reaches equilibrium with the capture rate. This occurs when

$$\sqrt{C^{\odot} A^{\odot}} t_{\odot} \gg 1. \quad (141)$$

For many of the particle physics models which are most often considered (most supersymmetry or Kaluza-Klein models, for example), the WIMP capture and annihilation rates reach, or nearly reach, equilibrium in the Sun. This is often not the case for the Earth. This is true for two reasons. First, the Earth is less massive than the Sun and, therefore, provides fewer targets for WIMP scattering and a less deep gravitational well for capture. Second, the Earth accretes WIMPs only by scalar (spin-independent) interactions. For these reasons, it is unlikely that the Earth will provide any observable neutrino signals from WIMP annihilations in any planned experiments (for a recent analysis of WIMP capture in the Earth, see Ref. [365]).

The flux of neutrinos produced in WIMP annihilations is highly model dependent as the annihilation fractions to various products can vary a great deal from model to model. We will attempt to be as general in our discussion as possible while still considering some specific cases as well.

In supersymmetry, there are no tree level diagrams for direct neutralino annihilation to neutrinos. Many indirect channels exist, however. These include neutrinos from heavy quarks, gauge bosons, tau leptons and Higgs bosons. These processes result in a broad spectrum of neutrinos, but with typical energies of 1/2 to 1/3 of the neutralino mass. For experimental (muon) energy thresholds of 10-100 GeV, lighter WIMPs can be very difficult or impossible to detect for this reason.

For neutralinos lighter than the W^\pm mass (80.4 GeV), annihilation to $b\bar{b}$ typically dominates, with a small admixture of $\tau^+\tau^-$ as well. In these cases, neutrinos with less than about 30 GeV energy are produced and detection is difficult. For heavier neutralinos, annihilation into gauge bosons, top quarks and Higgs bosons are important in addition to $b\bar{b}$ and $\tau^+\tau^-$. In particular, gauge bosons can undergo two body decays ($Z \rightarrow \nu\nu$ or $W^\pm \rightarrow l^\pm\nu$) producing neutrinos with an energy of about half of the WIMP mass. Neutralinos with a substantial higgsino component often annihilate mostly into gauge bosons.

For Kaluza-Klein dark matter, the picture is somewhat different. Kaluza-Klein dark matter particles annihilate directly to a pair of neutrinos about 3-4% of the time [446, 150, 305]. Although this fraction is small, the neutrinos are of higher energy and are, therefore, easier to detect. The more frequent annihilation channels for Kaluza-Klein dark matter are charged leptons (60-70%) and up-type quarks (20-30%). Of these, the $\tau^+\tau^-$ mode contributes the most to the neutrino flux. Unlike in supersymmetry, a large fraction of lightest Kaluza-Klein particles annihilate into long lived particles, such as up quarks, electrons and muons, which lose their energy in the Sun long before decaying. Bottom and charm quarks lose some energy before decaying, but not as dramatically.

Neutrinos which are produced lose energy as they travel through the Sun [204, 318, 168]. The probability of a neutrino escaping the sun without interacting is given by

$$P = e^{-E_\nu/E_k} \quad (142)$$

where E_k is $\simeq 130$ GeV for ν_μ , $\simeq 160$ GeV for ν_τ , $\simeq 200$ GeV for $\bar{\nu}_\mu$ and $\simeq 230$ GeV for $\bar{\nu}_\tau$. Thus we see that neutrinos above a couple hundred GeV are

especially depleted. For a useful parameterization of solar effects, see Ref. [204]. Note that neutrino oscillations can also play an important role in calculating the flux of muon neutrinos in a detector [168].

6.4.2 Detection of high-energy neutrinos from the Sun

Several experiments are potentially able to detect the flux of high energy neutrinos from dark matter annihilations in the solar core. The AMANDA experiment is currently the largest operating neutrino telescope. The AMANDA B-10 array, due to its “soda can” geometry, was not very sensitive in the direction of the Sun (the horizon), although the current version of the experiment, AMANDA-II, does not have this problem and can place limits on dark matter annihilations from the center of the Sun and Earth. ANTARES, with a lower energy threshold (10 GeV) and IceCube, with a much greater effective area, will each function as effective dark matter experiments (see section 4.3 for a description of neutrino telescopes).

The background for this class of experiments consists of atmospheric neutrinos [243] and neutrinos generated in cosmic ray interactions in the Sun’s corona [82, 83]. In the direction of the Sun (up to the angular resolution of a neutrino telescope), tens of events above 100 GeV and on the order of 1 event per year above 1 TeV, per square kilometer are expected from the atmospheric neutrino flux. The rate of events from neutrinos generated by cosmic ray interactions in the Sun’s corona is predicted to be less than a few events per year per square kilometer above 100 GeV.

The sensitivity of a square kilometer neutrino detector with a moderate muon energy threshold (50 GeV) to supersymmetric dark matter is shown in Fig. 31. From this figure, it is clear that high-energy neutrinos will be an observable signature in only a small fraction of possible supersymmetry models, although such experiments are still certainly an important probe.

For Kaluza-Klein dark matter, the prospects for detection via high-energy neutrinos are substantially better. This is largely due to the dominating annihilation modes. The spectrum of muons in a detector due to LKP annihilations in the Sun is shown in Fig. 32 for various annihilation channels and for two choices of LKP mass. Unlike in the case of supersymmetry, annihilation to neutrinos and taus dominates the neutrino spectrum. In supersymmetry, b quarks and gauge bosons dominate, producing fewer observable neutrinos.

In Fig. 33, the event rates from Kaluza-Klein dark matter annihilation in the Sun are shown for a square kilometer detector with a threshold of 50 GeV. Each of the three lines correspond to variations in the Kaluza-Klein spectrum. For the spectrum predicted in Ref. [149], a kilometer scale neutrino telescope could be sensitive to a LKP with mass up to about 800 GeV. The relic density of the LKP varies from low to high values from left to right in the graph. The range of masses of the LKP that gives the appropriate relic density was estimated from Refs. [150, 446] and shown in the figure by the solid sections of the lines. Combining the expected size of the one-loop radiative corrections with a relic density appropriate for dark matter, we see that IceCube should see between a

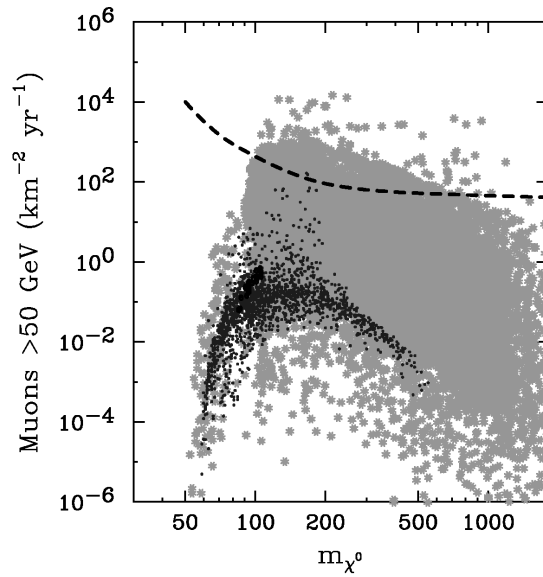


Figure 31: The number of events from neutralino annihilation in the Sun per year in a neutrino telescope with an effective area equal to one square kilometer and a 50 GeV muon threshold [310]. The lightly shaded region represents the general Minimal Supersymmetric Standard Model (MSSM), the darker region corresponds to mSUGRA models, a subset of the MSSM. For each point shown, the relic density is below the maximum value allowed by the WMAP data ($\Omega_\chi h^2 \leq 0.129$). The sensitivity projected for IceCube is shown as a dashed line [205].

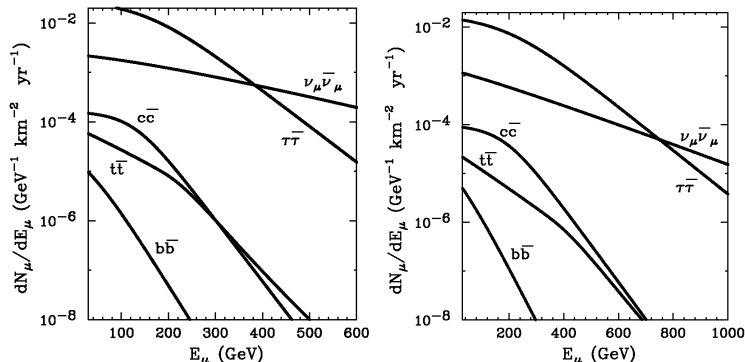


Figure 32: The spectrum of muons at the Earth generated in charged-current interactions of muon neutrinos generated in the annihilation of 600 GeV (left side) and 1000 GeV (right side) Kaluza-Klein dark matter particles in the Sun [305]. The elastic scattering cross section used for capture in the Sun was fixed at 10^{-6} pb for both graphs. The rates are proportional to that cross section.

few events and tens of events per year.

For detectors with smaller effective areas one simply has to scale the curves down by a factor $A/(1 \text{ km}^2)$ to obtain the event rate. In particular, for the first generation neutrino telescopes including AMANDA and ANTARES, with effective areas up to 0.1 km^2 , the event rate could be as high as ten events per year for a 500 GeV LKP. The current limits from AMANDA-II (with data up to 2001) is roughly 3000 muons per square kilometer per year from the Sun [12]. This sensitivity is expected to improve significantly with the analysis of more recent and future data.

6.5 e^+ and \bar{p} from Annihilations in the Galactic Halo

Charged particles, such as positrons and anti-protons, which are generated in dark matter annihilations do not travel in straight lines. Therefore, rather than observing a single region, such as the Galactic center or the Sun, the entire galactic halo can contribute to the flux of such particles. In this section, we will discuss the impact on dark matter annihilations in the galactic halo on the cosmic positron and anti-proton spectrum.

6.5.1 The positron excess

In 1994 and 1995, the High Energy Antimatter Telescope (HEAT) observed a flux of cosmic positrons well in excess of the predicted rate, peaking around ~ 10 GeV and extending to higher energies [64]. This result was confirmed by another HEAT flight in 2000 [162, 163]. Although the source of these positrons is not known, it has been suggested in numerous articles that this signal could

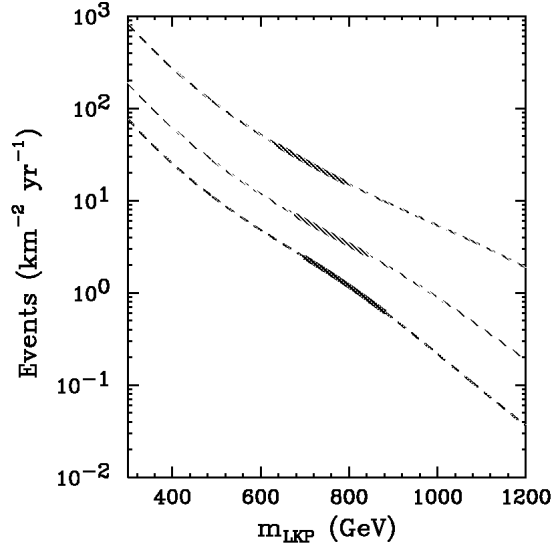


Figure 33: The number of events per year in a detector with effective area equal to one square kilometer and a muon energy threshold of 50 GeV [305]. Contours are shown, from bottom to top, for $r_{q_R^1} = 0.1, 0.2,$ and 0.3 , where $r_{q_R^1}$ is the mass splitting of the LKP and KK quarks over the LKP mass. The expected size of the one-loop radiative corrections predict $0.1 \lesssim r_{q_R^1} \lesssim 0.2$, therefore, the $r_{q_R^1} = 0.3$ contour is shown merely for comparison. The relic density of the LKP's lies within the range $\Omega_{B^1} h^2 = 0.16 \pm 0.04$ for the solid sections of each line. The relic density is smaller (larger) for smaller (larger) LKP masses.

be the product of dark matter annihilations, particularly within the context of supersymmetry [329, 324, 59, 474, 476, 328, 58] and Kaluza-Klein dark matter [150, 306].

If the dark matter is evenly distributed in our local region (within a few kpc), the rate of annihilations may be insufficient to produce the observed excess. It has been suggested, however, that if sufficient clumping were present in the galactic halo, that the rate at which such particles annihilate could be enhanced enough to accommodate the data.

Positrons can be produced in a variety of dark matter annihilation modes. Direct annihilation to e^+e^- is suppressed for neutralinos, but occurs frequently for Kaluza-Klein dark matter [150]. Also, annihilations to ZZ or W^+W^- can produce positrons with energy of half of the WIMP mass [324]. A continuum of positrons, extending to much lower energies, will in most cases also be produced in the cascades of annihilation products such as heavy leptons, heavy quarks, Higgs bosons and gauge bosons. The spectrum of positrons produced in dark matter annihilations can vary significantly depending on the mass and annihilation modes of the WIMP.

As positrons propagate, they move under the influence of the tangled galac-

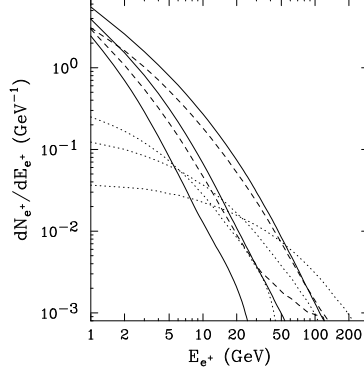


Figure 34: The positron spectrum from neutralino annihilations for the most important annihilation modes. Solid lines represent the positron spectrum, per annihilation, for $\chi^0\chi^0 \rightarrow b\bar{b}$, for LSPs with masses of 50, 150 and 600 GeV. The dotted lines are the same, but from the process $\chi^0\chi^0 \rightarrow \tau^+\tau^-$. Dashed lines represent positrons from the process $\chi\chi \rightarrow W^+W^-$ for LSPs with masses of 150 and 600 GeV. The spectrum from $\chi\chi \rightarrow ZZ$ is very similar.

tic magnetic fields, travelling in a random walk, and losing energy via inverse Compton and synchrotron processes. The diffusion-loss equation describing this process is given by

$$\begin{aligned} \frac{\partial}{\partial t} \frac{dn_{e^+}}{dE_{e^+}} &= \vec{\nabla} \cdot \left[K(E_{e^+}, \vec{x}) \vec{\nabla} \frac{dn_{e^+}}{dE_{e^+}} \right] \\ &+ \frac{\partial}{\partial E_{e^+}} \left[b(E_{e^+}, \vec{x}) \frac{dn_{e^+}}{dE_{e^+}} \right] + Q(E_{e^+}, \vec{x}), \end{aligned} \quad (143)$$

where dn_{e^+}/dE_{e^+} is the number density of positrons per unit energy, $K(E_{e^+}, \vec{x})$ is the diffusion constant, $b(E_{e^+}, \vec{x})$ is the rate of energy loss and $Q(E_{e^+}, \vec{x})$ is the source term.

The diffusion constant [489] and rate of energy loss can be parameterized by

$$K(E_{e^+}) = 3 \times 10^{27} \left[3^{0.6} + E_{e^+}^{0.6} \right] \text{cm}^2 \text{s}^{-1} \quad (144)$$

and

$$b(E_{e^+}) = 10^{-16} E_{e^+}^2 \text{s}^{-1}, \quad (145)$$

respectively. $b(E_{e^+})$ is the result of inverse Compton scattering on both starlight and the cosmic microwave background [361]. The diffusion parameters are constrained from analyzing stable nuclei in cosmic rays (primarily by fitting the boron to carbon ratio) [374, 375].

In equations 144 and 145, there is no dependence on location. This is due to the assumption of a constant diffusion zone. For our galaxy, the diffusion zone is best approximated as a slab of thickness $2L$, where L is chosen to be 4 kpc, the

best fit to observations [489, 374, 375]. The radius of the slab is unimportant, as it is much larger than the distances which positrons can propagate at these energies. Outside of the diffusion zone, the positron density is assumed to be (nearly) zero (free escape boundary conditions). For detailed descriptions of two zone diffusion models, see Refs. [58, 374, 375, 193, 376].

The effect of propagation on the positron spectrum depends strongly on the distance from the source. To compare to the data recorded by HEAT, a quantity called the “positron fraction” is typically considered. The positron fraction is the ratio of the positron flux to the combined positron and electron fluxes. The spectra for secondary positrons, secondary electrons and primary electrons can be found in Ref. [387].

Figure 35 shows the positron fraction, as a function of positron energy, for two scenarios with supersymmetric dark matter candidates. The various lines represent clumps of dark matter at different distances from Earth. Note the substantial variation in the positron spectrum which results. In all cases, the normalization was considered a free parameter. The predicted spectrum is compared to the error bars of the 1995 and 2000 HEAT data.

These results show that the spectral shape of the observed positron excess can be fit well by dark matter annihilation models. This neglects the issue of the annihilation rate (normalization), however. To produce the observed excess, a very high annihilation rate is required in the local region (within a few kpc). For supersymmetric dark matter, this requires very dramatic dark matter substructure [309]. For Kaluza-Klein dark matter, with larger cross sections and more favorable annihilation models, it may be more natural to accommodate the observed positron excess [306].

In the future, new experiments, such as AMS-02 [66], PAMELA [410] and Bess Polar [441], will refine the positron spectrum considerably. See section 4.4 for more details.

6.5.2 Anti-protons

Anti-protons travel much greater distances than positrons before losing their energy as they propagate through the galactic magnetic fields. Therefore, the dark matter distribution throughout much of the galaxy can contribute to the observed anti-proton spectrum [462, 432]. The measurement of the BESS experiment finds a cosmic anti-proton flux of $1.27_{-0.32}^{+0.37} \times 10^{-6} \text{cm}^{-2} \text{s}^{-1} \text{sr}^{-1} \text{GeV}^{-1}$ in the range of 400 to 560 MeV. This measurement is difficult to interpret in the context of dark matter annihilations due to large uncertainties in the size of the diffusion zone and other propagation characteristics [192]. Future experiments, especially those with sensitivity at greater energies, will be needed to identify signatures of dark matter in the cosmic anti-proton spectrum. For more information on anti-protons from dark matter annihilations, see Refs. [125, 192, 84].

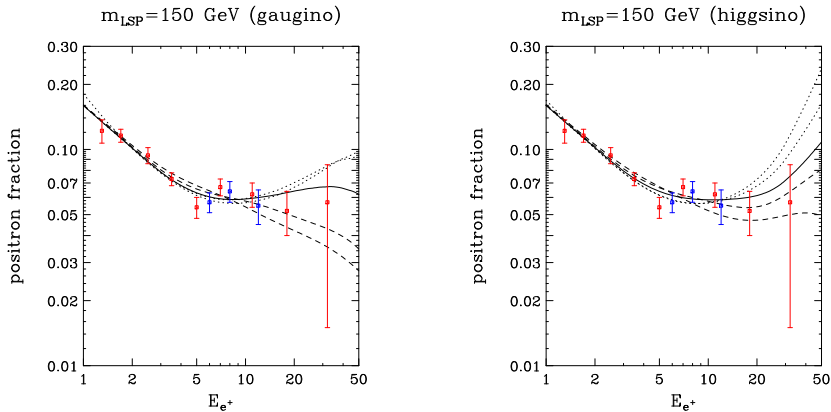


Figure 35: The predicted positron fraction, as a function of positron energy (in GeV), for a 150 GeV neutralino which annihilates 96% to $b\bar{b}$ and 4% to $\tau^+\tau^-$ (left) or 58% to W^+W^- and 42% to ZZ (right). The solid line represents the distance to the source (the dark matter clump) at which the predicted spectrum best fit the data (0.42 and 0.62 kpc for the left and right panels, respectively). Dotted lines represent the spectra for a source at a distance less than found for the best fit (0.23 and 0.19 kpc or 0.20 and 0.19 kpc for the left and right panels, respectively). For these two lines, the χ^2 is larger by 1 and 4, respectively (1 and $2\text{-}\sigma$). The dashed lines are the same, but for distances greater than found for the best fit (0.85 and 1.3 kpc or 1.1 and 1.6 kpc for the left and right panels, respectively). The normalization was considered a free parameter. The error bars shown are for the HEAT experiment. Red (lighter) error bars are from the 94-95 flight. The three blue (darker) errors bars between 6 and 12 GeV are from the 2000 flight.

6.6 The Role of Substructures

Annihilation radiation could be enhanced by the presence of substructures in the galactic halo. The actual effect depends crucially on the prescription of the profile and the spatial distribution of substructures.

Several groups focused on the signal enhancement due to the presence of “clumps” in dark matter distribution, a common feature of N-body simulations. The effect of the enhancement of the annihilation radiation on the gamma-ray flux has been studied by, *e.g.*, Bergstrom *et al.* [81], Calcaneo-Roldan and Moore [135], Tasitsiomi and Olinto [465], Berezhinsky, Dokuchaev and Eroshenko 2003 [77] and Stoehr *et al.* [463]).

Recently the problem has been carefully investigated by Koushiappas, Zentner and Walker [344], by means of a semi-analytic model of structure formation calibrated on high-resolution N-body simulations. The authors concluded that previous estimates were optimistic, and that it may be possible for the upcoming experiments GLAST and VERITAS to detect gamma-rays from dark matter clumps only if the neutralino is relatively light, *i.e.* $m_\chi \lesssim 100$ GeV.

Blasi *et al.* [114] studied the synchrotron emission produced by secondary electron-positron pairs, produced by neutralino annihilations, in the galactic magnetic field. If confirmed, their results would imply a microwave emission observable over CMB anisotropies, which is potentially identifiable by its spatial structure or its radio spectrum. As we mentioned before, the presence of substructure is also a possible explanation for the positron excess observed by HEAT [59, 309].

Clumps are not the only substructures that can potentially increase the annihilation flux. Among other structures considered in the literature, are the so-called caustics. In fact, continuous infall of dark matter on our galaxy should give rise to ring shaped overdensities, called caustics (see *e.g.* Ref. [453]). Unfortunately the prospects for the detection of annihilation radiation from these substructures do not appear promising (see Bergstrom, Edsjo and Gunnarsson [85]).

Apart from galactic substructures, one could ask what the annihilation flux from all structures and substructures in the Universe is, *i.e.* what extra-galactic background would be produced by dark matter annihilation. This problem has been investigated by Bergstrom, Edsjo and Ullio [87], Taylor and Silk [467], and Ullio *et al.* [482]. In particular, the authors of the last reference stressed the possibility of observing, for some specific regions of the SUSY parameter space, and sufficiently dense substructures, a spectacular feature in the gamma-ray spectrum produced by cosmological redshift and absorption along the line-of-sight of the gamma-ray line from dark matter annihilation.

6.7 Constraints from Helioseismology

The seismic diagnostics of the Sun’s interior puts important constraints on the internal thermodynamic structure of the Sun. Indeed, such research has led to significant improvements in our understanding of microphysics such as the equation of state and the opacity calculations, and to a better determination of specific cross-sections in the *pp* chain (see *e.g.* Ref. [363] and references therein).

It is intriguing to investigate whether the fact that the Sun evolves in a halo of WIMPs affects its internal structure and the details of its evolution. Modifying an existing numerical code for the Solar structure, Lopes *et al.* [363] estimated the influence of the WIMP halo on the evolution and structure of the Sun, and calculated the deviations of the “modified Sun” with respect to the Solar Standard Model and to helioseismic data. They then rejected the portions of the WIMP parameter space leading to Solar models in conflict with Helioseismic observations.

Although current measurement do not appear to impose strong constraints on dark matter particles (see also Lopes, Silk and Hansen [364] and Bottino *et al.* [127]), it is expected that future helioseismic experiments will be sensitive to luminosities from WIMP annihilations in the solar core larger than 10^{-5} times the solar core luminosity (see figure 36). Furthermore, if the dark matter density increases toward the central region of our galaxy, as is suggested by N-body simulations, stars nearer to the Galactic center would evolve in a WIMP

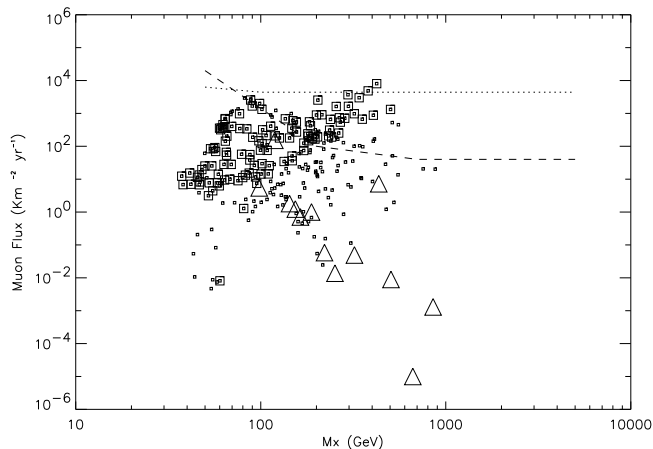


Figure 36: Predicted neutrino-induced muon flux produced by neutralino annihilation in the Sun. Small squares correspond to models within the phenomenological MSSM, triangles correspond to selected benchmark points within the mSUGRA framework. Big squares are used to highlight models leading to a local variation of luminosity of the solar core larger than 10^{-5} (which could thus be potentially probed by upcoming solar seismic observations). The dotted and dashed curves represent the current limit sensitivity of MACRO and the expected sensitivity of IceCube.

halo which is much more dense, where the effects of dark matter on the stellar structure could be of enormous importance.

Preliminary calculations [362] suggest that evolution times of stars evolving in dense dark matter halos are significantly shorter. If confirmed, these results would change our understanding of stellar evolution and shed new light on the stellar population near the center of our galaxy.

6.8 Constraints on Superheavy Dark Matter

In our discussion thus far, we have focused on the detection of weakly interacting dark matter particles with masses near the electroweak scale. Here, we will extend that discussion to include particles which are much more massive.

Recently, Albuquerque and Baudis [23] have studied the prospects for the direct detection of supermassive dark matter particles. They find that if such particles are strongly interacting (simpzillas), masses below $\sim 10^{15}$ GeV can be probed by current experiments. A superheavy, weakly interacting particle is not constrained by this method, however.

The prospects for the observation of supermassive dark matter annihilation from the galactic center are not very promising (see *e.g.* Ref. [91]). Nevertheless, portions of the relevant parameter space can be efficiently probed by gamma-ray experiments.

The prospects for the observation of high-energy neutrinos from the Sun are potentially interesting [24, 168]. For simpzillas, kilometer scale neutrino

telescopes, such as IceCube can test a broad range of masses. A signature unique to this scenario would be a predominance of tau neutrinos with energies above $\sim\text{TeV}$.

The compilation of results in the work of Starkman *et al.* [460] considers the constraints on superheavy dark matter found from double- β decays, cosmic-ray detectors, galactic-halo stability, cooling of molecular clouds, proton-decay detectors and longevity of neutron stars.

The constraints derived from old neutron stars is particularly interesting. The argument goes as follows: if WIMPs exist they would accrete on neutron stars, the same way as they do on the Sun (see Sec. 6.4 and Sec. 6.7) [257]. For certain regions of the WIMP parameter space, the accretion can be so efficient that WIMPs become self-gravitating, then collapse to a mini black hole, which finally destroys the star. However, a large portion of the parameter space of modern superheavy candidates would escape these constraint, since the collapse could be prevented by self-annihilations.

7 Conclusions

There is compelling evidence for the existence of dark matter. Although our understanding of its nature and distribution is still incomplete, many independent observations suggest that about 30% of the total energy density of the Universe is made of some sort of non-baryonic dark matter. We have reviewed such observations and discussed how they compare with theoretical predictions, and in particular with the results of N-body simulations.

The dark matter problem is not only relevant to astrophysicists but also to the particle and high-energy physics community. In fact, some of the best dark matter candidates come from possible extensions of the Standard Model of particle physics. There is certainly no shortage of particle dark matter candidates found in such models. Among those proposed in literature, we have focused on the dark matter particles found in models of supersymmetry (the lightest neutralino) and models with Universal Extra Dimensions (Kaluza-Klein dark matter). Although many simple models of supersymmetry, extra dimensions or other scenarios are widely discussed by the particle and astroparticle communities, the phenomenology of the actual physical theory could be more rich and complex. Collider experiments are probing significant regions of the parameter space of these hypothetical particles. Conversely, a positive astrophysical detection of dark matter would provide invaluable information regarding the physics “beyond the Standard Model”.

The astroparticle community has started a vigorous and broad program of experiments that may be able to shed new light on the physics and astrophysics of dark matter. Before discussing the results of direct and indirect searches, we have reviewed the present and future experiments on which they are based.

Among the most promising dark matter searches appears to be direct detection. The current situation is complicated by the claim of a positive detection by the DAMA experiment, which have been contradicted by several other ex-

periments. It is unclear, but more and more improbable, whether it is possible to find a theoretical scenario that accommodates all the experimental findings. The much higher (several orders of magnitude) sensitivity of future experiments should be able to solve this controversy.

Indirect dark matter detection via annihilations in the Galactic center region is also an exciting possibility, although the prospects for the observation of gamma-rays, neutrinos and synchrotron radiation from that direction strongly depend on astrophysical parameters, such as the profile of dark matter in the innermost regions, which unfortunately are poorly known. Nevertheless, the development of next-generation gamma-ray and neutrino telescopes will allow us to test many scenarios, especially if effects such as the adiabatic accretion onto the central black hole significantly enhance the dark matter density and corresponding annihilation signal. If the Galactic center turns out to contain less dark matter, observations of dwarf galaxies, external galaxies and local dark substructure may play an important role for indirect searches.

Indirect searches for dark matter through the observation of high energy neutrinos produced in dark matter annihilations in the Sun are also promising. These rates do not depend strongly on the dark matter halo distribution and are thus fairly unambiguous probes of particle dark matter models. Measurement of the positron and anti-proton spectra, which are soon to improve dramatically, can also provide an opportunity to observe products of dark matter annihilations in the galactic halo.

Collectively, the direct, indirect and collider searches for particle dark matter have incredible prospects for discovery in the coming years. We hope that this review can be a useful tool in guiding members of the scientific community closer to the goal of dark matter identification which has eluded us for so long.

8 Acknowledgements

We wish to thank G.Sigl for earlier collaboration and countless stimulating discussions. We thank K. Abazajian, J. Beacom, A. Birkedal-Hansen, B. Dobrescu, S. Hansen, I. Liubarsky, I. Lopes, E. Nezri, J. Orloff, I. Perez, G. Servant, C. Skordis, P. Salati, C. Spiering, F. Stoehr, T. Tait, J. Taylor and A. Zentner for illuminating comments and discussions. Special thanks to P. Salati for careful reading of an earlier version of the manuscript and T. Plehn and L. Wang for numerous useful comments. The work of GB was supported at an earlier stage by an “Allocation de Recherche”, PhD program Universite Paris 7 at the Institut d’Astrophysique de Paris, and is now supported by the DOE and the NASA grant NAG 5-10842 at Fermilab. DH is supported by the Leverhulme trust.

A Neutralino Mass Eigenstates

In the Minimal Supersymmetric Standard Model (MSSM), the neutral electroweak gauginos (\tilde{B}, \tilde{W}^3) and higgsinos ($\tilde{H}_1^0, \tilde{H}_2^0$) have the same quantum numbers and, therefore, mix into four mass eigenstates called neutralinos. The neutralino mass matrix in the $\tilde{B}-\tilde{W}^3-\tilde{H}_1^0-\tilde{H}_2^0$ basis is given by

$$\mathcal{M}_N = \begin{pmatrix} M_1 & 0 & -M_Z \cos \beta \sin \theta_W & M_Z \sin \beta \sin \theta_W \\ 0 & M_2 & M_Z \cos \beta \cos \theta_W & -M_Z \sin \beta \cos \theta_W \\ -M_Z \cos \beta \sin \theta_W & M_Z \cos \beta \cos \theta_W & 0 & -\mu \\ M_Z \sin \beta \sin \theta_W & -M_Z \sin \beta \cos \theta_W & -\mu & 0 \end{pmatrix}, \quad (146)$$

where M_1 , M_2 and μ are the bino, wino and higgsino mass parameters, respectively, θ_W is the Weinberg angle and $\tan \beta$ is the ratio of the vacuum expectation values of the Higgs bosons. This matrix can be diagonalized by the matrix, N .

$$M_{\chi^0}^{\text{diag}} = N^\dagger M_{\chi^0} N. \quad (147)$$

The masses of the four mass eigenstates are then given by [207, 62]

$$\epsilon_1 M_{\chi_1^0} = -\left(\frac{1}{2}a - \frac{1}{6}C_2\right)^{1/2} + \left[-\frac{1}{2}a - \frac{1}{3}C_2 + \frac{C_3}{(8a - \frac{8}{3}C_2)^{1/2}}\right]^{1/2} + \frac{1}{4}(M_1 + M_2), \quad (148)$$

$$\epsilon_2 M_{\chi_2^0} = +\left(\frac{1}{2}a - \frac{1}{6}C_2\right)^{1/2} - \left[-\frac{1}{2}a - \frac{1}{3}C_2 - \frac{C_3}{(8a - \frac{8}{3}C_2)^{1/2}}\right]^{1/2} + \frac{1}{4}(M_1 + M_2), \quad (149)$$

$$\epsilon_3 M_{\chi_3^0} = -\left(\frac{1}{2}a - \frac{1}{6}C_2\right)^{1/2} - \left[-\frac{1}{2}a - \frac{1}{3}C_2 + \frac{C_3}{(8a - \frac{8}{3}C_2)^{1/2}}\right]^{1/2} + \frac{1}{4}(M_1 + M_2), \quad (150)$$

$$\epsilon_4 M_{\chi_4^0} = +\left(\frac{1}{2}a - \frac{1}{6}C_2\right)^{1/2} + \left[-\frac{1}{2}a - \frac{1}{3}C_2 - \frac{C_3}{(8a - \frac{8}{3}C_2)^{1/2}}\right]^{1/2} + \frac{1}{4}(M_1 + M_2), \quad (151)$$

where ϵ_i is the sign of the i th eigenvalue of the neutralino mass matrix, and

$$C_2 = (M_1 M_2 - M_Z^2 - \mu^2) - \frac{3}{8}(M_1 + M_2)^2, \quad (152)$$

$$C_3 = -\frac{1}{8}(M_1 + M_2)^3 + \frac{1}{2}(M_1 + M_2)(M_1 M_2 - M_Z^2 - \mu^2) + (M_1 + M_2)\mu^2 + (M_1 \cos^2 \theta_W + M_2 \sin^2 \theta_W)M_Z^2 + \mu M_Z^2 \sin 2\beta, \quad (153)$$

$$C_4 = -(M_1 \cos^2 \theta_W + M_2 \sin^2 \theta_W)M_Z^2 \mu \sin 2\beta - M_1 M_2 \mu^2 + \frac{1}{4}(M_1 + M_2)[(M_1 + M_2)\mu^2 + (M_1 \cos^2 \theta_W + M_2 \sin^2 \theta_W)M_Z^2 + \mu M_Z^2 \sin 2\beta] + \frac{1}{16}(M_1 M_2 - M_Z^2 - \mu^2)(M_1 + M_2)^2 - \frac{3}{256}(M_1 + M_2)^4, \quad (154)$$

$$a = \frac{1}{2^{1/3}} \operatorname{Re} \left[-S + i(D/27)^{1/2} \right]^{1/3}, \quad (155)$$

$$D = -4U^3 - 27S^2, \quad U = -\frac{1}{3}C_2^2 - 4C_4, \quad S = -C_3^2 - \frac{2}{27}C_2^3 + \frac{8}{3}C_2C_4. \quad (156)$$

The four masses above are not generally in the order $M_{\chi_1^0} < M_{\chi_2^0} < M_{\chi_3^0} < M_{\chi_4^0}$, although it is conventional to relabel the states, from lightest to heaviest.

The mixing matrix, N , is then given by [207, 62]

$$\frac{N_{i2}}{N_{i1}} = -\frac{1}{\tan \theta_W} \frac{M_1 - \epsilon_i M_{\chi_i^0}}{M_2 - \epsilon_i M_{\chi_i^0}}, \quad (157)$$

$$\frac{N_{i3}}{N_{i1}} = \frac{-\mu[M_2 - \epsilon_i M_{\chi_i^0}][M_1 - \epsilon_i M_{\chi_i^0}] - M_Z^2 \sin \beta \cos \beta [(M_1 - M_2) \cos^2 \theta_W + M_2 - \epsilon_i M_{\chi_i^0}]}{M_Z[M_2 - \epsilon_i M_{\chi_i^0}] \sin \theta_W [-\mu \cos \beta + \epsilon_i M_{\chi_i^0} \sin \beta]}, \quad (158)$$

$$\frac{N_{i4}}{N_{i1}} = \frac{-\epsilon_i M_{\chi_i^0} [M_2 - \epsilon_i M_{\chi_i^0}] [M_1 - \epsilon_i M_{\chi_i^0}] - M_Z^2 \cos^2 \beta [(M_1 - M_2) \cos^2 \theta_W + M_2 - \epsilon_i M_{\chi_i^0}]}{M_Z[M_2 - \epsilon_i M_{\chi_i^0}] \sin \theta_W [-\mu \cos \beta + \epsilon_i M_{\chi_i^0} \sin \beta]}, \quad (159)$$

and

$$N_{i1} = \left[1 + \left(\frac{N_{i2}}{N_{i1}} \right)^2 + \left(\frac{N_{i3}}{N_{i1}} \right)^2 + \left(\frac{N_{i4}}{N_{i1}} \right)^2 \right]^{-1/2}. \quad (160)$$

The lightest neutralino (χ_1^0) is a mixture of gauginos and higgsinos:

$$\chi_1^0 = N_{11} \tilde{B} + N_{12} \tilde{W}^3 + N_{13} \tilde{H}_1^0 + N_{14} \tilde{H}_2^0. \quad (161)$$

The gaugino fraction of χ_1^0 is defined as

$$f_G = N_{11}^2 + N_{12}^2 \quad (162)$$

and its higgsino fraction as

$$f_H = N_{13}^2 + N_{14}^2. \quad (163)$$

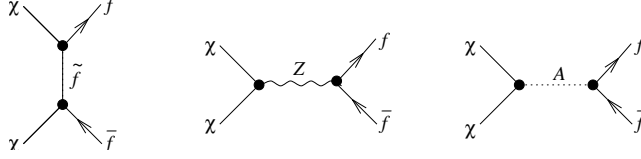


Figure 37: Tree level diagrams for neutralino annihilation into fermion pairs. From Ref. [319].

B Neutralino Annihilation Cross Sections in the Low Velocity Limit

In this appendix, we give the amplitudes and cross sections for the most important neutralino annihilation channels in the low velocity limit (the first term in the expansion $\sigma v = a + bv^2 + \dots$). This is sufficient for indirect detection but generally insufficient for relic density calculations in which velocity dependent contributions are important. For a more complete list, with all S and P-wave tree level annihilation amplitudes, see Refs. [195, 319, 397, 396, 106].

B.1 Annihilation Into Fermions

Neutralinos can annihilate to fermion pairs by three tree level diagrams [195, 213, 275, 276]. These processes consist of s-channel exchange of pseudoscalar Higgs and Z^0 -bosons and t-channel exchange of sfermions (see Fig. 37).

The amplitude for pseudoscalar Higgs exchange is given by

$$\mathcal{A}_A = 4\sqrt{2}gT_{A11}h_{Aff}\frac{1}{4 - (m_A/m_\chi)^2 + i\Gamma_A m_A/m_\chi^2}. \quad (164)$$

Here, m_A is the pseudoscalar Higgs mass and Γ_A is the pseudoscalar Higgs width. T_{A11} is the A^0 -neutralino-neutralino coupling and is given by

$$T_{A11} = -\sin\beta Q''_{1,1} + \cos\beta S''_{1,1}, \quad (165)$$

where $Q''_{1,1} = N_{3,1}(N_{2,1} - \tan\theta_W N_{1,1})$ and $S''_{1,1} = N_{4,1}(N_{2,1} - \tan\theta_W N_{1,1})$. N is the matrix which diagonalizes the neutralino mass matrix in the $\tilde{B}-\tilde{W}^3-\tilde{H}_1^0-\tilde{H}_2^0$ basis, $M_{\chi^0}^{\text{diag}} = N^\dagger M_{\chi^0} N$ (see Appendix A). θ_W is the Weinberg angle and $\tan\beta$ is the ratio of the Higgs vacuum expectation values. h_{Aff} is the A^0 -fermion-fermion Yukawa coupling. For up-type fermions, this is given by

$$h_{Aff} = -\frac{gm_f \cot\beta}{2m_{W^\pm}}. \quad (166)$$

For down-type fermions, it is

$$h_{Aff} = -\frac{gm_f \tan\beta}{2m_{W^\pm}}. \quad (167)$$

The amplitude for neutralino annihilation via sfermion exchange to a pair of fermions, $f_i \bar{f}_i$, is given by

$$\mathcal{A}_{\bar{f}} = \sqrt{2} \sum_{j=1}^6 \frac{1}{P_j} \left(\left[(X'_{ij1})^2 + (W'_{ij1})^2 \right] \frac{m_{f_i}}{m_\chi} + 2X'_{ij1} W'_{ij1} \right), \quad (168)$$

where $P_j = 1 + (m_{\bar{f}_j}/m_\chi)^2 - (m_{f_i}/m_\chi)^2$ and the sum is over the six sfermion states which couple to the final state fermion. The fermion-sfermion-neutralino couplings, X'_{ij1} and W'_{ij1} , are given by

$$X'_{ij1} = X_1 (\Pi_L \Theta_f)_{i,j} + Z_{i,k,1} (\Pi_R \Theta_f)_{k,j} \quad (169)$$

and

$$W'_{ij1} = Y_1 (\Pi_R \Theta_f)_{i,j} + Z_{i,k,1} (\Pi_L \Theta_f)_{k,j}, \quad (170)$$

where

$$X_1 = -g\sqrt{2} [T_3(f_i) N_{2,1}^* - \tan \theta_W (T_3(f_i) - e(f_i)) N_{1,1}^*], \quad (171)$$

and

$$Y_1 = g\sqrt{2} \tan \theta_W e(f_i) N_{1,1}^*. \quad (172)$$

For final state up-type quarks,

$$Z_{i,j,1} = -\frac{g}{\sqrt{2} m_{W^\pm} \sin \beta} \Theta_{i,j} N_{4,1}^*. \quad (173)$$

For final state down-type quarks,

$$Z_{i,j,1} = -\frac{g}{\sqrt{2} m_{W^\pm} \cos \beta} \Theta_{i,j} N_{3,1}^*. \quad (174)$$

And for final state leptons,

$$Z_{i,j,1} = -\frac{g}{\sqrt{2} m_{W^\pm} \cos \beta} \Theta_{i,j} N_{3,1}^*. \quad (175)$$

Here, $T_3(f_i)$ and $e(f_i)$ are the weak hypercharge and electric charge of the final state fermion. N , again, is the matrix which diagonalizes the neutralino mass matrix. Θ_f 's are the appropriate 6 x 6 sfermion mass matrices and $\Pi_{L,R}$ are left and right projection operators:

$$\Pi_L = \begin{pmatrix} 1 & 0 & 0 & 0 & 0 & 0 \\ 0 & 1 & 0 & 0 & 0 & 0 \\ 0 & 0 & 1 & 0 & 0 & 0 \end{pmatrix}, \quad (176)$$

$$\Pi_R = \begin{pmatrix} 0 & 0 & 0 & 1 & 0 & 0 \\ 0 & 0 & 0 & 0 & 1 & 0 \\ 0 & 0 & 0 & 0 & 0 & 1 \end{pmatrix}. \quad (177)$$

Lastly, the amplitude for neutralino annihilation to fermions via Z exchange is given by

$$\mathcal{A}_Z = 2\sqrt{2}\frac{g^2}{\cos^2\theta_W}O''_{1,1}{}^L T_3(f_i)\frac{m_{f_i}m_\chi}{m_Z^2}, \quad (178)$$

where $T_3(f_i)$ is the weak hypercharge of the fermion. The coupling $O''_{1,1}{}^L$ is given by $\frac{1}{2}(-N_{3,1}N_{3,1}^* + N_{4,1}N_{4,1}^*)$.

Summing these three contributions to the amplitude, we can calculate the cross section for this process:

$$\sigma v(\chi\chi \rightarrow \bar{f}_i f_i)_{v \rightarrow 0} = \frac{c_f \beta_f}{128\pi m_\chi^2} |\mathcal{A}_A(\chi\chi \rightarrow \bar{f}_i f_i) + \mathcal{A}_{\bar{f}}(\chi\chi \rightarrow \bar{f}_i f_i) + \mathcal{A}_Z(\chi\chi \rightarrow \bar{f}_i f_i)|^2, \quad (179)$$

where $\beta_f = \sqrt{1 - m_f^2/m_\chi^2}$. c_f is a color factor which is equal to three for quark final states and one otherwise.

We emphasize that all tree level (low velocity) neutralino annihilation diagrams to fermion pairs have amplitudes which are proportional to the final state fermion mass. For sfermion and Z^0 exchange, this is because the Z^0 -fermion-fermion and neutralino-fermion-fermion couplings preserve chirality. For pseudoscalar Higgs exchange, the amplitude introduces an explicit factor of the fermion mass in the Yukawa coupling. We also note that the Yukawa coupling which appears in the pseudoscalar Higgs exchange amplitude is proportional to $\tan\beta$ for down-type quarks and $\cot\beta$ for up-type quarks. The net result of these observations is that neutralino annihilation into fermions will be dominated by heavy final states, $b\bar{b}$, $\tau^-\tau^+$ and, if kinematically allowed, $t\bar{t}$. Furthermore, if $\tan\beta$ is large, bottom-type fermions may dominate over up-type fermions, even if less massive. For example, annihilations to $b\bar{b}$ may dominate over $t\bar{t}$, even for heavy neutralinos.

B.2 Annihilation Into Gauge Bosons

Generally, neutralinos can annihilate into gauge boson pairs via several processes (see Fig. 38) [195, 278, 404, 405]. In the low velocity limit, however, only t-channel processes via chargino or neutralino exchange are non-vanishing.

In the low velocity limit, the amplitude for neutralino annihilation to W^\pm -pairs is given by

$$\mathcal{A}(\chi\chi \rightarrow W^+W^-)_{v \rightarrow 0} = 2\sqrt{2}\beta_W g^2 \sum_{n=1}^2 [(O_{1,n}^L)^2 + (O_{1,n}^R)^2] \frac{1}{P_n}, \quad (180)$$

where $\beta_W = \sqrt{1 - m_W^2/m_\chi^2}$ and $P_n = 1 + (m_{\chi_n^\pm}/m_\chi)^2 - (m_W/m_\chi)^2$. The sum is over chargino states. $O_{1,n}^L$ and $O_{1,n}^R$ are the neutralino couplings to charginos given by $\frac{-1}{\sqrt{2}}N_{4,1}V_{2,n}^* + N_{2,1}V_{1,n}^*$ and $\frac{1}{\sqrt{2}}N_{3,1}^*U_{2,n} + N_{2,1}^*U_{1,n}$, respectively, where N , again, is the matrix which diagonalizes the neutralino mass matrix. The V 's and U 's are components of the chargino mass matrix, in the basis

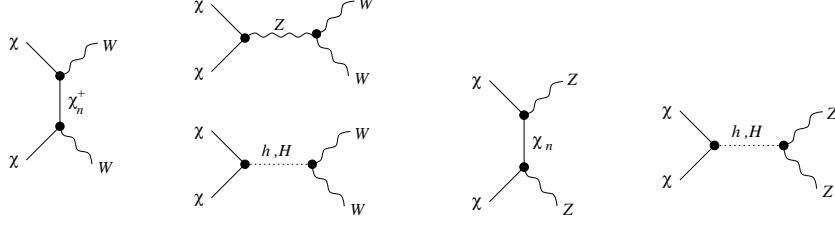


Figure 38: Tree level diagrams for neutralino annihilation into gauge boson pairs. From Ref. [319].

$$U = \begin{pmatrix} \cos \phi_- - \sin \phi_- \\ \sin \phi_- \cos \phi_+ \end{pmatrix} \quad (181)$$

and

$$V = \begin{pmatrix} \cos \phi_+ - \sin \phi_+ \\ \sin \phi_+ \cos \phi_- \end{pmatrix}, \quad (182)$$

where

$$\tan 2\phi_- = 2\sqrt{2}m_W \frac{(\mu \sin \beta + M_2 \cos \beta)}{(M_2^2 - \mu^2 + 2m_W^2 \cos 2\beta)} \quad (183)$$

and

$$\tan 2\phi_+ = 2\sqrt{2}m_W \frac{(\mu \cos \beta + M_2 \sin \beta)}{(M_2^2 - \mu^2 - 2m_W^2 \cos \beta)}. \quad (184)$$

The amplitude for annihilations to Z^0 -pairs is similar:

$$\mathcal{A}(\chi\chi \rightarrow Z^0 Z^0)_{v \rightarrow 0} = 4\sqrt{2}\beta_Z \frac{g^2}{\cos^2 \theta_W} \sum_{n=1}^4 (O''_{1,n}{}^L)^2 \frac{1}{P_n}. \quad (185)$$

Here, $\beta_Z = \sqrt{1 - m_Z^2/m_\chi^2}$, and $P_n = 1 + (m_{\chi_n}/m_\chi)^2 - (m_Z/m_\chi)^2$. The sum is over neutralino states. The coupling $O''_{1,n}{}^L$ is given by $\frac{1}{2}(-N_{3,1}N_{3,n}^* + N_{4,1}N_{4,n}^*)$.

The low velocity annihilation cross section for this mode is then given by

$$\sigma v(\chi\chi \rightarrow GG)_{v \rightarrow 0} = \frac{1}{S_G} \frac{\beta_G}{128\pi m_\chi^2} |\mathcal{A}(\chi\chi \rightarrow GG)|^2, \quad (186)$$

where G indicates which gauge boson is being considered. S_G is a statistical factor equal to one for W^+W^- and two for Z^0Z^0 .

It is useful to note that pure-gaugino neutralinos have a no S-wave annihilation amplitude to gauge bosons. Pure-higgsinos or mixed higgsino-gauginos, however, can annihilate efficiently via these channels, even at low velocities.

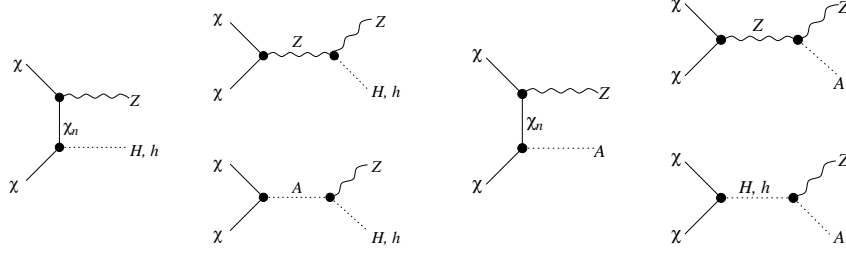


Figure 39: Tree level diagrams for neutralino annihilation into a Z and a Higgs boson. From Ref. [319].

B.3 Annihilation Into Higgs Bosons

There are many tree level diagrams which contribute to neutralino annihilation into Higgs boson pairs or a Higgs boson and a gauge boson (see Figs. 39, 40 and 41)[195, 278, 404, 405, 323, 429, 378].

In the low velocity limit, the amplitude for neutralino annihilation to a Z^0 and a light neutral Higgs, h^0 , is given by

$$\begin{aligned} \mathcal{A}(\chi\chi \rightarrow Z^0 h^0)_{v \rightarrow 0} &= -2\sqrt{2} \beta_{Zh} \frac{m_\chi}{m_Z} \frac{g^2}{\cos \theta_W} \left[-2 \sum_{n=1}^4 O_{1,n}^{\prime L} T_{h1,n} \right. & (187) \\ &\times \frac{m_{\chi_n} - m_\chi}{m_\chi P_n} + O_{1,1}^{\prime L} \frac{m_\chi \sin(\beta - \alpha)}{m_Z \cos \theta_W} - \frac{2 \cos(\alpha - \beta) T_{A1,1}}{4 - m_A^2/m_\chi^2 + i \Gamma_A m_A/m_\chi^2} \left. \right], \end{aligned}$$

where Γ_A is the pseudoscalar Higgs width and $T_{h1,n}$ is the $h^0 - \chi_0 - \chi_n$ Yukawa coupling (see below). The couplings, $O_{1,n}^{\prime L}$, is given by $N_{3,1}(N_{2,n} - \tan \theta_W N_{1,n})/2 + N_{3,n}(N_{2,1} - \tan \theta_W N_{1,1})/2$ and $P_n = 1 + (m_{\chi_n}/m_\chi)^2 - \frac{1}{2}(m_Z/m_\chi)^2 - \frac{1}{2}(m_h/m_\chi)^2$. $\tan \beta$ is the ratio of the Higgs vacuum expectation values and the mixing angle, α , is related to β by

$$\sin 2\alpha = -\sin 2\beta \left(\frac{m_H^2 + m_h^2}{m_H^2 - m_h^2} \right) \quad (188)$$

and

$$\cos 2\alpha = -\cos 2\beta \left(\frac{m_A^2 - m_Z^2}{m_H^2 - m_h^2} \right). \quad (189)$$

The three terms of Eq. 187 correspond to neutralino, Z^0 and A^0 exchange, from first to last.

The expression for neutralino annihilations to a Z^0 and a heavy Higgs boson, H^0 , is the same, but with $\sin(\beta - \alpha)$ and $\cos(\alpha - \beta)$ exchanged, and the couplings and masses of h^0 replaced by the couplings and masses of H^0 . These Yukawa couplings are given by

$$T_{h1,n} = \sin \alpha Q_{1,n}^{\prime\prime} + \cos \alpha S_{1,n}^{\prime\prime} \quad (190)$$

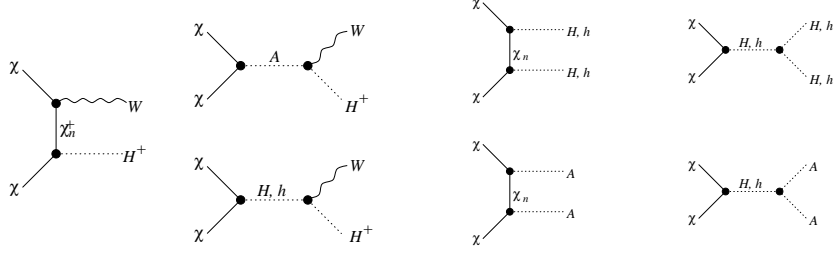


Figure 40: Tree level diagrams for neutralino annihilation into a W^\pm and a Higgs boson or a pair of Higgs bosons. From Ref. [319].

and

$$T_{H1,n} = -\cos\alpha Q''_{1,n} + \sin\alpha S''_{1,n}. \quad (191)$$

Here, $S''_{1,n} = N_{4,1}(N_{2,n} - \tan\theta_W N_{1,n})/2 + N_{4,n}(N_{2,1} - \tan\theta_W N_{1,1})/2$. $Q''_{1,n}$ is defined above.

The amplitude for annihilations to a W^\pm and a charged Higgs boson is given by

$$\begin{aligned} \mathcal{A}(\chi\chi \rightarrow W^\pm H^\mp)_{v \rightarrow 0} = & 4\sqrt{2}\beta_{WH}g^2 \left[-\frac{1}{2} \sum_{n=1}^2 \frac{m_\chi}{m_W} \frac{O_{1,n}^R Q_{1,n}^{\prime R} - O_{1,n}^L Q_{1,n}^{\prime L}}{P_n} \right. \\ & \left. + \frac{1}{2} \sum_{n=1}^2 \frac{m_{\chi_n^\pm}}{m_W} \frac{O_{1,n}^R Q_{1,n}^{\prime L} - O_{1,n}^L Q_{1,n}^{\prime R}}{P_n} - \frac{m_\chi T_{A11}}{m_W(4 - m_A^2/m_\chi^2)} \right], \end{aligned} \quad (192)$$

where $P_n = 1 + (m_{\chi_n^\pm}/m_\chi)^2 - \frac{1}{2}(m_{H^\pm}/m_\chi)^2 - \frac{1}{2}(m_W/m_\chi)^2$. $O_{1,n}^R$ and $O_{1,n}^L$ are couplings given earlier in this appendix. $Q_{n,m}^{\prime L}$ and $Q_{n,m}^{\prime R}$ are the chargino-neutralino-charged Higgs couplings, given by

$$Q_{nm}^{\prime L} = \cos\beta \left[N_{4n}^* V_{1m}^* + \sqrt{\frac{1}{2}}(N_{2n}^* + \tan\theta_W N_{1n}^*) V_{2m}^* \right] \quad (193)$$

and

$$Q_{nm}^{\prime R} = \sin\beta \left[N_{3n} U_{1m} - \sqrt{\frac{1}{2}}(N_{2n} + \tan\theta_W N_{1n}) U_{2m} \right], \quad (194)$$

where each of the quantities used have been defined earlier in this appendix. The first and second terms of Eq. 192 correspond to chargino exchange. The third term corresponds to pseudoscalar Higgs exchange (there is no low velocity contribution from scalar Higgs exchange).

Finally, the low velocity amplitude for neutralino annihilation into one neutral Higgs boson and one pseudoscalar Higgs boson is given by

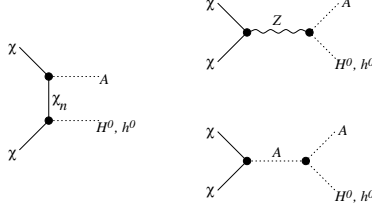


Figure 41: Tree level diagrams for neutralino annihilation into a neutral Higgs boson and a pseudoscalar Higgs boson. From Ref. [319].

$$\begin{aligned}
\mathcal{A}(\chi\chi \rightarrow h^0 A^0)_{v \rightarrow 0} = \sqrt{2} g^2 \left\{ -4 \sum_{n=1}^4 T_{h0n} T_{A0n} \left[\frac{m_{\chi_n}}{m_\chi P_n} - \frac{m_A^2 - m_h^2}{m_\chi^2} \right] \right. \\
\left. - 2 \frac{m_Z}{m_\chi} \frac{\sin(\alpha + \beta) \cos 2\beta}{2 \cos \theta_W} \frac{T_{A'00}}{4 - m_A^2/m_\chi^2} - \frac{\cos(\alpha - \beta) O'_{L00}}{2 \cos^2 \theta_W} \frac{m_A^2 - m_a^2}{m_Z^2} \right\}. \quad (195)
\end{aligned}$$

Here, $P_n = 1 + (m_{\chi_n}/m_\chi)^2 - \frac{1}{2}(m_A/m_\chi)^2 - \frac{1}{2}(m_h/m_\chi)^2$. The other quantities have been defined earlier in this appendix. Again, the amplitude for the analogous process with a heavy rather than light Higgs boson in the final state is the same, but with $\sin(\alpha + \beta)$ and $\cos(\alpha - \beta)$ exchanged and the light Higgs couplings and masses replaced with those for the heavy Higgs boson.

In the low velocity limit, there is no amplitude for neutralino annihilations to $H^+ H^-$, $h^0 h^0$, $H^0 H^0$, $A^0 A^0$ or $Z^0 A^0$.

The low velocity cross section for neutralino annihilation via any of these modes is

$$\sigma v(\chi\chi \rightarrow XY)_{v \rightarrow 0} = \frac{\beta_{XY}}{128\pi m_\chi^2} |\mathcal{A}(\chi\chi \rightarrow XY)_{v \rightarrow 0}|^2, \quad (196)$$

where X and Y are labels referring to the final state particles.

B.4 Annihilation Into Photons

Although there are no tree level processes for neutralino annihilation into photons, loop level processes to $\gamma\gamma$ and γZ^0 are very interesting, as they may provide a spectral line feature observable in indirect detection experiments.

In Fig. 42, all of the one-loop diagrams are shown for neutralino annihilation to a pair of photons. In Fig. 43, the corresponding diagrams to a photon and a Z^0 are shown. We do not include the corresponding amplitudes or cross sections here. For those results, see Ref. [79] and Ref. [480] for $\gamma\gamma$ and γZ^0 final states, respectively. Also see Ref. [271].

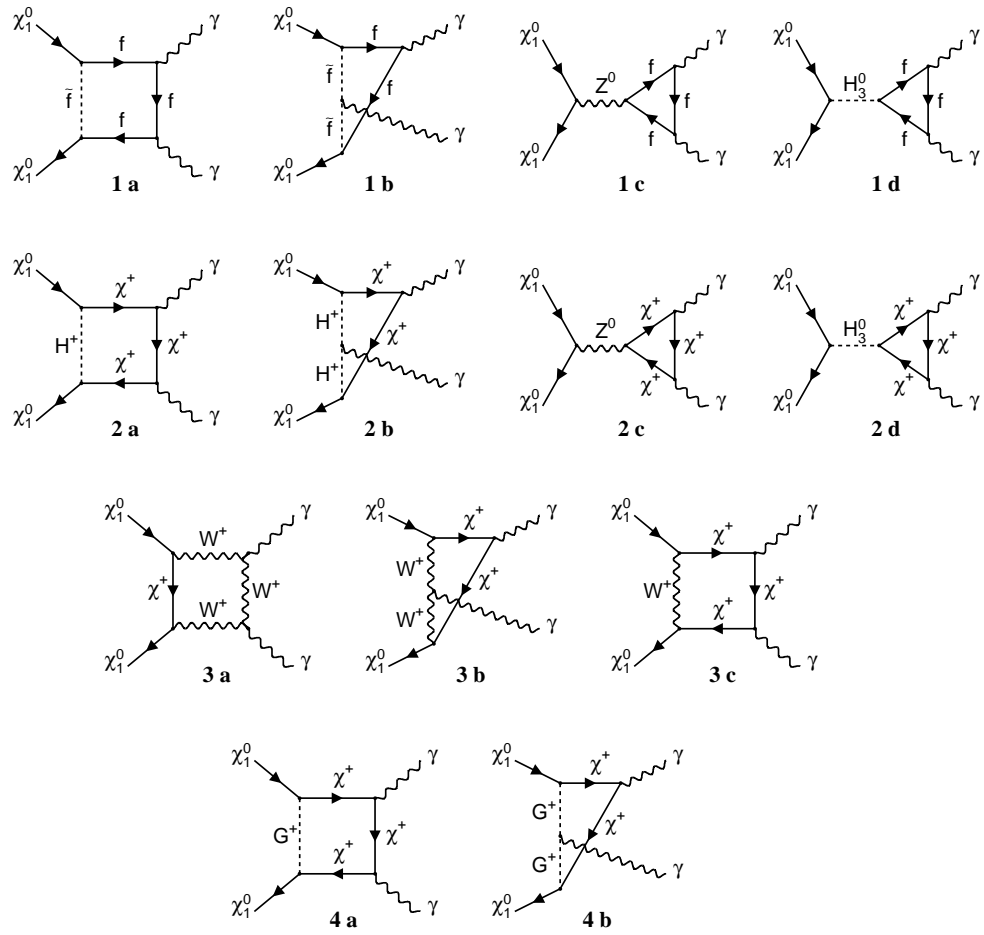
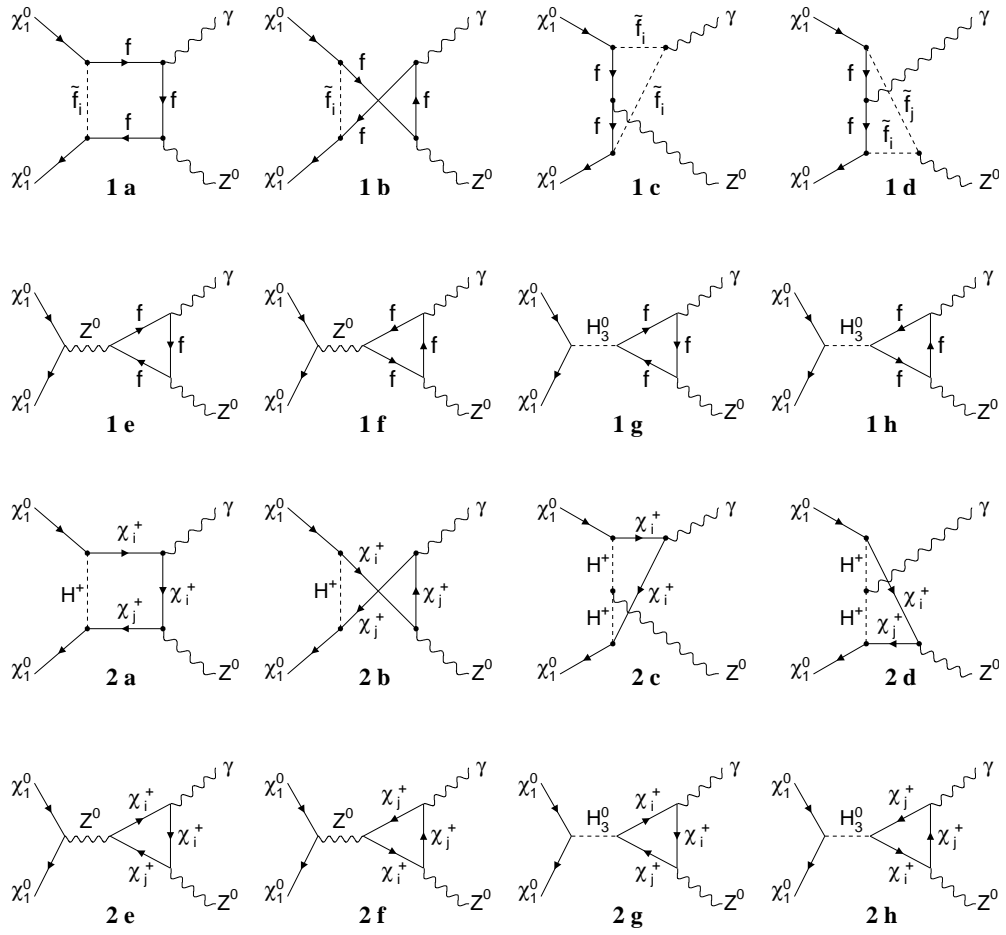


Figure 42: Diagrams contributing, at one loop level, to neutralino annihilation into two photons. From Ref. [79].



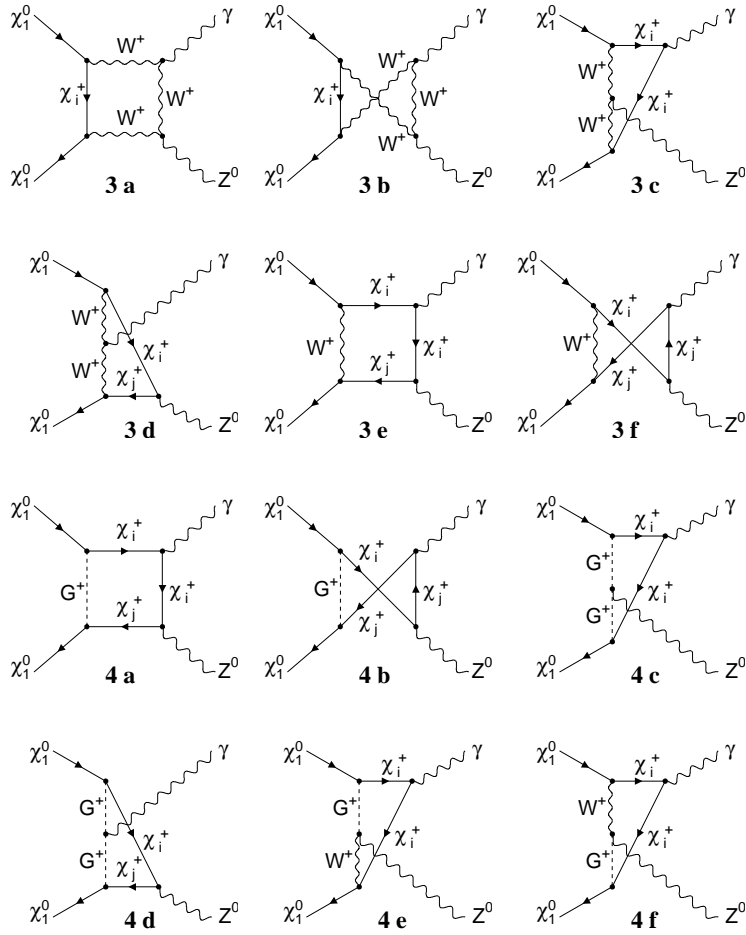


Figure 43: Diagrams contributing, at one loop level, to neutralino annihilation into a photon and a Z^0 . From Ref. [480].

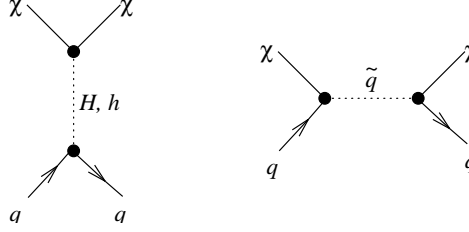


Figure 44: Tree level Feynman diagrams for neutralino-quark scalar (spin-independent) elastic scattering. From Ref. [319].

C Elastic Scattering Processes

C.1 Scalar Interactions

Consider a WIMP with scalar interactions with quarks given by

$$\mathcal{L}_{scalar} = a_q \bar{\chi} \chi \bar{q} q, \quad (197)$$

where a_q is the WIMP-quark coupling. Then the scattering cross section for the WIMP off of a proton or neutron is given by

$$\sigma_{scalar} = \int_0^{4m_r^2 v^2} \frac{d\sigma(v=0)}{d|\vec{v}|^2} = \frac{4m_r^2}{\pi} f_{p,n}^2, \quad (198)$$

where v is the relative velocity of the WIMP, m_r is the reduced mass of the nucleon ($m_r \simeq m_{p,n}$ for WIMPs heavier than ~ 10 GeV) and $f_{p,n}$ is the WIMP coupling to protons or neutrons, given by

$$f_{p,n} = \sum_{q=u,d,s} f_{Tq}^{(p,n)} a_q \frac{m_{p,n}}{m_q} + \frac{2}{27} f_{TG}^{(p,n)} \sum_{q=c,b,t} a_q \frac{m_{p,n}}{m_q}, \quad (199)$$

where $f_{Tu}^{(p)} = 0.020 \pm 0.004$, $f_{Td}^{(p)} = 0.026 \pm 0.005$, $f_{Ts}^{(p)} = 0.118 \pm 0.062$, $f_{Tu}^{(n)} = 0.014 \pm 0.003$, $f_{Td}^{(n)} = 0.036 \pm 0.008$ and $f_{Ts}^{(n)} = 0.118 \pm 0.062$ [209]. $f_{TG}^{(p,n)}$ is related to these values by

$$f_{TG}^{(p,n)} = 1 - \sum_{q=u,d,s} f_{Tq}^{(p,n)}. \quad (200)$$

The term in Eq. 199 which includes $f_{TG}^{(p,n)}$ results from the coupling of the WIMP to gluons in the target nuclei through a heavy quark loop. The couplings of squarks and Higgs bosons to heavy quarks leads to a loop level coupling of the WIMP to gluons [276, 61, 323]. Such diagrams are shown in Fig. 45.

To attain the scalar cross section for a WIMP scattering off of a target nucleus, one should sum over the protons and neutrons in the target:

$$\sigma = \frac{4m_r^2}{\pi} \left(Z f_p + (A - Z) f_n \right)^2, \quad (201)$$

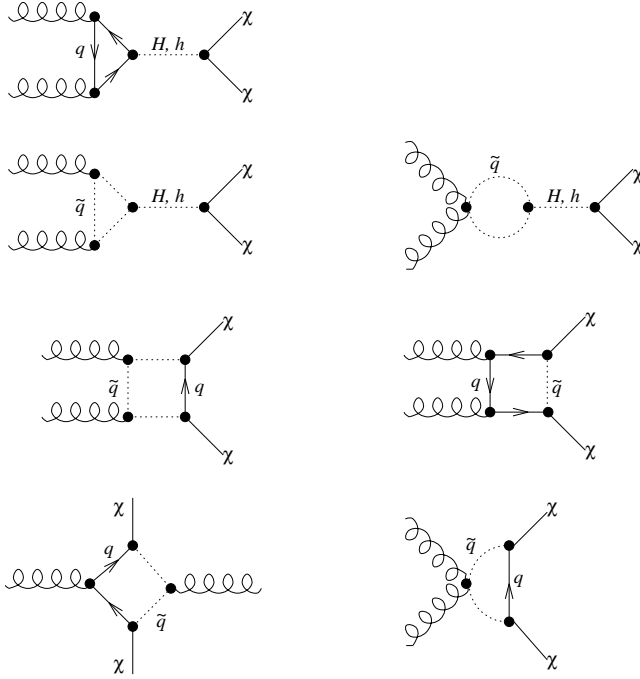


Figure 45: Feynman diagrams for neutralino-gluon scalar (spin-independent) elastic scattering. Notice that no tree level processes exist. From Ref. [319].

where Z and $A - Z$ are the numbers of protons and neutrons in the nucleus, respectively.

The above expression is valid only at zero momentum transfer between the WIMP and the nucleon. For finite momentum transfer, the differential cross section must be multiplied by a nuclear form factor. The appropriate factor, called the *Woods-Saxon* form factor, is given by [221]

$$F(Q) = \left(\frac{3j_1(qR_1)}{qR_1} \right)^2 \exp[-(qs)^2], \quad (202)$$

where j_1 is the first spherical bessel function and the momentum transferred is $q = \sqrt{sm_N Q}$. R_1 is given by $\sqrt{R^2 - 5s^2}$, where R and s are approximately equal to $1.2 \text{ fm } A^{1/3}$ and 1 fm , respectively.

Although less accurate than the Woods-Saxon form factor, the following simple form factor is sometimes used in its place [17, 240]:

$$F(Q) = \exp[-Q/2Q_0]. \quad (203)$$

Here, Q is the energy transferred from the WIMP to the target and $Q_0 = 1.5/(m_N R_0^2)$ where $R_0 = 10^{-13} \text{ cm } [0.3 + 0.91(m_N/\text{GeV})^{1/3}]$.

In the context of neutralino scattering, the value of a_q can be calculated from the parameters of the MSSM [248, 459, 197, 196]. Following Ref. [209], a_q

is in this case given by:

$$\begin{aligned}
a_q &= -\frac{1}{2(m_{1i}^2 - m_\chi^2)} \text{Re} [(X_i)(Y_i)^*] - \frac{1}{2(m_{2i}^2 - m_\chi^2)} \text{Re} [(W_i)(V_i)^*] \\
&\quad - \frac{gm_q}{4m_W B} \left[\text{Re} (\delta_1 [gN_{12} - g'N_{11}]) DC \left(-\frac{1}{m_H^2} + \frac{1}{m_h^2} \right) \right. \\
&\quad \left. + \text{Re} (\delta_2 [gN_{12} - g'N_{11}]) \left(\frac{D^2}{m_H^2} + \frac{C^2}{m_h^2} \right) \right], \tag{204}
\end{aligned}$$

where

$$\begin{aligned}
X_i &\equiv \eta_{11}^* \frac{gm_q N_{1,5-i}^*}{2m_W B} - \eta_{12}^* e_i g' N_{11}^*, \\
Y_i &\equiv \eta_{11}^* \left(\frac{y_i}{2} g' N_{11} + g T_{3i} N_{12} \right) + \eta_{12}^* \frac{gm_q N_{1,5-i}}{2m_W B}, \\
W_i &\equiv \eta_{21}^* \frac{gm_q N_{1,5-i}^*}{2m_W B} - \eta_{22}^* e_i g' N_{11}^*, \\
V_i &\equiv \eta_{22}^* \frac{gm_q N_{1,5-i}}{2m_W B} + \eta_{21}^* \left(\frac{y_i}{2} g' N_{11} + g T_{3i} N_{12} \right) \tag{205}
\end{aligned}$$

where y_i and T_{3i} denote hypercharge and isospin, and

$$\begin{aligned}
\delta_1 &= N_{13}(N_{14}), \quad \delta_2 = N_{14}(-N_{13}), \\
B &= \sin \beta (\cos \beta), \quad C = \sin \alpha (\cos \alpha), \\
D &= \cos \alpha (-\sin \alpha). \tag{206}
\end{aligned}$$

Here, $i = 1$ for up-type and 2 for down-type quarks. α is the Higgs mixing angle. m_{1i}, m_{2i} denote elements of the appropriate 2×2 squark mass matrix. N_{1n} are elements of the matrix which diagonalizes the neutralino mass matrix in the $\tilde{B}-\tilde{W}^3-\tilde{H}_1^0-\tilde{H}_2^0$ basis (see Appendix A). η is the matrix which diagonalizes the appropriate squark mass matrices.

To crudely estimate what scale we expect for the scalar cross section between a neutralino and nucleon, we can carry out a back-of-the-envelope estimate. Considering a gaugino-like neutralino, we see that as δ_1 and δ_2 both vanish, so do most of the terms in Eq. 204. We are left with a neutralino-quark coupling of $a_q \sim A/m_q^2$, where A is the product of the various order 1 couplings, mixing matrix parameters, etc. which contribute. For a typical case, A might be $\sim 10^{-3}$ or so, although it can vary a great deal. Inserting this coupling into Eqs. 198 and 199, we estimate a neutralino-nucleon scalar cross section of $\sim A^2 m_p / m_q^4$, which is roughly 10^{-9} picobarns, for TeV mass squarks. These results can vary dramatically, however, depending on the characteristics of the model being considered (see Figs. 21 and 22).

We can contrast this with the much larger neutralino annihilation cross sections. Considering again a gaugino-like neutralino, its amplitude for annihilations into $b\bar{b}$ via pseudoscalar Higgs exchange (see Eq. 164) is roughly $\mathcal{A}_A \sim$

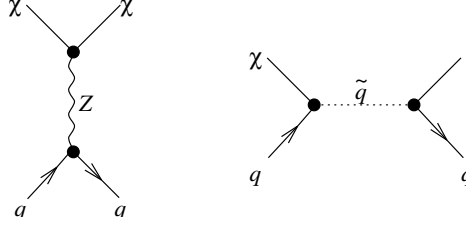


Figure 46: Tree level Feynman diagrams for neutralino-quark axial-vector (spin-dependent) elastic scattering. From Ref. [319].

$m_b \tan \beta \sqrt{f_h}/m_{W^\pm}$ where f_h is the higgsino fraction of the WIMP. The annihilation cross section (Eq. 179) is then roughly $\sigma \sim 3 m_b^2 \tan^2 \beta f_h / 128 \pi m_\chi^2 m_{W^\pm}^2$. For even a very small higgsino fraction, say 1%, and a 200 GeV neutralino, we find a cross section of $\sim 10^{-3}$ picobarns for small values of $\tan \beta$ and a few picobarns for $\tan \beta = 30$.

C.2 Axial-Vector Interactions

Next, we consider a WIMP with axial-vector interactions with quarks given by

$$\mathcal{L}_A = d_q \bar{\chi} \gamma^\mu \gamma_5 \chi \bar{q} \gamma_\mu \gamma_5 q, \quad (207)$$

where d_q is the generic coupling.

For such a WIMP, the spin-dependent scattering cross section can be written as [259]

$$\frac{d\sigma}{d|\vec{v}|^2} = \frac{1}{2\pi v^2} \overline{|T(v^2)|^2}, \quad (208)$$

where v , again, is the relative velocity of the WIMP, and $T(v^2)$ is the scattering matrix element. This expression can be integrated over the Boltzman velocity distribution of halo WIMPs to arrive at an average elastic scattering cross section. At zero momentum, the matrix element, $T(v^2)$, is given by

$$\overline{|T(0)|^2} = \frac{4(J+1)}{J} |(d_u \Delta_u^p + d_d \Delta_d^p + d_s \Delta_s^p) \langle S_p \rangle + (d_u \Delta_u^n + d_d \Delta_d^n + d_s \Delta_s^n) \langle S_n \rangle|^2, \quad (209)$$

where J is the nuclear spin and the Δ 's are the fraction of the nucleon spin carried by a given quark. Their values are measured to be $\Delta_u^p = \Delta_d^n = 0.78 \pm 0.02$, $\Delta_d^p = \Delta_u^n = -0.48 \pm 0.02$ and $\Delta_s^p = \Delta_s^n = -0.15 \pm 0.02$. $\langle S_p \rangle$ and $\langle S_n \rangle$ are the expectation values of the total spin of protons and neutrons, respectively. Notice that for target nuclei with even numbers of protons and neutrons, there is zero total spin, and the cross section vanishes.

The values of $\langle S_p \rangle$ and $\langle S_n \rangle$ depend on the nucleus being considered. For ^{73}Ge , the interacting shell model finds $\langle S_p \rangle$ and $\langle S_n \rangle$ to be 0.011 and 0.468, respectively. For ^{28}Si , they are given by -0.0019 and 0.133. For ^{27}Al , they are 0.3430 and 0.269. And for ^{39}K , they are -0.184 and 0.054 [368].

For non-zero momenta, a more complex form of equation 209 is needed. This equation is given by

$$\begin{aligned} \overline{|T(v^2)|^2} &= \frac{(J+1)}{J} |(d_u \Delta_u^p + d_d \Delta_d^p + d_s \Delta_s^p + d_u \Delta_u^n + d_d \Delta_d^n + d_s \Delta_s^n) \\ &< S_p + S_n > F^0(v^2) + (d_u \Delta_u^p + d_d \Delta_d^p + d_s \Delta_s^p - d_u \Delta_u^n + d_d \Delta_d^n + d_s \Delta_s^n) \\ &< S_p - S_n > F^1(v^2)|^2, \end{aligned} \quad (210)$$

where the F 's are nuclear form factors given by

$$F^0(v^2) \simeq \exp(-r_0^2 v^2 / \hbar^2) \quad (211)$$

and

$$F^1(v^2) \simeq \exp(-r_1^2 v^2 / \hbar^2 + icv/\hbar), \quad (212)$$

where r_0 and r_1 are parameters which depend on the nucleus being considered, with typical values of $1.3 - 2.1 \text{ fm}^{-1}$.

Again, within the context of neutralino scattering, the value of d_2 can be calculated from the parameters of the MSSM [266, 223, 275, 276, 211, 426]. Following Ref. [209], d_2 is in this case given by:

$$\begin{aligned} d_2 &= \frac{1}{4(m_{1i}^2 - m_\chi^2)} \left[|Y_i|^2 + |X_i|^2 \right] + \frac{1}{4(m_{2i}^2 - m_\chi^2)} \left[|V_i|^2 + |W_i|^2 \right] \\ &- \frac{g^2}{4m_Z^2 \cos^2 \theta_W} \left[|N_{13}|^2 - |N_{14}|^2 \right] \frac{T_{3i}}{2}, \end{aligned} \quad (213)$$

where the quantities used are defined in Appendix C.1.

C.3 Vector Interactions

As a third case, consider a WIMP with vector interactions with quarks, given by

$$\mathcal{L}_{vec}^q = b_q \bar{\chi} \gamma_\mu \chi \bar{q} \gamma^\mu q. \quad (214)$$

Here, b_q is the WIMP-quark vector coupling. In this case, the contributions of each quark in the nucleus add coherently and large cross sections result for large nuclei. The WIMP-nucleus cross section in this case is straight forward [266]

$$\sigma_{0vec} = \frac{m_\chi^2 m_N^2 b_N^2}{64\pi(m_\chi + m_N)^2}, \quad (215)$$

where b_N is simply $b_N = 2Zb_p + (A - Z)b_n$.

As an example of a WIMP with vector interactions, consider a Dirac neutrino. In this case, $b_q = G_F(T_q^3 - 2e_q \sin^2 \theta_W) / \sqrt{2}$, where G_F is the Fermi constant, T_q^3 and e_q are the weak isospin and electric charge of the quark q , respectively, and θ_W is the Weinberg angle. Summing over the quarks in a proton or neutron, we get $b_p = G_F(1 - 4 \sin^2 \theta_W) / (2\sqrt{2})$ and $b_n = -G_F / (2\sqrt{2})$. Since

$4 \sin^2 \theta_W \cong 1$, the neutron-neutrino cross section is much larger than the analogous proton-neutrino interaction. The Dirac neutrino-neutron cross section is then given by $\sigma_{\nu,n} = G_F^2 m_\nu^2 m_n^2 / (512\pi(m_\nu + m_n)^2)$. A cross section of this size has been ruled out by direct scattering experiments, except perhaps in the case of a very light WIMP. Similar calculations show that other similar particles, such as sneutrinos, are also excluded by this method [226].

Neutralinos, being Majorana fermions, do not have vector interactions with quarks.

References

- [1] K. Abazajian, G. M. Fuller and M. Patel, Phys. Rev. D **64** (2001) 023501 [arXiv:astro-ph/0101524].
- [2] G. Abbiendi *et al.* [OPAL Collaboration], Phys. Lett. B **551**, 35 (2003).
- [3] G. Abbiendi *et al.* [OPAL Collaboration], Eur. Phys. J. C **14**, 51 (2000).
- [4] B. Abbott *et al.* [D0 Collaboration], Phys. Rev. D **60**, 031101 (1999).
- [5] B. Abbott *et al.* [D0 Collaboration], Phys. Rev. D **63**, 091102 (2001).
- [6] F. Abe *et al.* [CDF Collaboration], Phys. Rev. D **56**, 1357 (1997).
- [7] K. Abe *et al.* [Belle Collaboration], *Talk at the 20th International Symposium on Lepton and Photon Interactions at High Energies (LK 01), Rome, Italy, (2001)*, [arXiv:hep-ex/0107065].
- [8] F. Abe, *et al.* [CDF Collaboration], Phys. Rev. Lett. **84**, 5716 (2000).
- [9] S. Abel *et al.* [SUGRA Working Group Collaboration], Report of the SUGRA working group for run II of the Tevatron, arXiv:hep-ph/0003154.
- [10] J. Abdallah *et al.*, [DELPHI Collaboration], Phys. Lett. B **552**, 127 (2003).
- [11] M. Acciarri *et al.* [L3 Collaboration], Phys. Lett. B **471**, 280 (1999).
- [12] M. Ackermann *et al.* [AMANDA Collaboration], arXiv:hep-ex/0405035.
- [13] I. Affleck and M. Dine, Nucl. Phys. B **249** (1985) 361.
- [14] T. Affolder, *et al.* [CDF Collaboration], Phys. Rev. Lett. **87**, 231803 (2001).
- [15] K. Agashe and G. Servant, arXiv:hep-ph/0403143.
- [16] AGASA Homepage, www.icrr.u-tokyo.ac.jp/as/as.html; HIRES Homepage, www2.keck.hawaii.edu:3636/realpublic/inst/hires/hires.html
- [17] S. P. Ahlen, F. T. Avignone, R. L. Brodzinski, A. K. Drukier, G. Gelmini and D. N. Spergel, Phys. Lett. B **195**, 603 (1987).
- [18] J. Ahrens [IceCube Collaboration], arXiv:astro-ph/0305196.

- [19] J. Ahrens *et al.* [The IceCube Collaboration], Nucl. Phys. Proc. Suppl. **118**, 388 (2003) [arXiv:astro-ph/0209556].
- [20] D. S. Akerib *et al.* [CDMS Collaboration], arXiv:astro-ph/0405033.
- [21] D. S. Akerib *et al.* [CDMS Collaboration], Phys. Rev. D **68** (2003) 082002 [arXiv:hep-ex/0306001].
- [22] M. S. Alam *et al.* [CLEO Collaboration], Phys. Rev. Lett. **74**, 2885 (1995).
- [23] I. F. M. Albuquerque and L. Baudis, Phys. Rev. Lett. **90** (2003) 221301 [Erratum-ibid. **91** (2003) 229903] [arXiv:astro-ph/0301188].
- [24] I. F. M. Albuquerque, L. Hui and E. W. Kolb, Phys. Rev. D **64** (2001) 083504 [arXiv:hep-ph/0009017].
- [25] B. C. Allanach *et al.* [Beyond the Standard Model Working Group Collaboration], “Les Houches ‘Physics at TeV Colliders 2003’ Beyond the Standard Model Working Group: Summary report”, arXiv:hep-ph/0402295.
- [26] B. C. Allanach, C. G. Lester, M. A. Parker and B. R. Webber, JHEP **0009**, 004 (2000) [arXiv:hep-ph/0007009].
- [27] R. Aloisio, P. Blasi and A. V. Olinto, arXiv:astro-ph/0402588.
- [28] L. Alvarez-Gaume, M. Claudson and M. B. Wise, Nucl. Phys. B **207**, 96 (1982).
- [29] U. Amaldi, W. de Boer and H. Furstenuau, Phys. Lett. B **260**, 447 (1991).
- [30] M. Amenomori, *et al.*, *Proceedings of the GeV-TeV Gamma Ray Astrophysics Workshop, Snowbird, Utah*, AIP Proc. Conf. **515**, 459 (1999).
- [31] K.R. Anantharamaiah, A. Pedlar, R.D. Ekers, W.M. Goss, Mon. Not. Roy. Astron. Soc., **249** (1991).
- [32] E. Andres *et al.*, Astropart. Phys. **13** (2000) [arXiv:astro-ph/9906203].
- [33] E. Andres *et al.*, Nature **410**, 441 (2001).
- [34] K. Anikeev *et al.*, arXiv:hep-ph/0201071.
- [35] T. Appelquist, H. C. Cheng and B. A. Dobrescu, Phys. Rev. D **64** (2001) 035002 [arXiv:hep-ph/0012100].
- [36] T. Appelquist and H. U. Yee, T. Appelquist and H. U. Yee, Phys. Rev. D **67**, 055002 (2003) [arXiv:hep-ph/0211023].
- [37] E. Aprile *et al.*, Published in: Kashiwa 2001, Technique and application of xenon detectors 165-178, arXiv:astro-ph/0207670.
- [38] N. Arkani-Hamed, A. G. Cohen and H. Georgi, Phys. Lett. B **513**, 232 (2001) [arXiv:hep-ph/0105239].
- [39] N. Arkani-Hamed, A. G. Cohen, T. Gregoire and J. G. Wacker, JHEP **0208**, 020 (2002) [arXiv:hep-ph/0202089].

- [40] N. Arkani-Hamed, A. G. Cohen, E. Katz and A. E. Nelson, JHEP **0207**, 034 (2002) [arXiv:hep-ph/0206021].
- [41] N. Arkani-Hamed, A. G. Cohen, E. Katz, A. E. Nelson, T. Gregoire and J. G. Wacker, JHEP **0208**, 021 (2002) [arXiv:hep-ph/0206020].
- [42] N. Arkani-Hamed, S. Dimopoulos and G. R. Dvali, Phys. Lett. B **429** (1998) 263 [arXiv:hep-ph/9803315].
- [43] E. Aslanides *et al.* [ANTARES Collaboration], arXiv:astro-ph/9907432.
- [44] ATLAS TDR, report CERN/LHCC/99-15 (1999).
- [45] B. Aubert *et al.* [BABAR Collaboration], *Talk at the 31st International Conference on High Energy Physics (ICHEP 2002), Amsterdam, The Netherlands, (2002)*, [arXiv:hep-ex/0207074].
- [46] M. Azzaro, F. Prada and C. M. Gutierrez, arXiv:astro-ph/0310487.
- [47] H. Baer and C. Balazs, JCAP **0305**, 006 (2003) [arXiv:hep-ph/0303114].
- [48] H. Baer, C. Balazs, A. Belyaev and J. O’Farrill, JCAP **0309**, 007 (2003) [arXiv:hep-ph/0305191].
- [49] H. Baer, C. Balazs, A. Belyaev, T. Krupovnickas and X. Tata, JHEP **0306**, 054 (2003) [arXiv:hep-ph/0304303].
- [50] K. G. Begeman, A. H. Broeils and R. H. Sanders, 1991, MNRAS, 249, 523.
- [51] Bahcall, J. N., Flynn, C., and Gould, A. 1992, ApJ, 389, 234.
- [52] N. Bahcall and X. Fan, Astrophys. J. **504** (1998) 1.
- [53] J. N. Bahcall, M. Schmidt and R. M. Soneira, Astrophys. J. 265 (1983) 730.
- [54] D. Bailey, PhD thesis, unpublished.
- [55] C. Balazs, M. Carena and C. E. M. Wagner, arXiv:hep-ph/0403224.
- [56] V. A. Balkanov *et al.* [BAIKAL Collaboration], Nucl. Phys. Proc. Suppl. **87**, 405 (2000) [arXiv:astro-ph/0001145].
- [57] E. A. Baltz, C. Briot, P. Salati, R. Taillet and J. Silk, Phys. Rev. D **61** (2000) 023514 [arXiv:astro-ph/9909112].
- [58] E. A. Baltz and J. Edsjo, Phys. Rev. D **59** (1999) 023511 [arXiv:astro-ph/9808243].
- [59] E. A. Baltz, J. Edsjo, K. Freese and P. Gondolo, Phys. Rev. D **65** (2002) 063511 [arXiv:astro-ph/0109318].
- [60] R. Barate *et al.* [ALEPH Collaboration], Phys. Lett. B **499**, 67 (2001)
- [61] R. Barbieri, M. Frigeni and G. F. Giudice, Nucl. Phys. B **313**, 725 (1989).
- [62] V. Barger, M. S. Berger and P. Ohmann, Phys. Rev. D **49**, 4908 (1994).

- [63] V. D. Barger, F. Halzen, D. Hooper and C. Kao, *Phys. Rev. D* **65**, 075022 (2002).
- [64] S. W. Barwick *et al.* [HEAT Collaboration], *Astrophys. J.* **482**, L191 (1997) [arXiv:astro-ph/9703192].
- [65] M. Battaglia, A. De Roeck, J. Ellis, F. Gianotti, K. A. Olive and L. Pape, arXiv:hep-ph/0306219.
- [66] R. Battiston, *Frascati Physics Series* **24**, 261.
- [67] U. Baur *et al.*, in *Proc. of the APS/DPF/DPB Summer Study on the Future of Particle Physics (Snowmass 2001)* ed. N. Graf, eConf **C010630**, E4001 (2001) [arXiv:hep-ph/0201227].
- [68] G. Belanger, *Talk at the Workshop on Computer Particle Physics (CPP 2001): Automatic Calculation for Future Colliders, Tokyo, Japan, (2001)*, [arXiv:hep-ph/0210350].
- [69] P. Belli, R. Bernabei, A. Bottino, F. Donato, N. Fornengo, D. Prosperi and S. Scopel, *Phys. Rev. D* **61** (2000) 023512 [arXiv:hep-ph/9903501].
- [70] G. W. Bennett *et al.* [Muon g-2 Collaboration], *Phys. Rev. Lett.* **89**, 101804 (2002); [Erratum-ibid. **89** (2002) 129903] [arXiv:hep-ex/0208001].
- [71] A. Benoit *et al.*, *Phys. Lett. B* **545** (2002) 43 [arXiv:astro-ph/0206271].
- [72] V. Berezhinsky, A. Bottino, J. Ellis, N. Fornengo, G. Mignola and S. Scopel, *Astropart. Phys.* **5**, 333 (1996) [hep-ph/9603342].
- [73] J. F. Beacom and N. F. Bell, *Phys. Rev. D* **65** (2002) 113009 [arXiv:hep-ph/0204111].
- [74] J. F. Beacom, N. F. Bell and S. Dodelson, arXiv:astro-ph/0404585.
- [75] V. Berezhinsky, A. Bottino and G. Mignola, *Phys. Lett. B* **325** (1994) 136 [arXiv:hep-ph/9402215].
- [76] V. Berezhinsky, A. Bottino and G. Mignola, *Phys. Lett. B* **391** (1997) 355 [arXiv:astro-ph/9610060].
- [77] V. Berezhinsky, V. Dokuchaev and Y. Eroshenko, *Phys. Rev. D* **68** (2003) 103003 [arXiv:astro-ph/0301551].
- [78] V. Berezhinsky, M. Kachelriess and A. Vilenkin, *Phys. Rev. Lett.* **79**, 4302 (1997) [arXiv:astro-ph/9708217].
- [79] L. Bergstrom and P. Ullio, *Nucl. Phys. B* **504**, 27 (1997) [arXiv:hep-ph/9706232].
- [80] L. Bergstrom, P. Ullio and J. H. Buckley, *Astropart. Phys.* **9** (1998) 137 [arXiv:astro-ph/9712318].
- [81] L. Bergstrom, J. Edsjo and P. Ullio, *Phys. Rev. D* **58** (1998) 083507 [arXiv:astro-ph/9804050].
- [82] L. Bergstrom, J. Edsjo and P. Gondolo, *Phys. Rev. D* **58** (1998) 103519 [arXiv:hep-ph/9806293].

- [83] L. Bergstrom, J. Edsjo and P. Gondolo, Phys. Rev. D **55**, 1765 (1997) [arXiv:hep-ph/9607237].
- [84] L. Bergstrom, J. Edsjo and P. Ullio, arXiv:astro-ph/9902012.
- [85] L. Bergstrom, J. Edsjo and C. Gunnarsson, Phys. Rev. D **63** (2001) 083515 [arXiv:astro-ph/0012346].
- [86] L. Bergstrom, Rept. Prog. Phys. **63** (2000) 793 [arXiv:hep-ph/0002126].
- [87] L. Bergstrom, J. Edsjo and P. Ullio, Phys. Rev. Lett. **87** (2001) 251301 [arXiv:astro-ph/0105048].
- [88] R. Bernabei *et al.*, *Talk at the 10th International Workshop on Neutrino Telescopes, Venice, Italy*, (2003), [arXiv:astro-ph/0305542].
- [89] V. Bertin, E. Nezri and J. Orloff, Eur. Phys. J. C **26** (2002) 111 [arXiv:hep-ph/0204135].
- [90] V. Bertin, E. Nezri and J. Orloff, JHEP **0302**, 046 (2003) [arXiv:hep-ph/0210034].
- [91] G. Bertone, G. Sigl and J. Silk, Mon. Not. Roy. Astron. Soc. **326**, 799 (2001) [arXiv:astro-ph/0101134].
- [92] G. Bertone, G. Sigl and J. Silk, Mon. Not. Roy. Astron. Soc. **337** (2002) [arXiv:astro-ph/0203488].
- [93] G. Bertone, G. Servant and G. Sigl, Phys. Rev. D **68** (2003) 044008 [arXiv:hep-ph/0211342].
- [94] G. Bertone, E. Nezri, J. Orloff and J. Silk, arXiv:astro-ph/0403322.
- [95] G. Bertone, P. Binetruy, Y. Mambrini and E. Nezri, arXiv:hep-ph/0406083.
- [96] E. Bertschinger, Astrophys. J. Suppl. **58** (1985) 39.
- [97] C. L. Bhat, et al., *Proceedings of the Workshop on VHE Gamma Ray Astronomy, Kruger Park*, (1997).
- [98] P. N. Bhat, et al., *Proceedings of the 26th International Cosmic Ray Conference, Salt Lake City*, **5**, 191 (1999).
- [99] P. Binetruy, Y. Mambrini and E. Nezri, arXiv:hep-ph/0312155.
- [100] P. Binetruy, A. Birkedal-Hansen, Y. Mambrini and B. D. Nelson, arXiv:hep-ph/0308047.
- [101] P. Binetruy, Lecture course notes: “Supersymmetry: from concepts to searches”.
- [102] P. Binetruy, M. K. Gaillard and B. D. Nelson, Nucl. Phys. B **604** (2001) 32 [arXiv:hep-ph/0011081].
- [103] P. Binetruy, G. Girardi and P. Salati, Nucl. Phys. B **237** (1984) 285.
- [104] J. J. Binney and N. W. Evans, arXiv:astro-ph/0108505.

- [105] A. Birkedal-Hansen, D. Hooper, G. Kribs and J. G. Wacker, in preparation.
- [106] A. Birkedal-Hansen and E. h. Jeong, *JHEP* **0302**, 047 (2003) [arXiv:hep-ph/0210041].
- [107] A. Birkedal, K. Matchev and M. Perelstein, arXiv:hep-ph/0403004.
- [108] A. Birkedal-Hansen and B. D. Nelson, *Phys. Rev. D* **64**, 015008 (2001) [arXiv:hep-ph/0102075].
- [109] A. Birkedal-Hansen and B. D. Nelson, gaugino *Phys. Rev. D* **67**, 095006 (2003) [arXiv:hep-ph/0211071].
- [110] A. Birkedal-Hansen and J. G. Wacker, arXiv:hep-ph/0306161.
- [111] M. Birkel and S. Sarkar, *Astropart. Phys.* **9**, 297 (1998) [arXiv:hep-ph/9804285].
- [112] F. Blanc *et al.* [ANTARES Collaboration], *Presented by L. Thompson on behalf of the ANTARES Collaboration, to appear in the proceedings of 28th International Cosmic Ray Conferences (ICRC 2003), Tsukuba, Japan, 31 Jul - 7 Aug 2003.*
- [113] P. Blasi, R. Dick and E. W. Kolb, *Astropart. Phys.* **18**, 57 (2002) [arXiv:astro-ph/0105232].
- [114] P. Blasi, A. V. Olinto and C. Tyler, *Astropart. Phys.* **18**, 649 (2003) [arXiv:astro-ph/0202049].
- [115] I. Blokland, A. Czarnecki and K. Melnikov, *Phys. Rev. Lett.* **88**, 071803 (2002).
- [116] J. Bijnens, E. Pallante and J. Prades, *Nucl. Phys.* **B626** (2002) 410.
- [117] C. Boehm, T. A. Ensslin and J. Silk, arXiv:astro-ph/0208458.
- [118] C. Boehm and P. Fayet, arXiv:hep-ph/0305261.
- [119] C. Boehm, P. Fayet and J. Silk, arXiv:hep-ph/0311143.
- [120] C. Boehm, D. Hooper, J. Silk and M. Casse, *Phys. Rev. Lett.* **92**, 101301 (2004) [arXiv:astro-ph/0309686].
- [121] M. Boezio *et al.* [WiZard/CAPRICE Collaboration], *Astrophys. J.* **561**, 787 (2001) [arXiv:astro-ph/0103513].
- [122] J. R. Bond, G. Efstathiou and J. Silk, *Phys. Rev. Lett.* **45** (1980) 1980.
- [123] J. R. Bond and A. S. Szalay, *Astrophys. J.* **274** (1983) 443.
- [124] S. A. Bonometto, F. Gabbiani and A. Masiero, *Phys. Rev. D* **49**, 3918 (1994) [arXiv:hep-ph/9305237].
- [125] A. Bottino, F. Donato, N. Fornengo and P. Salati, *Phys. Rev. D* **58**, 123503 (1998).
- [126] A. Bottino, F. Donato, N. Fornengo and S. Scopel, *Phys. Rev. D* **68**, 043506 (2003) [arXiv:hep-ph/0304080].

- [127] A. Bottino, G. Fiorentini, N. Fornengo, B. Ricci, S. Scopel and F. L. Villante, Phys. Rev. D **66** (2002) 053005 [arXiv:hep-ph/0206211].
- [128] A. Bouquet, P. Salati, J. Silk, 1989 Phys. Rev. D, 40 (1989) 3168
- [129] M. Brhlik and L. Roszkowski, Phys. Lett. B **464**, 303 (1999) [arXiv:hep-ph/9903468].
- [130] H. N. Brown *et al.* [Muon g-2 Collaboration], Phys. Rev. Lett., **86** (2001) 2227.
- [131] R. Brown, in *Galactic and Extragalactic Radio Astronomy*, eds.: G. L. Verschuur and K. I. Kellermann (Springer, New York, 1974), p. 1.
- [132] W. Buchmuller, K. Hamaguchi and M. Ratz, Phys. Lett. B **574**, 156 (2003) [arXiv:hep-ph/0307181].
- [133] A. J. Buras, A. Czarnecki, M. Misiak and J. Urban, Nucl. Phys. B **631**, 219 (2002) [arXiv:hep-ph/0203135].
- [134] A. J. Buras, A. Poschenrieder, M. Spranger and A. Weiler, eConf **C0304052**, WG302 (2003) [arXiv:hep-ph/0307202].
- [135] C. Calcano-Roldan and B. Moore, Phys. Rev. D **62** (2000) 123005 [arXiv:astro-ph/0010056].
- [136] R. R. Caldwell and J. P. Ostriker, Astrophys. J. 251 (1981) 61.
- [137] H. V. Cane, Mon. Not. Roy. Astron. Soc. **189** (1979) 189.
- [138] M. Carena, D. Garcia, U. Nierste and C. E. M. Wagner, Phys. Lett. B **499**, 141 (2001) [arXiv:hep-ph/0010003].
- [139] R. G. Carlberg *et al.*, Astrophys. J. **516** (1999) 552.
- [140] M. F. Cawley, *et al.*, Exp. Ast. **1**, 185 (1990).
- [141] J. A. R. Cembranos, A. Dobado and A. L. Maroto, Phys. Rev. Lett. **90**, 241301 (2003) [arXiv:hep-ph/0302041].
- [142] A. Cesarini, F. Fucito, A. Lionetto, A. Morselli and P. Ullio, arXiv:astro-ph/0305075.
- [143] P. M. Chadwick, *et al.*, *Proceedings of the Workshop on VHE Gamma Ray Astronomy, Snowbird*, (1999).
- [144] S. Chang, C. Coriano and A. E. Faraggi, Nucl. Phys. B **477**, 65 (1996) [arXiv:hep-ph/9605325].
- [145] P. Chardonnet, G. Mignola, P. Salati and R. Taillet, Phys. Lett. B **384** (1996) 161 [arXiv:astro-ph/9606174].
- [146] Z. Chacko, M. A. Luty, A. E. Nelson and E. Ponton, JHEP **0001**, 003 (2000) [arXiv:hep-ph/9911323].
- [147] H. C. Cheng and I. Low, JHEP **0309**, 051 (2003) [arXiv:hep-ph/0308199].

- [148] H. C. Cheng, K. T. Matchev and M. Schmaltz, Phys. Rev. D **66** (2002) 056006 [arXiv:hep-ph/0205314].
- [149] H. C. Cheng, K. T. Matchev and M. Schmaltz, Phys. Rev. D **66**, 036005 (2002) [arXiv:hep-ph/0204342].
- [150] H. C. Cheng, J. L. Feng and K. T. Matchev, Phys. Rev. Lett. **89**, 211301 (2002) [arXiv:hep-ph/0207125].
- [151] K. M. Cheung and G. Landsberg, Phys. Rev. D **65**, 076003 (2002) [arXiv:hep-ph/0110346].
- [152] K. Choi, K. Hwang, H. B. Kim and T. Lee, Phys. Lett. B **467**, 211 (1999) [arXiv:hep-ph/9902291].
- [153] D. J. H. Chung, L. L. Everett, G. L. Kane, S. F. King, J. Lykken and L. T. Wang, arXiv:hep-ph/0312378.
- [154] D. J. Chung, E. W. Kolb and A. Riotto, Phys. Rev. D **59** (1999) 023501 [arXiv:hep-ph/9802238].
- [155] CMS TP, report CERN/LHCC/94-38 (1994).
- [156] A. Coc, E. Vangioni-Flam, P. Descouvemont, A. Adahchour and C. Angulo, Astrophys. J. **600**, 544 (2004) [arXiv:astro-ph/0309480].
- [157] P. D. Collins, A. D. Martin and E. J. Squires, “Particle Physics And Cosmology,” New York, USA, Wiley (1989).
- [158] F. Combes, arXiv:astro-ph/0404210.
- [159] C. R. Contaldi, H. Hoekstra and A. Lewis, Phys. Rev. Lett. **90** (2003) 221303 [arXiv:astro-ph/0302435].
- [160] C. J. Copi and L. M. Krauss, Phys. Rev. D **67** (2003) 103507 [arXiv:astro-ph/0208010].
- [161] C. Coriano, A. E. Faraggi and M. Plumacher, Nucl. Phys. B **614**, 233 (2001) [arXiv:hep-ph/0107053].
- [162] S. Coutu *et al.* [HEAT-pbar Collaboration], *Proceedings of the 27th International Cosmic Ray Conference* (2001).
- [163] S. Coutu *et al.*, Astropart. Phys. **11**, 429 (1999), [arXiv:astro-ph/9902162].
- [164] L. Covi, J. E. Kim and L. Roszkowski, Phys. Rev. Lett. **82**, 4180 (1999) [arXiv:hep-ph/9905212].
- [165] L. Covi, H. B. Kim, J. E. Kim and L. Roszkowski, JHEP **0105**, 033 (2001) [arXiv:hep-ph/0101009].
- [166] L. Covi, L. Roszkowski, R. R. de Austri and M. Small, arXiv:hep-ph/0402240.
- [167] R. A. C. Croft *et al.*, Astrophys. J. **581** (2002) 20 [arXiv:astro-ph/0012324].
- [168] P. Crotty, Phys. Rev. D **66**, 063504 (2002) [arXiv:hep-ph/0205116].

- [169] C. Csaki, J. Hubisz, G. D. Kribs, P. Meade and J. Terning, Phys. Rev. D **67**, 115002 (2003) [arXiv:hep-ph/0211124].
- [170] R. H. Cyburt, J. R. Ellis, B. D. Fields and K. A. Olive, Phys. Rev. D **67**, 103521 (2003) [arXiv:astro-ph/0211258].
- [171] N. Dalal and C. R. Keeton, arXiv:astro-ph/0312072.
- [172] A. Daum, et al., Astropart. Phys. **8**, 1 (1997).
- [173] R. Dave, D. N. Spergel, P. J. Steinhardt and B. D. Wandelt, Astrophys. J. **547**, 574 (2001) [arXiv:astro-ph/0006218].
- [174] M. Davier, S. Eidelman, A. Hocker and Z. Zhang, Eur. Phys. J. C **27**, 497 (2003) [arXiv:hep-ph/0208177].
- [175] R.D. Davies, D. Walsh and R.S. Booth , Mon. Not. Roy. Astron. Soc. , **177** (1976) 319
- [176] S. Dawson, E. Eichten and C. Quigg, Phys. Rev. D **31**, 1581 (1985).
- [177] V. Debattista and J. A. Sellwood, Astrophys. J. **493**, L5 (1998) [arXiv:astro-ph/9710039].
- [178] V. P. Debattista and J. A. Sellwood, Astrophys. J. **543**, 704 (2000), [arXiv:astro-ph/0006275].
- [179] W. J. de Blok, S. S. McGaugh, A. Bosma and V. C. Rubin, arXiv:astro-ph/0103102.
- [180] H. I. DeJager, et al., South African of J. Phys., **9** 107 (1986).
- [181] M. de Naurois, *Proceedings of the 26th International Cosmic Ray Conference, Salt Lake City*, **5**, 211 (1999).
- [182] A. De Rujula, S. L. Glashow and U. Sarid, Nucl. Phys. B **333**, 173 (1990).
- [183] S. Dimopoulos and H. Georgi, Nucl. Phys. B **193**, 150 (1981).
- [184] S. Dimopoulos, G. F. Giudice and A. Pomarol, Phys. Lett. B **389**, 37 (1996) [arXiv:hep-ph/9607225].
- [185] S. Dimopoulos, S. Raby and F. Wilczek, Phys. Lett. B **112**, 133 (1982).
- [186] M. Dine and W. Fischler, Phys. Lett. B **110**, 227 (1982).
- [187] M. Dine and A. E. Nelson, Phys. Rev. D **48**, 1277 (1993) [arXiv:hep-ph/9303230].
- [188] M. Dine, A. E. Nelson and Y. Shirman, Phys. Rev. D **51**, 1362 (1995) [arXiv:hep-ph/9408384].
- [189] M. Dine, A. E. Nelson, Y. Nir and Y. Shirman, Phys. Rev. D **53**, 2658 (1996) [arXiv:hep-ph/9507378].
- [190] A. Djouadi *et al.* [MSSM Working Group Collaboration], *Talk at Groupement de Recherche-Supersymetrie, Montpellier, France*, (1998) [arXiv:hep-ph/9901246].

- [191] S. Dodelson and L. M. Widrow, Phys. Rev. Lett. **72** (1994) 17 [arXiv:hep-ph/9303287].
- [192] F. Donato, N. Fornengo, D. Maurin, P. Salati and R. Taillet, arXiv:astro-ph/0306207.
- [193] F. Donato, D. Maurin, P. Salati, R. Taillet, A. Barrau and G. Boudoul, Astrophys. J. **563**, 172 (2001).
- [194] M. Drees and S. P. Martin, *Report of Subgroup 2 of the DPF Working Group on Electroweak Symmetry Breaking and Beyond the Standard Model*, [arXiv:hep-ph/9504324].
- [195] M. Drees and M. M. Nojiri, Phys. Rev. D **47**, 376 (1993) [arXiv:hep-ph/9207234].
- [196] M. Drees and M. Nojiri, Phys. Rev. D **48**, 3483 (1993) [arXiv:hep-ph/9307208].
- [197] M. Drees and M. M. Nojiri, Phys. Rev. D **47**, 4226 (1993) [arXiv:hep-ph/9210272].
- [198] M. Drees, M. M. Nojiri, D. P. Roy and Y. Yamada, Phys. Rev. D **56**, 276 (1997) [Erratum-ibid. D **64**, 039901 (2001)] [arXiv:hep-ph/9701219].
- [199] A. K. Drukier, K. Freese and D. N. Spergel, Phys. Rev. D **33**, 3495 (1986).
- [200] A. Drukier and L. Stodolsky, Phys. Rev. D **30**, 2295 (1984).
- [201] G. Duda, G. Gelmini, P. Gondolo, J. Edsjo and J. Silk, Phys. Rev. D **67** (2003) 023505 [arXiv:hep-ph/0209266].
- [202] J. Edsjo and P. Gondolo, Phys. Rev. D **56** (1997) 1879 [arXiv:hep-ph/9704361].
- [203] J. Edsjo, Ph. D Thesis, arXiv:hep-ph/9704384.
- [204] J. Edsjo, Nucl. Phys. Proc. Suppl. **43**, 265 (1995) [arXiv:hep-ph/9504205].
- [205] J. Edsjo, arXiv:astro-ph/0211354.
- [206] J. Edsjo, M. Schelke, P. Ullio and P. Gondolo, JCAP **0304** (2003) 001 [arXiv:hep-ph/0301106].
- [207] M. M. El Kheishen, A. A. Aboshousha and A. A. Shafik, Phys. Rev. D **45** (1992) 4345.
- [208] J. R. Ellis, Phys. Scripta **T85** (2000) 221 [arXiv:astro-ph/9812211].
- [209] J. R. Ellis, A. Ferstl and K. A. Olive, Phys. Lett. B 481, (2000) 304, [arXiv:hep-ph/0001005].
- [210] J. Ellis and R. A. Flores, Phys. Lett. B 212 (1988) 375.
- [211] J. R. Ellis and R. A. Flores, Phys. Lett. B **263**, 259 (1991).
- [212] J. R. Ellis, G. B. Gelmini, J. L. Lopez, D. V. Nanopoulos and S. Sarkar, Nucl. Phys. B **373**, 399 (1992).

- [213] J. R. Ellis, J. S. Hagelin, D. V. Nanopoulos, K. A. Olive and M. Srednicki, Nucl. Phys. B **238**, 453 (1984).
- [214] J. R. Ellis, J. E. Kim and D. V. Nanopoulos, Phys. Lett. B **145**, 181 (1984).
- [215] J. R. Ellis, J. L. Lopez and D. V. Nanopoulos, Phys. Lett. B **247**, 257 (1990).
- [216] J. R. Ellis, D. V. Nanopoulos and S. Sarkar, Nucl. Phys. B **259**, 175 (1985).
- [217] J. R. Ellis, K. A. Olive, Y. Santoso and V. C. Spanos, Phys. Lett. B **565** (2003) 176 [arXiv:hep-ph/0303043].
- [218] J. R. Ellis, K. A. Olive, Y. Santoso and V. C. Spanos, Phys. Rev. D **69**, 095004 (2004) [arXiv:hep-ph/0310356].
- [219] J. R. Ellis, K. A. Olive, Y. Santoso and V. Spanos, arXiv:hep-ph/0312262.
- [220] J. Ellis, S. Kelley and D.V. Nanopoulos, Phys. Lett., **260** (1991) 131
- [221] J. Engel, Phys. Lett. B, 264 (1991) 114.
- [222] J. Engel, S. Pittel, E. Ormand and P. Vogel, Phys. Lett. B, 275 (1992) 119.
- [223] J. Engel, S. Pittel and P. Vogel, Int. J. Mod. Phys. E **1**, 1 (1992).
- [224] N. W. Evans, F. Ferrer and S. Sarkar, arXiv:astro-ph/0311145.
- [225] A. C. Fabian and S. W. Allen, *Proceedings of the 21st Texas Symposium on Relativistic Astrophysics (Texas in Tuscany), Florence, Italy, 2002* [arXiv:astro-ph/0304020].
- [226] T. Falk, K. A. Olive and M. Srednicki, Phys. Lett. B **339**, 248 (1994) [arXiv:hep-ph/9409270].
- [227] A. Falvard *et al.*, Astropart. Phys. **20**, 467 (2004) [arXiv:astro-ph/0210184].
- [228] G. R. Farrar and P. Fayet, Phys. Lett. B **76**, 575 (1978).
- [229] J. L. Feng, K. T. Matchev and T. Moroi, Phys. Rev. Lett. **84**, 2322 (2000) [arXiv:hep-ph/9908309].
- [230] J. L. Feng, K. T. Matchev and T. Moroi, Phys. Rev. D **61**, 075005 (2000) [arXiv:hep-ph/9909334].
- [231] J. L. Feng, K. T. Matchev and F. Wilczek, Phys. Lett. B **482**, 388 (2000) [arXiv:hep-ph/0004043].
- [232] J. L. Feng, K. T. Matchev and F. Wilczek, Phys. Rev. D **63**, 045024 (2001).
- [233] J. L. Feng, A. Rajaraman and F. Takayama, Phys. Rev. D **68**, 063504 (2003) [arXiv:hep-ph/0306024].
- [234] J. L. Feng, A. Rajaraman and F. Takayama, Phys. Rev. Lett. **91** (2003) 011302 [arXiv:hep-ph/0302215].
- [235] B. D. Fields and S. Sarkar, Phys. Rev. D **66**, 010001 (2002).

- [236] C.P. Fong and B.R. Webber, Nucl. Phys. B355 (1991) 54.
- [237] R. Foot, Phys. Rev. D **69**, 036001 (2004) [arXiv:hep-ph/0308254].
- [238] R. Foot and Z. K. Silagadze, arXiv:astro-ph/0404515.
- [239] K. Freese, Phys. Lett. B **167**, 295 (1986).
- [240] K. Freese, J. A. Frieman and A. Gould, Phys. Rev. D **37**, 3388 (1988).
- [241] K. Freese, P. Gondolo and H. J. Newberg, arXiv:astro-ph/0309279.
- [242] T. Fukushige, A. Kawai and J. Makino, arXiv:astro-ph/0306203.
- [243] T. K. Gaiser, F. Halzen and T. Stanev, Phys. Rept. **258**, 173 (1995) [Erratum-ibid. **271**, 355 (1996)] [arXiv:hep-ph/9410384].
- [244] T. K. Gaiser, G. Steigman and S. Tilav, Phys. Rev. D **34**, 2206 (1986).
- [245] W. Galbraith, J. V. Jelley, Nature, 171, 349 (1953).
- [246] R. Gandhi, C. Quigg, M. H. Reno and I. Sarcevic, Astropart. Phys. **5** (1996) 81 [arXiv:hep-ph/9512364].
- [247] G. Gelmini and P. Gondolo, arXiv:hep-ph/0405278.
- [248] G. B. Gelmini, P. Gondolo and E. Roulet, Nucl. Phys. B **351**, 623 (1991).
- [249] T. Gherghetta, G. F. Giudice and A. Riotto, Phys. Lett. B **446**, 28 (1999) [arXiv:hep-ph/9808401].
- [250] T. Gherghetta, G. F. Giudice and J. D. Wells, Nucl. Phys. B **559**, 27 (1999) [arXiv:hep-ph/9904378].
- [251] A. M. Ghez, S. Salim, S. D. Hornstein, A. Tanner, M. Morris, E. E. Becklin and G. Duchene, arXiv:astro-ph/0306130.
- [252] A. M. Ghez, B. L. Klein, M. Morris and E. E. Becklin, Astrophys. J. **509** (1998) 678 [arXiv:astro-ph/9807210].
- [253] K. Giesel, J. H. Jureit and E. Reya, Astropart. Phys. **20**, 335 (2003) [arXiv:astro-ph/0303252].
- [254] G. Gilmore and R. F. G. Wyse, arXiv:astro-ph/0104242.
- [255] G. F. Giudice, M. A. Luty, H. Murayama and R. Rattazzi, JHEP **9812**, 027 (1998) [arXiv:hep-ph/9810442].
- [256] H. Goldberg, Phys. Rev. Lett. **50**, 1419 (1983).
- [257] I. Goldman and S. Nussinov, Phys. Rev. D **40** (1989) 3221.
- [258] P. Gondolo, *et al.*, as found at <http://dendera.berkeley.edu/plotter/entryform.html>.
- [259] P. Gondolo, *Talk at the XXXI Rencontres de Moriond, "Dark Matter in Cosmology, Quantum Measurements, Experimental Gravitation", Les Arcs, France*, (1996), [arXiv:hep-ph/9605290].

- [260] P. Gondolo and G. Gelmini, Nucl. Phys. B **360** (1991) 145.
- [261] P. Gondolo and J. Silk, Phys. Rev. Lett. **83** (1999) 1719 [arXiv:astro-ph/9906391].
- [262] P. Gondolo, Phys. Lett. B **494** (2000) 181 [arXiv:hep-ph/0002226].
- [263] P. Gondolo, J. Edsjo, P. Ullio, L. Bergstrom, M. Schelke and E. A. Baltz, Publically released at Dark Matter 2004, Marina del Ray, CA, USA.
- [264] P. Gondolo, J. Edsjo, P. Ullio, L. Bergstrom, M. Schelke and E. A. Baltz, arXiv:astro-ph/0211238.
- [265] M. C. Gonzalez-Garcia and Y. Nir, Rev. Mod. Phys. **75** (2003) 345 [arXiv:hep-ph/0202058].
- [266] M. W. Goodman and E. Witten, Phys. Rev. D **31**, 3059 (1985).
- [267] P. Goret, et al., *Proceedings of the 25th International Cosmic Ray Conference, Durban*, **3**, 173 (1997).
- [268] T. Goto and M. Yamaguchi, Phys. Lett. B **276**, 103 (1992).
- [269] A. Gould, Astrophys. J. **388**, 338 (1991).
- [270] A. Gould, Astrophys. J. **321**, 571 (1987).
- [271] G. J. Gounaris, J. Layssac, P. I. Porfyriadis and F. M. Renard, Phys. Rev. D **69**, 075007 (2004) [arXiv:hep-ph/0309032].
- [272] A. M. Green, Phys. Rev. D **68** (2003) 023004 [arXiv:astro-ph/0304446].
- [273] K. Greisen, Phys. Rev. Lett. **16** (1966) 748.
- [274] P. K. Grieder [DUMAND Collaboration], Nucl. Phys. Proc. Suppl. **43** (1995) 145.
- [275] K. Griest, Phys. Rev. Lett. **61**, 666 (1988).
- [276] K. Griest, Phys. Rev. D **38**, 2357 (1988) [Erratum-ibid. D **39**, 3802 (1989)].
- [277] K. Griest and M. Kamionkowski, Phys. Rev. Lett. **64** (1990) 615.
- [278] K. Griest, M. Kamionkowski and M. S. Turner, Phys. Rev. D **41**, 3565 (1990).
- [279] K. Griest and D. Seckel, Phys. Rev. D **43** (1991) 3191.
- [280] K. Griest and D. Seckel, Nucl. Phys. B **283**, 681 (1987) [Erratum-ibid. B **296**, 1034 (1988)].
- [281] D. E. Groom *et al.* [Particle Data Group Collaboration], Eur. Phys. J. C **15** (2000) 1, pp 152.
- [282] R. Haag, J. T. Lopuszanski and M. Sohnius, Nucl. Phys. B **88**, 257 (1975).
- [283] K. Hagiwara, A. D. Martin, D. Nomura and T. Teubner, arXiv:hep-ph/0209187.

- [284] F. Halzen and D. Hooper, Rept. Prog. Phys. **65**, 1025 (2002) [arXiv:astro-ph/0204527].
- [285] F. Halzen, T. Stelzer and M. Kamionkowski, Phys. Rev. D **45**, 4439 (1992).
- [286] S. Hannestad, JCAP **0305** (2003) 004 [arXiv:astro-ph/0303076].
- [287] S. H. Hansen and Z. Haiman, Astrophys. J. **600** (2004) 26 [arXiv:astro-ph/0305126].
- [288] S. H. Hansen, S. Pastor and D. V. Semikoz, Astrophys. J. **573** (2002) L69 [arXiv:astro-ph/0205295].
- [289] T. Hara, et al., Nucl.Inst. Meth. A. **332**, 300 (1993).
- [290] M. Hayakawa and T. Kinoshita, arXiv:hep-ph/0112102.
- [291] E. Hayashi *et al.*, arXiv:astro-ph/0310576.
- [292] N. Hayashida *et al.* [AGASA Collaboration], J. Phys. G **21** (1995) 1101.
- [293] A. Heister *et al.* [ALEPH Collaboration], Phys. Lett. B **526**, 206 (2002).
- [294] A. Heister *et al.* [ALEPH Collaboration], Phys. Lett. B **543**, 1 (2002).
- [295] A. Heister *et al.* [ALEPH Collaboration], Phys. Lett. B **544**, 16 (2002).
- [296] C. T. Hill, Nucl. Phys. B **224** (1983) 469.
- [297] I. Hinchliffe, F. E. Paige, M. D. Shapiro, J. Soderqvist and W. Yao, Phys. Rev. D **55**, 5520 (1997) [arXiv:hep-ph/9610544].
- [298] H. M. Hodges, Phys. Rev. D **47**, 456 (1993).
- [299] H. Hoekstra, H. Yee and M. Gladders, New Astron. Rev. **46**, 767 (2002) [arXiv:astro-ph/0205205].
- [300] G. P. Holder and J. E. Carlstrom, arXiv:astro-ph/9904220.
- [301] E. Holmberg, ApJ, **94** (1941) 385.
- [302] D. Hooper and B. Dingus, [arXiv:astro-ph/0212509]
- [303] D. Hooper and B. Dingus, Talk given at the 34th COSPAR Scientific Assembly: The 2nd World Space Congress, Houston, Texas, 10-19 Oct 2002, arXiv:astro-ph/0212509.
- [304] D. Hooper, F. Ferrer, C. Boehm, J. Silk, J. Paul, N. W. Evans and M. Casse, arXiv:astro-ph/0311150.
- [305] D. Hooper and G. D. Kribs, Phys. Rev. D **67**, 055003 (2003) [arXiv:hep-ph/0208261].
- [306] D. Hooper and G. D. Kribs, In preparation.
- [307] D. Hooper, I. Perez, J. Silk, F. Ferrer and S. Sarkar, arXiv:astro-ph/0404205.

- [308] D. Hooper and T. Plehn, Phys. Lett. B **562**, 18 (2003) [arXiv:hep-ph/0212226].
- [309] D. Hooper, J. E. Taylor and J. Silk, Phys. Rev. D, in press, arXiv:hep-ph/0312076.
- [310] D. Hooper and L. T. Wang, Phys. Rev. D **69**, 035001 (2004) [arXiv:hep-ph/0309036].
- [311] D. Hooper and L. T. Wang, arXiv:hep-ph/0402220.
- [312] W. Hu and S. Dodelson, Ann. Rev. Astron. Astrophys. **40**, 171 (2002) [arXiv:astro-ph/0110414].
- [313] W. Hu, N. Sugiyama and J. Silk, Nature **386**, 37 (1997) [arXiv:astro-ph/9604166].
- [314] P. Hut, Phys. Lett. B **69** (1977) 85.
- [315] A. Y. Ignatiev and R. R. Volkas, Phys. Rev. D **68**, 023518 (2003) [arXiv:hep-ph/0304260].
- [316] F. Jegerlehner (unpublished, as reported in M. Krawczyk, *Acta Phys. Polon.* **B33** (2002) 2621 [arXiv:hep-ph/0208076].
- [317] M. Joyce and M. E. Shaposhnikov, Phys. Rev. Lett. **79** (1997) 1193 [arXiv:astro-ph/9703005].
- [318] G. Jungman and M. Kamionkowski, Phys. Rev. D **51** (1995) 328 [arXiv:hep-ph/9407351].
- [319] G. Jungman, M. Kamionkowski and K. Griest, Phys. Rept. **267** (1996) 195 [arXiv:hep-ph/9506380].
- [320] F. D. Kahn and L. Woltjer, 1959, ApJ, 130, 705.
- [321] K. Kainulainen and K. A. Olive, arXiv:hep-ph/0206163.
- [322] T. Kaluza, Sitzungsber. Preuss. Akad. Wiss. Berlin (Math. Phys.) **1921** (1921) 966. English translation available at <http://www.slac.stanford.edu/spires/find/hep/www?r=hupd-8401>
- [323] M. Kamionkowski, Phys. Rev. D **44**, 3021 (1991).
- [324] M. Kamionkowski and M. S. Turner, Phys. Rev. D **43**, 1774 (1991).
- [325] T. Kamon [CDF Collaboration], arXiv:hep-ex/0301019.
- [326] G. L. Kane, J. Lykken, S. Mrenna, B. D. Nelson, L. T. Wang and T. T. Wang, Phys. Rev. D **67** (2003) 045008 [arXiv:hep-ph/0209061].
- [327] G. L. Kane, C. F. Kolda, L. Roszkowski and J. D. Wells, Phys. Rev. D **49** (1994) 6173 [arXiv:hep-ph/9312272].
- [328] G. L. Kane, L. T. Wang and T. T. Wang, Phys. Lett. B **536**, 263 (2002).
- [329] G. L. Kane, L. T. Wang and J. D. Wells, Phys. Rev. D **65**, 057701 (2002).

- [330] D. E. Kaplan, G. D. Kribs and M. Schmaltz, Phys. Rev. D **62**, 035010 (2000) [arXiv:hep-ph/9911293];
- [331] A. Kashlinsky, Phys. Rep. **307** (1998) 67.
- [332] U. F. Katz [The ANTARES Collaboration], *Proceedings of International Europhysics Conference on High-Energy Physics, Aachen, Germany, (2003)* [arXiv:astro-ph/0310736].
- [333] H. V. Klapdor-Kleingrothaus, *Talk at the International Workshop on Low Energy Solar Neutrinos, Tokyo, Japan, (2000)* [arXiv:hep-ph/0104028].
- [334] A. Klypin, H. Zhao and R. S. Somerville, arXiv:astro-ph/0110390.
- [335] J. Knapp, D. Heck, S. J. Sciutto, M. T. Dova and M. Risse, Astropart. Phys. **19** (2003) 77 [arXiv:astro-ph/0206414].
- [336] M. Knecht and A. Nyffeler, Phys. Rev. Lett. **D65** (2002) 073034.
- [337] M. Knecht, A. Nyffeler, M. Perrottet and E. De Rafael, Phys. Rev. Lett. **88**, 071802 (2002).
- [338] E. W. Kolb and R. Slansky, Phys. Lett. B **135** (1984) 378.
- [339] E. W. Kolb, D. J. Chung and A. Riotto, *Proceedings of the 2nd International Conference on Dark Matter in Astro and Particle Physics (DARK98), Heidelberg, Germany, (1998)* [arXiv:hep-ph/9810361].
- [340] E. W. Kolb and M. S. Turner, "The Early Universe".
- [341] L. V. Koopmans and T. Treu, Astrophys. J. **583** (2003) 606 [arXiv:astro-ph/0205281].
- [342] J. Kormendy and L. C. Ho, arXiv:astro-ph/0003268.
- [343] K. Kosack [the VERITAS Collaboration], arXiv:astro-ph/0403422.
- [344] S. M. Koushiappas, A. R. Zentner and T. P. Walker, Phys. Rev. D **69**, 043501 (2004) [arXiv:astro-ph/0309464].
- [345] L. M. Krauss, M. Srednicki and F. Wilczek, Phys. Rev. D **33**, 2079 (1986).
- [346] A. V. Kravtsov, A. A. Klypin, J. S. Bullock, J. R. Primack, Astrophys. J., **502**, 48 (1998)[arXiv:astro-ph/9708176]
- [347] S. Kretzer, Phys. Rev. D **62**, 054001 (2000) [arXiv:hep-ph/0003177]. FORTRAN routines available at: www.pv.infn.it/~radici/FFdatabase/parametrizations.html
- [348] C. I. Kuo *et al.* [ACBAR collaboration], Astrophys. J. **600** (2004) 32 [arXiv:astro-ph/0212289].
- [349] A. Kurylov and M. Kamionkowski, Phys. Rev. D **69**, 063503 (2004) [arXiv:hep-ph/0307185].
- [350] A. Kusenko, V. Kuzmin, M. E. Shaposhnikov and P. G. Tinyakov, Phys. Rev. Lett. **80**, 3185 (1998) [arXiv:hep-ph/9712212].

- [351] A. Kusenko and M. E. Shaposhnikov, Phys. Lett. B **418**, 46 (1998) [arXiv:hep-ph/9709492].
- [352] T.N. La Rosa, N.E. Kassim, T.J. Lazio and S.D. Hyman, Astron. Journ. **119** (2000) 207.
- [353] J. G. Learned and K. Mannheim, Ann. Rev. Nucl. Part. Sci. **50**, 679 (2000).
- [354] S. Lee, Phys. Rev. D **58** (1998) 043004 [arXiv:astro-ph/9604098].
- [355] B. W. Lee and S. Weinberg, Phys. Rev. Lett. **39**, 165 (1977).
- [356] LEP Higgs Working Group (standard model Higgs), OPAL, ALEPH, DELPHI and L3 Collaborations, arXiv:hep-ex/0107029.
- [357] LEP Higgs Working Group (MSSM Higgs), arXiv:hep-ex/0107030.
- [358] A. D. Lewis, D. A. Buote and J. T. Stocke, Astrophys. J. **586** (2003) 135 [arXiv:astro-ph/0209205].
- [359] L. Lista [BABAR Collaboration], *Proceedings of the International Conference on Flavor Physics (ICFP), Zhang-Jia-Jie City, Hunan, China*, (2001) [arXiv:hep-ex/0110010].
- [360] S. M. Liu, V. Petrosian and F. Melia, arXiv:astro-ph/0403487.
- [361] M. S. Longair, *High Energy Astrophysics*, Cambridge University Press, New York, 1994.
- [362] Lopes, Ilidio, private communication.
- [363] I. P. Lopes, G. Bertone and J. Silk, Mon. Not. Roy. Astron. Soc. **337** (2002) 1179 [arXiv:astro-ph/0205066].
- [364] I. P. Lopes, J. Silk and S. H. Hansen, Mon. Not. Roy. Astron. Soc. **331**, 361 (2002) [arXiv:astro-ph/0111530].
- [365] J. Lundberg and J. Edsjo, arXiv:astro-ph/0401113.
- [366] E. J. Chun, H. B. Kim and D. H. Lyth, Phys. Rev. D **62** (2000) 125001 [arXiv:hep-ph/0008139].
- [367] D. Majumdar, J. Phys. G **28**, 2747 (2002) [arXiv:hep-ph/0209278].
- [368] G. K. Mallot, Int. J. Mod. Phys. A, **1581**, 521 (2000).
- [369] M. Maltoni, T. Schwetz, M. A. Tortola and J. W. Valle, Phys. Rev. D **68**, 113010 (2003) [arXiv:hep-ph/0309130].
- [370] T. Maeno *et al.* [BESS Collaboration], Astropart. Phys. **16**, 121 (2001) [arXiv:astro-ph/0010381].
- [371] G. Marchesini *et al.*, Comp. Phys. Comm. **67** (1992) 465.
- [372] S. P. Martin, arXiv:hep-ph/9709356.

- [373] M. Mateo, *Ann. Rev. Astron. Astrophys.* **36**, 435 (1998) [arXiv:astro-ph/9810070].
- [374] D. Maurin, F. Donato, R. Taillet and P. Salati, *Astrophys. J.* **555**, 585 (2001) [arXiv:astro-ph/0101231].
- [375] D. Maurin, R. Taillet and F. Donato, *Astron. Astrophys.* **394**, 1039 (2002) [arXiv:astro-ph/0206286].
- [376] D. Maurin, R. Taillet, F. Donato, P. Salati, A. Barrau and G. Boudoul, arXiv:astro-ph/0212111.
- [377] H.A. Mayer-Haesselwander *et al.*, *A&A* 335, 161 (1998)
- [378] J. McDonald, K. A. Olive and M. Srednicki, *Phys. Lett. B* **283**, 80 (1992).
- [379] F. Melia, *Astrophys. J.* **387** (1992) L25.
- [380] D. Merritt, Center," arXiv:astro-ph/0311594.
- [381] D. Merritt, M. Milosavljevic, L. Verde and R. Jimenez, *Phys. Rev. Lett.*, 88, (2002), 191301 [arXiv:astro-ph/0201376.]
- [382] R. B. Metcalf, L. A. Moustakas, A. J. Bunker and I. R. Parry, arXiv:astro-ph/0309738.
- [383] R. N. Mohapatra, S. Nussinov and V. L. Teplitz, *Phys. Rev. D* **66**, 063002 (2002) [arXiv:hep-ph/0111381].
- [384] B. Moore, T. Quinn, F. Governato, J. Stadel and G. Lake, *Mon. Not. Roy. Astron. Soc.* **310** (1999) 1147 [arXiv:astro-ph/9903164].
- [385] T. Moroi, H. Murayama and M. Yamaguchi, *Phys. Lett. B* **303**, 289 (1993).
- [386] A. Morselli, A. Lionetto, A. Cesarini, F. Fucito and P. Ullio [GLAST Collaboration], *Nucl. Phys. Proc. Suppl.* **113** (2002) 213 [arXiv:astro-ph/0211327].
- [387] I. V. Moskalenko and A. W. Strong, *Astrophys. J.* **493** (1998) 694 [arXiv:astro-ph/9710124].
- [388] L. A. Moustakas and R. B. Metcalf, *Mon. Not. Roy. Astron. Soc.* **339**, 607 (2003) [arXiv:astro-ph/0206176].
- [389] H. Murayama, G. Raffelt, C. Haggmann, K. van Bibber, and L. J. Rosenberg, *Eur. Phys. J.* **C3** (1998) 264.
- [390] D. V. Nanopoulos, K. A. Olive and M. Srednicki, *Phys. Lett. B* **127**, 30 (1983).
- [391] C. R. Nappi and B. A. Ovrut, *Phys. Lett. B* **113**, 175 (1982).
- [392] R. Narayan, R. Mahadevan, J. E. Grindlay, R. G. Popham and C. Gammie, *Astrophys. J.* **492** (1998) 554.
- [393] J. F. Navarro, C. S. Frenk and S. D. White, *Astrophys. J.* **462** (1996) 563 [arXiv:astro-ph/9508025].

- [394] J. F. Navarro, arXiv:astro-ph/0110680.
- [395] J. F. Navarro *et al.*, arXiv:astro-ph/0311231.
- [396] T. Nihei, L. Roszkowski and R. Ruiz de Austri, JHEP **0105**, 063 (2001) [arXiv:hep-ph/0102308].
- [397] T. Nihei, L. Roszkowski and R. Ruiz de Austri, JHEP **0203**, 031 (2002) [arXiv:hep-ph/0202009].
- [398] S. I. Nikolsky and V. G. Sinityna, *Proceedings of the Workshop on VHE Gamma Ray Astronomy, Crimea*, (1989).
- [399] P. L. Nolan, W. F. Tompkins, I. A. Grenier, P. F. Michelson, *Astrophys. J.* **597**, 615 (2003) [arXiv:astro-ph/0307188].
- [400] H. Ohanian and R. Ruffini, "Gravitation And Space-Time," New York, USA, Norton (1994).
- [401] K. i. Okumura and L. Roszkowski, arXiv:hep-ph/0208101.
- [402] K. i. Okumura and L. Roszkowski, JHEP **0310**, 024 (2003) [arXiv:hep-ph/0308102].
- [403] K. A. Olive, TASI lectures on dark matter, arXiv:astro-ph/0301505.
- [404] K. A. Olive and M. Srednicki, *Phys. Lett. B* **230**, 78 (1989).
- [405] K. A. Olive and M. Srednicki, *Nucl. Phys. B* **355**, 208 (1991).
- [406] R. A. Ong, arXiv:astro-ph/0304336.
- [407] R. A. Ong, *Proceedings of the GeV-TeV Gamma Ray Astrophysics Workshop, Snowbird, Utah*, (1999) AIP Proc. Conf. **515**, 401.
- [408] S. Orito *et al.* [BESS Collaboration], *Phys. Rev. Lett.* **84**, 1078 (2000) [arXiv:astro-ph/9906426].
- [409] H. Pagels and J. R. Primack, *Phys. Rev. Lett.* **48**, 223 (1982).
- [410] For particle physics prospects of PAMELA, see: <http://www.cerncourier.com/main/article/42/8/17>
- [411] T. J. Pearson *et al.*, *Astrophys. J.* **591** (2003) 556 [arXiv:astro-ph/0205388].
- [412] P. J. E. Peebles, *Gen. Rel. Grav.* **3** (1972), 63.
- [413] P. J. E. Peebles, *Science* **224** (1984) 1385.
- [414] W. J. Percival *et al.*, *Mon. Not. Roy. Astron. Soc.* **327** (2001) 1297 [arXiv:astro-ph/0105252].
- [415] D. Petry [the MAGIC Telescope Collaboration], *Astron. Astrophys. Suppl. Ser.* **138** (1999) 601 [arXiv:astro-ph/9904178].
- [416] C. Picciotto and M. Pospelov, arXiv:hep-ph/0402178.

- [417] P. Picozza and A. Morselli, *J. Phys. G* **29**, 903 (2003) [arXiv:astro-ph/0211286].
- [418] L. Pieri and E. Branchini, arXiv:astro-ph/0307209.
- [419] T. Plehn, *et al.*, Prospino program available at: <http://pheno.physics.wisc.edu/~plehn/prospino/prospino.html>
- [420] G. Polesello and D. R. Tovey, arXiv:hep-ph/0403047.
- [421] F. Prada, A. Klypin, J. Flix, M. Martinez and E. Simonneau, arXiv:astro-ph/0401512.
- [422] G. Prezeau, A. Kurylov, M. Kamionkowski and P. Vogel, *Phys. Rev. Lett.* **91**, 231301 (2003) [arXiv:astro-ph/0309115].
- [423] L. Randall and R. Sundrum, *Phys. Rev. Lett.* **83** (1999) 3370 [arXiv:hep-ph/9905221].
- [424] L. Randall and R. Sundrum, *Nucl. Phys. B* **557**, 79 (1999) [arXiv:hep-th/9810155].
- [425] D. Reed *et al.*, arXiv:astro-ph/0312544.
- [426] T. Ressel, *et al.*, *Phys. Rev. D.* **48** (1993) 5519.
- [427] G. Rhee, A. Klypin and O. Valenzuela, arXiv:astro-ph/0311020.
- [428] L. J. Rosenberg and K. A. van Bibber, *Phys. Rept.* **325** (2000) 1.
- [429] L. Roszkowski, *Phys. Lett. B* **262**, 59 (1991).
- [430] L. Roszkowski, R. Ruiz de Austri and T. Nihei, *JHEP* **0108**, 024 (2001) [arXiv:hep-ph/0106334].
- [431] P. Roy, ICNAPP 1994:0225-237, [arXiv:hep-ph/9501209].
- [432] S. Rudaz and F. W. Stecker, *Astrophys. J.* **325**, 16 (1988).
- [433] S. Rudaz and F. W. Stecker, *Astrophys. J.* **368**, 406 (1991).
- [434] G.B. Rybicki., A.P. Lightman , *Radiative Processes in Astrophysics*, 1979, John Wiley & Sons.
- [435] H. F. Sadrozinski, *Nucl. Instrum. Meth. A* **466** (2001) 292.
- [436] N. Sakai and T. Yanagida, *Nucl. Phys. B* **197**, 533 (1982).
- [437] P. Salati, *Phys. Lett. B* **571** (2003) 121 [arXiv:astro-ph/0207396].
- [438] A. Salucci, P. Borriello, *MNRAS*, **323**, 285 (2001).
- [439] P. Salucci and A. Borriello, arXiv:astro-ph/0203457.
- [440] D. J. Sand, T. Treu and R. S. Ellis, *Astrophys. J.* **574** (2002) L129 [arXiv:astro-ph/0207048].
- [441] T. Sanuki, *Int. J. Mod. Phys. A* **17**, 1635 (2002).

- [442] S. Sarkar, *Talk given at COSMO 99: 3rd International Conference on Particle Physics and the Early Universe, Trieste, Italy*, (1999) [arXiv:hep-ph/0005256].
- [443] S. Sarkar, Proc. Indian Natl. Sci. Acad. **70A**, 163 (2004) [arXiv:hep-ph/0302175].
- [444] S. Sarkar and R. Toldra, Nucl. Phys. B **621**, 495 (2002) [arXiv:hep-ph/0108098].
- [445] R. Schoedel, R. Genzel, T. Ott, A. Eckart, N. Mouawad and T. Alexander, Astrophys. J. **596**, 1015 (2003) [arXiv:astro-ph/0306214].
- [446] G. Servant and T. M. Tait, Nucl. Phys. B **650** (2003) 391 [arXiv:hep-ph/0206071].
- [447] G. Servant and T. M. Tait, New J. Phys. **4**, 99 (2002) [arXiv:hep-ph/0209262].
- [448] X. D. Shi and G. M. Fuller, Phys. Rev. Lett. **82** (1999) 2832 [arXiv:astro-ph/9810076].
- [449] G. Shiu and L. T. Wang, arXiv:hep-ph/0311228.
- [450] V. F. Shvartsman, 1971, Soviet Astronomy, 15, 377.
- [451] G. Sigl, S. Lee, P. Bhattacharjee and S. Yoshida, Phys. Rev. D **59**, 043504 (1999) [arXiv:hep-ph/9809242].
- [452] J. Silk, K. Olive and M. Srednicki, Phys. Rev. Lett. **55**, 257 (1985).
- [453] P. Sikivie, Phys. Rev. D **60** (1999) 063501 [arXiv:astro-ph/9902210].
- [454] T. Sjöstrand, Comp. Phys. Comm. 82 (1994) 74.
- [455] A. Slyz, T. Kranz and H. W. Rix, Mon. Not. Roy. Astron. Soc. **346**, 1162 (2003) [arXiv:astro-ph/0309597].
- [456] D. R. Smith and N. Weiner, Phys. Rev. D **64**, 043502 (2001) [arXiv:hep-ph/0101138].
- [457] D. N. Spergel *et al.*, Astrophys. J. Suppl. **148**, 175 (2003) [arXiv:astro-ph/0302209].
- [458] D. N. Spergel and P. J. Steinhardt, Phys. Rev. Lett. **84**, 3760 (2000) [arXiv:astro-ph/9909386].
- [459] M. Srednicki and R. Watkins, Phys. Lett. B **225**, 140 (1989).
- [460] G. D. Starkman, A. Gould, R. Esmailzadeh and S. Dimopoulos, Phys. Rev. D **41** (1990) 3594.
- [461] F. W. Stecker, Phys. Lett. B **201**, 529 (1988).
- [462] F. W. Stecker, S. Rudaz and T. F. Walsh, Phys. Rev. Lett. **55**, 2622 (1985).
- [463] F. Stoehr, S. D. White, V. Springel, G. Tormen and N. Yoshida, Mon. Not. Roy. Astron. Soc. **345**, 1313 (2003) [arXiv:astro-ph/0307026].

- [464] A. W. Strong, I. V. Moskalenko and O. Reimer, *Astrophys. J.* **537** (2000) 763 [Erratum-ibid. **541** (2000) 1109] [arXiv:astro-ph/9811296].
- [465] A. Tasitsiomi and A. V. Olinto, *Phys. Rev. D* **66** (2002) 083006 [arXiv:astro-ph/0206040].
- [466] A. Tasitsiomi, J. Gaskins and A. V. Olinto, arXiv:astro-ph/0307375.
- [467] J. E. Taylor and J. Silk, *Mon. Not. Roy. Astron. Soc.* **339** (2003) 505 [arXiv:astro-ph/0207299].
- [468] J. Taylor and J. Navarro, *ApJ*, 563:483-488, 2001.
- [469] M. Tegmark *et al.* [SDSS Collaboration], arXiv:astro-ph/0310723.
- [470] Home page of Max Tegmark: <http://www.hep.upenn.edu/~max/main.html>
- [471] K. Tsuchiya *et al.* [CANGAROO-II Collaboration], arXiv:astro-ph/0403592.
- [472] D. Tucker-Smith and N. Weiner, arXiv:hep-ph/0402065.
- [473] M. S. Turner, *Phys. Rev. D* **33**, 889 (1986).
- [474] M. S. Turner and F. Wilczek, *Phys. Rev. D*, **42**, 1001 (1990).
- [475] C. Tyler, *Phys. Rev. D* **66** (2002) 023509 [arXiv:astro-ph/0203242].
- [476] A. J. Tylka, *Phys. Rev. Lett.*, **63**, 840 (1989).
- [477] J.A. Tyson, G.P. Kochanski and I.P. Dell'Antonio, *Astrophys. J. Lett.* **498** (1998) 107.
- [478] P. Ullio, M. Kamionkowski and P. Vogel, *JHEP* **0107** (2001) 044 [arXiv:hep-ph/0010036].
- [479] P. Ullio, *JHEP* **0106**, 053 (2001) [arXiv:hep-ph/0105052].
- [480] P. Ullio and L. Bergstrom, *Phys. Rev. D* **57**, 1962 (1998) [arXiv:hep-ph/9707333].
- [481] P. Ullio, H. Zhao and M. Kamionkowski, *Phys. Rev. D* **64** (2001) 043504 [arXiv:astro-ph/0101481].
- [482] P. Ullio, L. Bergstrom, J. Edsjo and C. Lacey, *Phys. Rev. D* **66** (2002) 123502 [arXiv:astro-ph/0207125].
- [483] F. C. van den Bosch and R. A. Swaters, arXiv:astro-ph/0006048.
- [484] B. M. Vladimirovsky, *et al.*, *Proceedings of the Workshop on VHE Gamma Ray Astronomy, Crimea*, (1989).
- [485] H. J. Volk, *Talk at the 27th International Cosmic Ray Conference (ICRC), Hamburg, Germany*, (2001) [arXiv:astro-ph/0202421].
- [486] S. S. Vogt, M. Mateo, E. W. Olszewski and M. J. Keane, *Astron. Journal*, **109** (1995) 151.

- [487] I. Wasserman, Phys. Rev. D **33** (1986) 2071.
- [488] B. R. Webber, *Lectures given at NATO Advanced Study Institute on Particle Production Spanning MeV and TeV Energies, Nijmegen, Netherlands*, (1999) [arXiv:hep-ph/9912399].
- [489] W. R. Webber, M. A. Lee and M. Gupta, Astrophys. J. **390** (1992) 96.
- [490] T. C. Weekes, *et al.*, Astrophys. J. **342** (1998) 379.
- [491] T. C. Weekes, arXiv:astro-ph/0010431.
- [492] G. Weiglein (editor), Report of the LHC/LC study group, 2004.
- [493] S. Weinberg, 1995, *The Quantum Theory of Fields Vol 1: Foundations*, Cambridge University Press.
- [494] S. Weinberg, Phys. Rev. Lett. **48**, 1303 (1982).
- [495] S. Weinberg, Phys. Rev. D **26**, 287 (1982).
- [496] C. Weinheimer, *Proceedings of 10th International Workshop on Neutrino Telescopes, Venice, Italy*, 2003 [arXiv:hep-ex/0306057].
- [497] J. Wess and J. Bagger, “Supersymmetry And Supergravity”, Princeton, USA: Univ. Pr. (1992).
- [498] J. Wess and B. Zumino, Nucl. Phys. B **70**, 39 (1974).
- [499] R. Wischnewski [the AMANDA Collaboration], arXiv:astro-ph/0204268.
- [500] R. F. G. Wyse, arXiv:astro-ph/0012270.
- [501] T. Yamamoto *et al.*, *Proceedings of the 26th International Cosmic Ray Conference, Salt Lake City*, **5**, 275 (1999).
- [502] J. Yinlin, *et al.*, *Proceedings of the 21st International Cosmic Ray Conference, Adelaide*, **4**, 220 (1990).
- [503] G. B. Yodh, Space. Sci. Rev. **75**, 199 (1996).
- [504] N. Yoshida, A. Sokasian, L. Hernquist and V. Springel, Astrophys. J. **591** (2003) L1 [arXiv:astro-ph/0303622].
- [505] M. Yu, Khlopov and A. D. Linde, Phys. Lett. B **138** (1984) 265.
- [506] G. T. Zatsepin and V. A. Kuzmin, Pis'ma Zh. Eksp. Teor. Fiz. **4** (1966) 114 [JETP. Lett. **4** (1966) 78].
- [507] D. Zaritsky, R. Smith, C. Frenk and S. D. M. White, Astroph. Journal, **478** (1997) 39.
- [508] H. Ziaepour, Astropart. Phys. **16**, 101 (2001) [arXiv:astro-ph/0001137].
- [509] J. A. Zweerink, *et al.*, *Proceedings of the 26th International Cosmic Ray Conference, Salt Lake City*, bf **5**, 223 (1999).

- [510] F. Zwicky, 1933, *Helv. Phys. Acta* 6, 110.
- [511] <http://hegra1.mppmu.mpg.de/MAGICWeb/>
- [512] <http://icrhp9.icrr.u-tokyo.ac.jp/index.html>
- [513] <http://www.mpi-hd.mpg.de/hfm/HESS/HESS.html>
- [514] <http://veritas.sao.arizona.edu/index.html>